Univerza v Ljubljani

Fakulteta za elektrotehniko

Andraž Polak

Električne lastnosti ravninskih dvoslojev sestavljenih iz mešanic lipidov

DOKTORSKA DISERTACIJA

Mentor: prof. dr. Damijan Miklavčič

Somentor: dr. Mounir Tarek

Ljubljana, 2014

University of Ljubljana

Faculty of Electrical Engineering

Andraž Polak

Electrical properties of planar lipid bilayers formed from lipid mixtures

DOCTORAL THESIS

Mentor: Prof.: Damijan Miklavčič, Ph.D.

Co-mentor: Mounir Tarek, Ph.D.

Ljubljana, 2014

Očkotu v zahvalo

Preface

The present PhD thesis is a result of hardware development for planar lipid bilayer properties' measuring system, experiments on planar lipid bilayers and molecular dynamics simulations of lipid bilayers carried out during the PhD study period at the Laboratory of Biocybernetrics, Faculty of Electrical Engineering, University of Ljubljana. The molecular dynamics simulations were performed at Équipe Théorie Simulations et Modélisation, Université de Lorraine, Nancy, France. The results of the present work have been published or were submitted in the following papers in international scientific journals:

Paper 1: Polak A, Mulej B, Kramar P. **System for measuring planar lipid bilayer properties**. *J. Membrane Biol.* 245: 625-632, 2012.

Paper 2: Polak A, Bonhenry D, Dehez F, Kramar P, Miklavčič D, Tarek M. **On the electroporation thresholds of lipid bilayers: Molecular dynamics simulation investigations.** *J. Membrane Biol.* 246: 843-850, 2013.

Paper 3: Polak A, Tarek M, Tomšič M, Valant J, Poklar Ulrih N, Jamnik A, Kramar P, Miklavčič D. **Electroporation of archaeal lipid membranes using MD simulations.** *Bioelectrochemistry*, 2014.

Paper 4: Polak A, Tarek M, Tomšič M, Valant J, Poklar Ulrih N, Jamnik A, Kramar P, Miklavčič D. **Structural Properties of Archaeal Lipid Bilayers: Small-Angle X-Ray Scattering and Molecular Dynamics Simulation Study.** *Langmuir*, Submitted.

Paper 5: Polak A, Velikonja A, Kramar P, Tarek M, Miklavčič D. **Polyoxyethylene glycol ($C_{12}E_8$) decreases the electroporation threshold of POPC lipid bilayers.** *Langmuir*, Submitted.

Acknowledgements

Za strokovno vodstvo in videnju mojega potenciala se iskreno zahvaljujem mentorju prof. dr. Damijanu Miklavčiču.

Thanks to my co-mentor dr. Mounir Tarek who introduced and lead me into the world of molecular dynamics simulations. Thank you for your hospitality and for teaching me how to be a better scientist.

Hvala doc. dr. Petru Kramarju za dolgoletno mentorstvo, ki se je začelo že v času študija elektrotehnike in nadaljevalo do doktorske disertacije.

Thanks to all the colleagues at the Équipe Théorie Simulations et Modélisation Laboratory, who helped me at work and spent free time with me in Nancy.

Hvala vsem sodelavcem Laboratorija za biokibernetiko za nepozabne trenutke, ki smo jih skupaj preživeli. Posebna zahvala gre Barbari, Mariji in Boštjanu za pomoč in zanimive pogovore.

Hvala Mateji in Dunji za pregled doktorske disertacije.

Hvala najboljšim prijateljem za vso izkazano podporo.

Hvala mami in bratu, ki sta me in me še podpirata na vseh področjih mojega življenja.

Table of contents

Abstract

Electroporation is related to a cascade of events which follows the application of high electric field and leads to cell membrane permeabilization. The electroporation is divided into two different fields: irreversible electroporation and reversible electroporation. In reversible electroporation, the cell membrane does not reseal pores after voltage is applied and the cell dies. In reversible electroporation, the cell membrane pores are resealed after the electric field application. Both effects are used in biology, biotechnology and medicine. Despite a wide range of applications, little is known on how electroporation thresholds vary with the membrane lipids' composition. The influence of lipid bilayer composition on electroporation threshold and other electrical properties of bilayers were studied, using experiments on planar lipid bilayers and molecular dynamics' simulations. First a system for measuring planar lipid bilayer properties was developed. It measures properties using voltage and current-clamp methods. The planar lipid bilayer can be formed by painting or folding method and its temperature can be regulated between 15 and 55 °C.

Systematic electroporation study of those lipids which are predominant component in membranes of archaea *Aeropyrum pernix* was performed, using molecular dynamics simulations. These lipids are one of the features which enable life in harsh environments. *Aeropyrum pernix* has 2,3-di-O-sesterterpanyl-sn-glicerol-1-phospho-myo-inositol (AI) and 2,3-di-O-sesterterpanyl-sn-glicerol-1-phospho-1'(2'-O-α-D-glucosyl)-myo-inositol (AGI) in its membrane. These two lipids have complex structures, therefore first the effect of two main moieties on the electroporation process was studied, by comparing dipalmitoyl-phosphatidylcholine (DPPC), dipalmitoyl-phosphatidylcholine (DPhPC-ester) and diphytanoyl-phosphocholine-ether (DPhPC-ether) bilayers. Comparison of DPPC and DPhPC-ester revealed that additional methyl groups in lipid tails increase the electroporation threshold. Comparison of DPhPC-ester and DPhPC-ether revealed that changing ester linkages with ether linkages increases the electroporation threshold even further. The AI and AGI molecules have longer tails and contain carbohydrates in the head group in comparison to the DPhPC-ether. The molecular dynamics study revealed that they have very high electroporation threshold, which can be decreased by adding DPPC molecules into the bilayer. Here we for the first time observed conducting hydrophobic pore formation. Other properties which increase the stability of the bilayers are: low water permeability in hydrophobic region, due to methyl groups in lipid tails; high lateral pressure in hydrophobic region; low lateral diffusion of lipids and hydrogen bonds among lipid head groups. The electron density profiles obtained from molecular dynamics simulations were in good agreement with the measured electron density profiles, measured using Small Angle X-ray Scattering, which gives confidence in the programmed models.

Using the system for measuring planar lipid bilayers properties, experiments on palmitoy-oleoyl-phosphatidylcholine (POPC) planar lipid bilayers and POPC planar lipid bilayers with incorporated surfactant polyoxyethylene glycol ($C_{12}E_8$) were performed. Small increase of capacitance in the POPC planar lipid bilayers with $C_{12}E_8$ incorporated was noticed. On the other hand, the incorporation of $C_{12}E_8$ into the POPC planar lipid bilayer drastically decreased electroporation threshold. Drastic decrease of electroporation threshold was explained using molecular dynamics simulations. At $C_{12}E_8$ incorporation special pore formation in POPC bilayers was observed. First the hydrophilic parts of $C_{12}E_8$ molecules gather in the hydrophobic region and later water penetrates into the interior of the bilayer, to form hydrophilic pore.

Razširjeni povzetek

Uvod

Elektroporacija je pojav pri katerem se lastnosti celične membrane spremenijo, če je le-ta izpostavljena električnemu polju. Elektroporacija je lahko ireverzibilna ali reverzibilna. Pri ireverzibilni elektroporaciji celica izpostavljena električnemu polju umre zaradi posledic poškodb na celični membrani (Goldman 1943). Poškodbe celične membrane so lahko tudi reverzibilne. To pomeni, da se celična membrana po izpostavitvi električnemu polju zaceli nazaj (Stampfli 1958). Tako ireverzibilna kot reverzibilna elektroporacija se uporabljata v biologiji, medicini in biotehnologiji (Haberl et al. 2013). Najbolj znane aplikacije ireverzibilne elektroporacije se uporabljajo pri proizvodnji hrane (Toepfl et al. 2007), oblaciji tkiv (Al-Sakere et al. 2007; Rubinsky 2007) in čiščenju vode (Gusbeth et al. 2009). Reverzibilna elektroporacija se uporablja pri elektrokemoterapiji (Sersa et al. 2012; Miklavčič et al. 2014), vnosu genov v celice (C. Heller in Heller 2010), prenosu zdravil preko kože (Zorec et al. 2013), fuziji celic (Usaj et al. 2010) in vstavljanju proteinov v membrane (Teissié 1998).

Čeprav se elektroporacija uporablja na veliko področjih, pa nastanek in obstoj por v bioloških membranah še vedno niso povsem razjasnjeni. Raziskave se vršijo na več področjih s poskusi in na modelih tkiv, celic in membran (Kotnik et al. 2012). Modele uporabljamo za načrtovanje poskusov, uporabljajo se lahko tudi za razlago in pojasnitev poskusov. Za modeliranje elektroporacije uporabljamo modele končnih diferenc, končnih elementov, molekularne dinamike in kvantne mehanike. Prvi dve metodi se uporabljata za simulacije večjih sistemov kot so tkiva, celice in liposomi (Pavšelj in Miklavčič 2008; Corovic et al. 2013; Rems in Miklavčič 2014). Molekularna dinamika se uporablja za simulacije liposomov in membran. Kvantna mehanika se v kombinaciji z molekularno dinamiko uporablja za simulacije membran in manjših sistemov (Vries et al. 2003; Tarek 2005).

Umetni vezikli so najpreprostejši model celične membrane, saj so po svoji geometriji podobni celični membrani, vendar nimajo notranjih struktur (Tekle et al. 2001). Umetne vezikle med drugim uporabljajo tudi za enkapsulacijo zdravilnih učinkovin, ki se lahko sprostijo v izbranih področjih, npr. v celici (Immordino et al. 2006; Elbayoumi and Torchilin 2010). Ena od učinkovitih metod za sprostitev učinkovine iz umetnih liposomov je tudi elektroporacija (Napotnik et al. 2010). Učinkovitost elektroporacije umetnih veziklov je predvsem odvisna od strukture membrane in dovedenega električnega polja (Portet et al. 2009). Za proučevanje sproščanja učinkovine iz umetnih veziklov moramo poznati strukturo membrane in njeno obnašanje pod vplivom električnega polja. Ravninski lipidni dvosloji predstavljajo majhen košček membrane celice ali vezikla. Ravninske lipidne dvosloje tvorimo med dvema tekočinama. Tako je ravninski lipidni dvosloj dostopen z obeh strani,

zato so tudi eksperimenti na ravninskih lipidnih dvoslojih preprostejši kot eksperimenti na umetnih veziklih (Mueller et al. 1963; Huang et al. 1964; Benz et al. 1975; Ottova in Tien 2002).

Poznamo različne tehnike tvorjenja ravninskih lipidnih dvoslojev med dvema tekočinama: metoda barvanja (Mueller et al. 1963), metoda dvigovanja gladine vode (Montal in Mueller 1972), metoda potopitve konice (Coronado in Latorre 1983), metoda z dvojnim prekatom (Funakoshi et al. 2006) in metoda s križnim kanalom (Funakoshi et al. 2006). Z elektrotehniškega stališča lahko ravninski lipidni dvosloj smatramo kot paralelno vezavo kondenzatorja in upora. Pri proučevanju elektroporacije, nas zanima tudi pod kakšnimi pogoji (napetost) se ravninski lipidni dvosloj poruši. Električne lastnosti ravninskih lipidnih dvoslojev merimo z metodo vsiljene napetosti ali metodo vsiljenega toka. Pri metodi vpete napetosti ravninskemu lipidnemu dvosloju vpnemo napetost in izmerimo tok, ki teče skozi dvosloj. Pri metodi vsiljenega toka preko ravninskega lipidnega dvosloja vsilimo tok in merimo napetost, ki se pri tem ustvari. Pri obeh metodah lahko uporabimo različne oblike signalov, kot so: pulzi, linearno naraščajoč signal, sinusoida ali trikotni signal (Kramar et al. 2007; Kramar et al. 2009; Sabotin et al. 2009; Kramar et al. 2010).

Simulacija molekularne dinamike je računalniška metoda, ki se v zadnjih letih zelo hitro razvija. Z njo lahko simuliramo sisteme na molekularni ravni. Eno od področij raziskovanja so tudi biološke membrane. S to metodo lahko zgradimo matematični model koščka ravninskega lipidnega dvosloja. Osnovni gradniki sistemov molekularne dinamike so atomi, ki se z vezmi povezujejo v molekule. Lastnosti atomov in vezi so zbrani v posebnih knjižnicah, ki se v angleščini imenujejo "force fields". Najbolj znane knjižnice molekularne dinamike so: CHARMM (Brooks et al. 2009), AMBER (Salomon-Ferrer et al. 2013), GROMACS (Hess et al. 2008) in MARTINI (Marrink et al. 2007). Sile, ki delujejo na atome, izračunamo iz Newtonovih zakonov gibanja. Pozicije atomov izračunamo v diskretnih časovnih trenutkih. Tako je vsak položaj atoma izračunan iz prejšnjega položaja z upoštevanjem Newtonovih zakonov gibanja. Postopek je računsko zelo zahteven, zato lahko simuliramo le relativno majhne sisteme, pri katerih so problematični robni pogoji. Zato pri simulacijah uporabimo periodične robne pogoje. Najpogosteje uporabljeni programi za računanje simulacij molekularne dinamike so: NAMD2 (Kalé et al. 1999; Phillips et al. 2005), GROMACS (Hess et al. 2008) and AMBER (Salomon-Ferrer et al. 2013).

Za simulacijo in proučevanje elektroporacije bioloških membran, je potrebno zgraditi sistem, sestavljen iz lipidnega dvosloja in raztopine, ki ga obdaja. V lipidni dvosloj lahko vgradimo tudi druge nelipidne molekule. Celoten sistem uravnotežimo, nato ga izpostavimo električnemu polju. Izpostavitev električnemu polju lahko proučujemo na dva načina. Prvi način je predstavil Tieleman (2004). Pri tem načinu usmerimo zunanje električno polje (E) pravokotno na površino lipidnega dvosloja. Predpostavimo, da je električno polje enakomerno razporejeno po celotnem simulacijskem prostoru in na vsak nabit atom deluje sila q_iE (Slika 1A). Drugi način vsili električno polje preko

membrane kot posledica ionskega neravnovesja preko lipidnega dvosloja (Sachs et al. 2004). Ker pa ima simulacijski prostor periodične mejne pogoje, moramo simulirati dva vzporedna lipidna dvosloja (Slika 1B). Ta način simulacije je izboljšala Delemotte et al. (2008). Simulacija dveh paralelnih lipidnih dvoslojev je računsko potratna, zato so avtorji uporabili ionsko neravnovesje le na eni membrani. Simulaciji drugega lipidnega dvosloja so se izognili z dodatkom praznega prostora na obeh straneh lipidnega dvosloja (Slika 1C). Obstaja tudi izvedba, kjer uporabimo konstanten tlak, tako kot pri Tielemanovi metodi, in električno polje ustvarimo z neravnovesjem nabojev. Prehajanje ionov z ene na drugo stran dvosloja preprečimo s silo na ione, ki je odvisna od razdalje od lipidnega dvosloja (Herrera in Pantano 2009). Vernier et al. (2006) je pokazal, da sta Tilemanova in metoda z neravnovesjem nabojev primerljivi in dajeta primerljive rezultate.

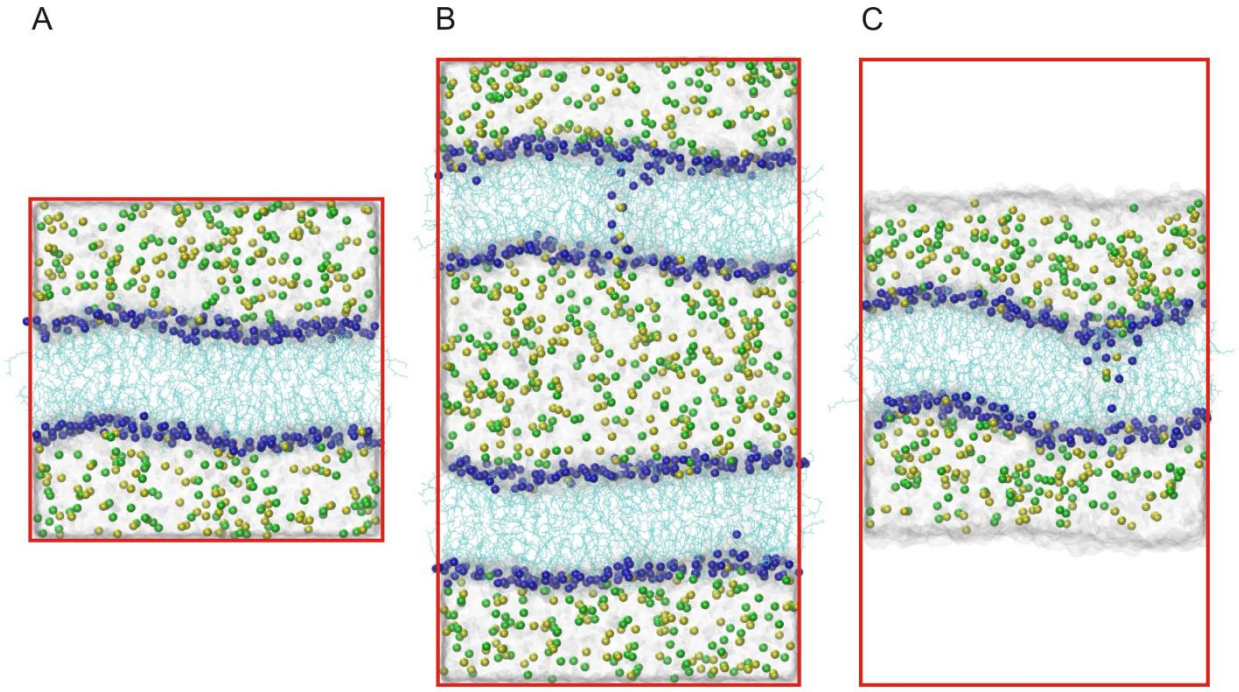

Slika 1: Metode elektroporacije v molekularni dinamiki. A) Vsiljeno električno polje preko sile na vsak nabiti delec v sistemu; B) Sach-ova metoda; C) Delemotte-jina metoda (modra – fosfor, rumena – kalijev ion, zelena – kloridni ion, siva površina – voda, modrozelena -lipidni repi, redeči pravokotnik – simulacijska celica).

Lipidne molekule, ki jih najdemo v membranah prokariontov in evkariontov, so razdeljene v štiri skupine: glicerofosfolipidi, galaktolipidi, sfingolipidi in steroli (Luckey 2008; Lehninger et al. 2008). V membranah arhej pa najdemo posebne lipidne molekule. Arheje so ekstremofilni organizmi, ki se optimalno razmnožujejo v izjemno negostoljubnih okoljih. Glede na okolje v katerem živijo jih delimo na: halofilne, anaerobne, termofilne in psihrofilne. Ti organizmi se od drugih ločijo v sestavi lipidnih membran (Benvegnu et al. 2004; Ulrih et al. 2007; Ulrih et al. 2009). Zaradi stabilnosti lipidov arhej v negostoljubnih okoljih so primerni tudi za tvorjenje umetnih liposomov, ki vsebujejo različne zdravilne učinkovine (Hanford in Peeples 2002; Ulrih et al. 2009).

Aeropyrum pernix spada med hipertermofilne arheje. Prvič so ga izolirali na obalnih žveplenih vrelcih otoka Kodakara-Jima, blizu Japonske. Ta vrsta je aerobni organizem, ki najbolje raste pri temperaturah med 90 °C in 95 °C, pH 7,0 in slanosti 3,5 %. Celice so okrogle oblike s premerom med 0,8 µm in 1,2 µm (Sako et al. 1996). Ta arheja ima posebno strukturo membrane, zgrajeno iz dveh lipidov: 2,3-di-O-sesterterpanil-sn-glicerol-1-fosfo-mio-inozitol (AI) in 2,3-di-O-sesterterpanil-sn-glicerol-1-fosfo-1'(2'-O-α-D-glucozil)-mio-inozitol (AGI). Jedro obeh lipidov je 2,3-di-o-sesterterpanil-sn-glicerol ($C_{25,25}$-arheol). Polarna glava enega od lipidov je zgrajena iz inozitola, polarno glavo drugega lipida pa sestavljata inozitol in glukoza (Morii et al. 1999).

Lipidne strukture obstajajo v gel kristalinični ali v tekoči kristalinični fazi. Faza lipidne strukture je določena z mobilnostjo lipidnih molekul v njej, ta pa je odvisna od temperature. Pri višjih temperaturah je mobilnost lipidnih molekul večja, kar določa tekočo fazo. Pri nižjih temperaturah je mobilnost manjša, kar določa gel kristalično fazo. Med prehodom faz sespremeni tudi debelina lipidnega dvosloja (Tokumasu et al. 2002; Luckey 2008). Kapacitivnost ravninskega lipidnega dvosloja je obratno sorazmerna z debelino dvosloja, zato lahko pri faznem prehodu opazimo tudi spremembo kapacitivnosti (Basu et al. 2001). Basu s sodelavci je pokazal, da je tudi prevodnost ravninskega lipidnega dvosloja odvisna od temperature.

Prvi cilj doktorske disertacije je bil izdelava sistema za merjenje lastnosti ravninskih lipidnih dvoslojev, ki bo omogočal avtomatizirano merjenje pri določeni temperaturi ter vzbujanje ravninskega lipidnega dvosloja z napetostjo ali tokom. Drugi cilj doktorske disertacije je bil izmeriti lastnosti ravninskih lipidnih dvoslojev iz različnih mešanic lipidov. Tretji cilj doktorske disertacije je bil proučiti, kaj se dogaja v lipidnem dvosloju, ki ga izpostavimo električnemu polju na molekularni ravni z uporabo simulacije molekularne dinamike. Rezultate simulacije molekularne dinamike smo primerjali z eksperimentalnimi podatki pridobljenimi na ravninskih lipidnih dvoslojih.

Materiali in metode

Celotna doktorska disertacija je sestavljena iz treh področij dela: razvoja sistema za merjenje lastnosti ravninskih lipidnih dvoslojev, merjenja lastnosti ravninskih lipidnih dvoslojev in simulacij lipidnih dvoslojev z molekularno dinamiko.

Sistem za merjenje lastnosti ravninskih lipidnih dvoslojev

Sistem za merjenje lastnosti ravninskih lipidnih dvoslojev je zgrajen iz kontrolne enote, izhodne enote, LCR metra, črpalk za polnjenje prekatov, kopeli z regulirano temperaturo in merilne komore s štirimi elektrodami. Kontrolno enoto sestavlja vgradni računalnik, kontrolno vezje, analogno digitalni in digitalno analogni pretvornik. Kontrolna enota kontrolira vsa stikala, aktuatorje in generatorje ter zajema signale s senzorjev. Grafični vmesnik, nameščen na vgradnem računalniku, omogoča nastavitve metod merjenja lastnosti ravninskih lipidnih dvoslojev in nastavitev temperature. Pretvorniki so most med analognim in digitalnim delom naprave. LCR meter se uporablja za merjenje kapacitivnosti ravninskih lipidnih dvoslojev. Izhodna enota je vezje, ki omogoča generiranje in merjenje signalov poljubnih oblik z metodama vpete napetosti in vsiljenega toka. Sistem omogoča merjenje lastnosti ravninskih lipidnih dvoslojev tvorjenih z metodama barvanja in dvigovanja gladine vode. Merilni komori sta izdelani iz teflona. V prekata merilne komore sta vstavljeni dve tokovni in dve referenčni elektrodi. Za zagotovitev regulirane temperature ravninskega lipidnega dvosloja je merilna komora vstavljena v temperaturno regulirano kopel, ki služi tudi kot oklop pred zunanjimi motnjami. Pri metodi dvigovanja gladine vode ravninske lipidne dvosloje tvorimo avtomatsko s polnjenjem in praznjenjem prekatov preko črpalk.

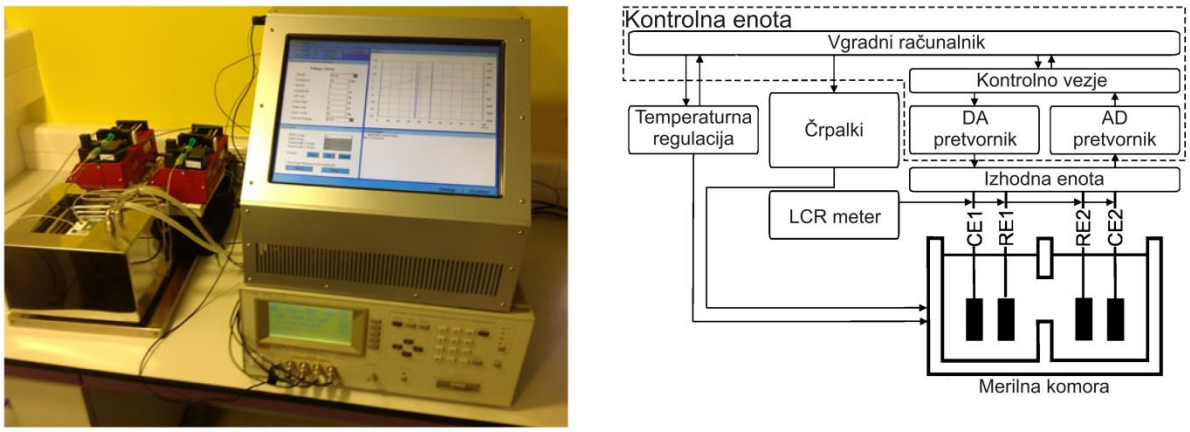

Slika 2: Levo: Slika sistema za merjenje lastnosti ravninskih lipidnih sistemov. Na levi strani sta črpalki za polnjenje prekatov merilne komore in kopel. V kopel je vstavljena merilna komora s štirimi elektrodami. Desno zgoraj je kontrolna enota. Pod njo pa LCR meter. Desno: Shema sistema za merjenje lastnosti ravninskih lipidnih dvoslojev, ki je sestavljen iz kontrolne enote, LCR metra, izhodne enote, črpalk za polnjenje prekatov, merilne komore s štirimi elektrodami in temperaturno regulirane kopeli. Kontrolna enota je sestavljena iz vgradnega računalnika, kontrolnega vezja, digitalno analognega (DA) in analogno digitalnega (AD) pretvornika.

Merjenje lastnosti ravninskih lipidnih dvoslojev

Lastnosti ravninskih lipidnih dvoslojev smo merili z izdelanim sistemom. Uporabili smo metodo vsiljenega toka in linearno naraščajoči vzbujalni signal. Ravninske lipidne dvosloje smo tvorili z metodo dvigovanja gladine vode pri 25 °C. Proučevali smo vpliv surfaktanta polietilen glikola ($C_{12}E_8$) v ravninskih lipidnih dvoslojih zgrajenih iz palmito-olein-fosfatholin (POPC) molekul na elektroporacijo. Ravninske lipidne dvosloje smo tvorili na luknjici premera 105 µm. Prah lipidov POPC smo raztopili v 9:1 heksan/etanolu tako, da smo dobili 10 mg/ml mešanico. Za torus smo uporabili mešanico heksana in dekana v razmerju 3:7. Okoliška raztopina je bila pripravljena iz mešanice 0,1 M KCl in 0,01 M HEPES v enakem razmerju. Z dodajanjem 1 M NaOH smo dosegli, da je imela raztopina pH 7.4. Pri eksperimentih z vgrajenim surfaktantom smo v enega od prekatov vbrizgali 15 µl 1 mM raztopine s $C_{12}E_8$. Pri poskusu smo tvorili 42 POPC ravninskih lipidnih dvoslojev in 42 POPC ravninskih dvoslojev z vgrajenimi molekulami $C_{12}E_8$.

Izmerili smo tudi lastnosti veziklov zgrajenih iz lipidov arhej *Aeropyrum pernix* in njihovimi mešanicami z dipalmitol-fosfatholin (DPPC) molekulami v enakem razmerju z metodo sipanja X-žarkov pod majhnimi koti (SAXS). Dobili smo profile elektronske gostote preko membran, ki smo jih kasneje primerjali z rezultati molekularne dinamike.

Simulacija lipidnih dvoslojev z molekularno dinamiko

Z molekularno dinamiko smo simulirali elektroporacijo lipidnih dvoslojev zgrajenih iz dipalmitol-fosfatholin (DPPC), dipalmitol-fosfatidilholin (DPhPC-ester), di-palmitol-fosfatidilholin-eter (DPhPC-eter), 2,3-di-O-sesterterpanyl-sn-glicerol-1-phospho-myo-inositol (AI), 2,3-di-O-sesterterpanyl-sn-glicerol-1-phospho-1'(2'-O-α-D-glucosyl)-myo-inositol (AGI), palmito-olein-fosfatholin (POPC) in polietilen glikol ($C_{12}E_8$) molekul. Modela molekul DPPC in POPC sta v literaturi že opisana in zanju najdemo parametre v večini knjižnic molekularne dinamike. Pri simulacijah smo uporabili knjižnico CHARMM 36. Ostale modele molekul smo zgradili iz kombinacij različnih knjižnic CHARMM. Vsi dvosloji so bili najprej sestavljeni iz 64 lipidnih molekul in obdani z raztopino (KCl ali vodo z dodatnimi Na^+ ioni za nevtralizacijo). Nato smo sisteme uravnotežili pri konstantni temperaturi in tlaku ter jih s preslikanjem 4-krat povečali. Velike sisteme smo še enkrat uravnotežili pri želenih temperaturah. Časovni korak integracije smo nastavili na 2.0 fs. Takšna dolžina koraka je zadoščala, ker smo uporabili konstantne razdalje vezi, ki jih tvorijo vodikovi atomi. Sile, ki delujejo na krajši in daljši razdalji, smo izračunali vsak in vsak drugi časovni trenutek. Za izračun sil, ki delujejo na daljši razdalji, smo uporabili "particle mash Ewald" pristop (Essmann et al. 1995). Izračunali smo lastnosti lipidnih dvoslojev kot so: dipolni potencial membrane, porazdelitev posameznih molekul v sistemu, profile elektronskih gostot, difuzijo molekul v lateralni smeri na membrano in reorentacijo lipidnih glav arheolipidov.

Uravnotežene lipidne dvosloje smo izpostavili električnemu polju. Električno polje smo vzpostavili z neravnovesjem ionov preko lipidnih dvoslojev z Delemotte-jino metodo (Delemotte et al. 2008). Pri simulacijah uporabljamo periodične robne pogoje, zato smo na sredino raztopine vstavili prazen prostor in spremenili pogoje simulacije. Namesto nastavitve konstantnega tlaka smo nastavili konstanten volumen simulacijske celice. Tako smo se izognili prehajanju nosilcev naboja iz ene na drugo stran dvosloja. Iz odvisnosti transmembranske napetosti od neravnovesja nabojev (od 0e do 8e) smo izračunali kapacitivnost lipidnega dvosloja. Pri višjih vrednostih neravnovesja nabojev oziroma transmembranske napetosti pa pride do spremembe organizacije lipidnih molekul v membrani in tvorjenja por.

Rezultati in razprava

Sistem za merjenje lastnosti ravninskih lipidnih dvoslojev

Sistem za merjenje lastnosti ravninskih lipidnih dvoslojev omogoča merjenje kapacitivnosti s sinusnim signalom frekvenc od 20 Hz do 1 MHz z efektivno vrednostjo od 0,005 do 2 V. Ostale električne lastnosti ravninskih lipidnih dvoslojev meri sistem z metodama vpete napetosti ali vsiljenega toka poljubnih oblik. Pri metodi vpete napetosti lahko generiramo napetost na območju med -1,5 in 1,5 V s točnostjo 1 mV in merimo tok na območju med -15 in 15 µA s točnostjo do 0,05 µA. Pri metodi vsiljenega toka lahko tok generiramo med -15 in 15 µA s točnostjo 0,02 µA in merimo napetost s točnostjo 4 mV. Temperaturo tvorjenih ravninskih lipidnih dvoslojev lahko reguliramo med 15 in 55 °C s točnostjo 0,5 °C. Testirali smo izhodno enoto, ki generira in meri električne signale preko ravninskega lipidnega dvosloja. Ugotovili smo, da je mejna frekvenca metode vpete napetosti 11 kHz, mejna frekvenca metode vsiljenega toka pa 17 kHz.

Sistem je bil preizkušen na ravninskih lipidnih dvoslojih sestavljenih iz lecitina. Ravninske lipidne dvosloje smo tvorili z metodo dvigovanja gladine vode pri 25 °C. Tvorjeni so bili na okroglih luknjicah premera 126 in 197 µm. Izmerjene kapacitivnosti, normirane na površino, so bile $0{,}39 \pm 0{,}0302$ µF/cm^2 in $0{,}38 \pm 0{,}02$ µF/cm^2. Za obe velikosti luknjic smo tako dobili primerljive vrednosti, ki so tudi v skladu z vrednostmi iz literature (Naumowicz et al. 2003). Porušitveni napetosti za ravninskih lipidnih dvoslojev iz lecitina sta bili $480{,}0 \pm 5{,}0$ mV in $480{,}5 \pm 6{,}5$ mV. Izmerili smo jih z metodama vpete napetosti in vsiljenega toka. Pri obeh metodah smo uporabili linearno naraščajoči signal.

Merjenje lastnosti ravninskih lipidnih dvoslojev

Izmerili smo kapacitivnosti in porušitvene napetosti POPC ravninskih lipidnih dvoslojev in POPC ravninskih lipidnih dvoslojev z vgrajenimi molekulami $C_{12}E_8$ (Tabela 1). Ugotovili smo, da se z dodatkom molekul $C_{12}E_8$ kapacitivnost nekoliko zviša, porušitvena napetost pa zmanjša za 22%. Troiano et al. (1998) je ugotovil, da se pri enakih ravninskih lipidnih dvoslojih z vgrajenimi molekulami $C_{12}E_8$, vendar pri drugačnih metodah merjenja kapacitivnost ne spremeni, porušitvena napetost pa pade za 33%. Poskusi na celični liniji DC3F so pokazali, da vgradnja surfaktanta $C_{12}E_8$ v celično membrano zniža prag ireverizibilne elektroporacije, ne vpliva pa na prag reverzibilne elektroporacije (Kandušer et al. 2003).

Tabela 1: Lastnosti POPC ravninskih lipidnih dvoslojev in POPC ravninskih lipidnih dvoslojev z vgrajenimi molekulami $C_{12}E_8$ (n – število meritev, U_{br} – porušitvena napetost, C_{Esp} – kapacitivnost normirana na površino).

Bilayer	n	U_{br} [V]	C_{Esp} [µF/cm^2]
POPC	42	0,374 ± 0,046	0,59 ± 0,03
POPC + 10 µM $C_{12}E_8$	42	0,293 ± 0,044	0,63 ± 0,03

Vrednosti za U_{br} in C_{Esp} so podane kot povprečna vrednost ± standardna deviacija.

Simulacija lipidnih dvoslojev z molekularno dinamiko

Lastnosti uravnoteženih lipidnih dvoslojev so zbrane v Tabeli 2. Pri proučevanju lipidnih dvoslojev, vedno izračunamo, kakšno površino zavzame posamezna molekula v lipidnem dvosloju. Ta mora imeti čim manj fluktuacij, saj to potrdi uravnoteženost lipidnega dvosloja. S primerjavo z eksperimentalnimi podatki pa potrdimo, da so matematični modeli dobro zgrajeni. Pri izpostavitvi lipidnega dvosloja električnemu polju lahko izračunamo kapacitivnost in prag elektroporacije ($U_{EPthres}$). S primerjavo DPPC in DPhPC-ester lipidnih dvoslojev smo ugotovili, da dodatek metilnih skupin v repe lipidov zviša prag elektroporacije (Tabela 2). Primerjava DPhPC-ester in -eter lipidnih dvoslojev je pokazala, da etrske vezi še zvišajo prag elektroporacije. Membrane, zgrajene iz lipidov arhej imajo nekoliko nižje kapacitivnosti, saj so lipidni dvosloji debelejši. Prag elektroporacije pa se giblje med 4,1–4,5 V pri 50 °C, kar je veliko več kot pri PC-lipidih. Pri nižjih temperaturah se prag elektroporacije arheolipidov še zviša in znaša 5,0–5,4 V. Prag elektroporacije arheolipidov lahko znižamo tako, da dodamo v lipidni dvosloj DPPC molekule. Lipidnim dvoslojem, zgrajenim iz arheolipidov in njihovih mešanic z DPPC v enakem razmerju, smo izračunali tudi elektronsko gostoto in jo primerjali s SAXS meritvami. Dobili smo zelo dobro ujemanje, kar potrjuje, da so naši modeli AI in AGI molekul dobro zgrajeni. S primerjavo profilov tlaka smo ugotovili, da pri obravnavanih lipidnih dvoslojih obstaja povezava s pragom elektroporacije. Višji kot je tlak v hidrofobnem delu lipidnega dvosloja višji je prag elektroporacije.

Shinoda et al. (2004b) je naredil obširno študijo prepustnosti vode v DPPC in DPhPC dvoslojih. Pokazal je, da je prepustnost vode v notranjosti DPhPC dvosloja za 30% manjša kot pri DPPC dvoslojih. To je lahko razlog za večjo stabilnost lipidnih dvoslojev tvorjenih z lipidi, ki imajo razvejane repe. Formacija pore je povezana z nastankom vodnih prstov v lipidnem dvosloju. Ti pa so neposredno povezani s prepustnostjo vode v notranjosti lipidnega dvosloja.

Izvedli smo obsežno analizo porazdelitve in dinamično analizo molekul v lipidnem dvosloju, da bi ugotovili zakaj so lipidni dvosloji zgrajeni z arhealnih lipidov tako stabilni. Arhealne lipidne molekule s svojimi glavami tvorijo skupke, ki so povezani med seboj z vodikovimi vezmi. Izračun lateralnega difuzijskega koeficienta je pokazal, da je le-ta zelo odvisen od temperature. Višja temperatura pomeni hitrejše gibanje molekul v lateralni smeri. V primerjavi z ostalimi PC-lipidi imajo arhealni lipidi veliko manjši lateralni difuzijski koeficient. Primerjali smo tudi reorentacijski koeficient glukoze in inozitola v glavah arhealnih lipidov. Reorientacija lipidnih glav je odvisna od temperature. Opazimo pa tudi velike razlike med AI in AGI molekulami, saj AI molekule nimajo dodatne glukoze v glavi, zato se tudi hitreje gibljejo v prostoru. S primerjavo različnih okoliških raztopin smo ugotovili, da ta nima vpliva na strukturo arhealnega lipidnega dvosloja. V primerjavi s PC-lipidi so arhealni lipidi manj hidrirani. Vse te lastnosti pripomorejo k stabilnosti lipidnih dvoslojev.

Primerjava POPC lipidnih dvoslojev s POPC lipidnimi dvosloji z vgrajenimi molekulami $C_{12}E_8$ je pokazala, da molekule $C_{12}E_8$ zavzamejo različne položaje v lipidnem dvosloju. Molekule gredo lahko v celoti v hidrofobni del dvosloja, čeprav so zgrajene iz hidrofobnega in hidrofilnega dela. Tako je velika možnost za prehod molekul na drugo stran lipidnega dvosloja (i.e. flip-flop), ki je bil pri eksperimentih že opažen (le Maire et al. 1987; Kragh-Hansen et al. 1998). Preko lipidnih membran smo vzpostavili ionsko neravnovesje. Izmerili smo kapacitivnosti in pragove elektroporacije. Pri izmerjenih kapacitivnostih smo opazili majhne razlike, prag elektroporacije pa se je z dodatkom molekul $C_{12}E_8$ drastično zmanjšal (Tabela 2). Primerjava z eksperimentalnimi podatki je pokazala veliko razliko med absolutnimi vrednostmi. Ta razlika do sedaj v študijah še ni bila pojasnjena, domnevamo pa, da je vzrok razlike v časovnih okvirih, kjer se elektroporacija zgodi. Eksperimenti se odvijajo v milisekundah, simulacije molekularne dinamike pa v nanosekundah. Pri eksperimentih in simulacijah smo opazili majhno zvišanje kapacitivnosti dvoslojev, ko dodamo surfaktant $C_{12}E_8$. Z dodatkom surfaktanta $C_{12}E_8$ se porušitvena napetost POPC dvoslojev zmanjšala za 22%.

Tabela 2: Lastnosti uravnoteženih lipidnih dvoslojev izračunanih iz simulacij molekularne dinamike (T – temperatura, A_m – površina, ki jo zavzame ena molekula v lipidnem dvosloju, U_d – dipolni potencial membrane, C_{Msp} – specifična kapacitivnost, $U_{EPthres}$ – prag elektroporacije).

Dvosloj	Raztopina	T [°C]	A_m [Å^2]	U_d [V]	C_{Msp} [µF/cm^2]	$U_{EPthres}$ [V]
256 DPPC	0,45 M KCl	50	60,0 ± 0,9	0,70	0,94	1,8–2,2
256 DPhPC-ester	0,45 M KCl	50	80,1 ± 0,6	0,62	0,93	2,3–2,7
256 DPhPC-eter	0,45 M KCl	50	74,6 ± 0,7	0,36	0,90	3,0–3,4
12 AI, 116 AGI, 128 DPPC	0,45 M KCl	70	73,8 ± 0,7	0,42	-	-
	128 Na^+ ionov	70	74,6 ± 0,9	-	-	-
	0,45 M KCl	50	72,0 ± 0,9	0,42	0,68	3,6–4,1
	0,45 M KCl	25	69,1 ± 0,7	0,42	0,68	3,9–4,3
	128 Na^+ ionov	25	68,9 ± 0,4	-	-	-
24 AI, 232 AGI	0,45 M KCl	90	90,4 ± 0,7	0,18	-	-
	0,45 M KCl	70	86,8 ± 0,6	0,20	-	-
	256 Na^+ ionov	70	86,7 ± 0,7	-	-	-
	0,45 M KCl	50	86,0 ± 0,6	0,23	0,72	4,1–4,5
	0,45 M KCl	25	82,5 ± 0,3	0,23	0,67	5,0–5,4
	256 Na^+ ionov	25	83,4 ± 0,4	-	-	-
256 POPC	0,1 M KCl	25	60,4 ± 0,7	0,68	0,88	1,9–2,3
256 POPC, 32 $C_{12}E_8$	0,1 M KCl	25	60,7 ± 0,9	0,66	0,97	<1,1

Vrednosti za A_m so podane kot povprečna vrednost ± standardna deviacija.

V okviru naloge smo opazovali tudi, kako nastajajo pore v lipidnih dvoslojih, ki jih izpostavimo električnemu polju. V lipidnih dvoslojih, sestavljenih iz DPPC, DPhPC-ester in -eter lipidov (Slika 3),

se elektroporacija začne z vstopom vodnih molekul (vodnih prstov) v notranjost lipidnega dvosloja z ene ali obeh strani. Voda nato tvori žico preko dvosloja (Slika 3B), ki se kasneje razširi. Razširjena pora se stabilizira z upogibom lipidnih molekul v notranjost lipidnega dvosloja (Slika 3C). Tako nastane hidrofilna pora, ki je v literaturi že dobro opisana (Tieleman et al. 2003; Leontiadou et al. 2004; Delemotte and Tarek 2012).

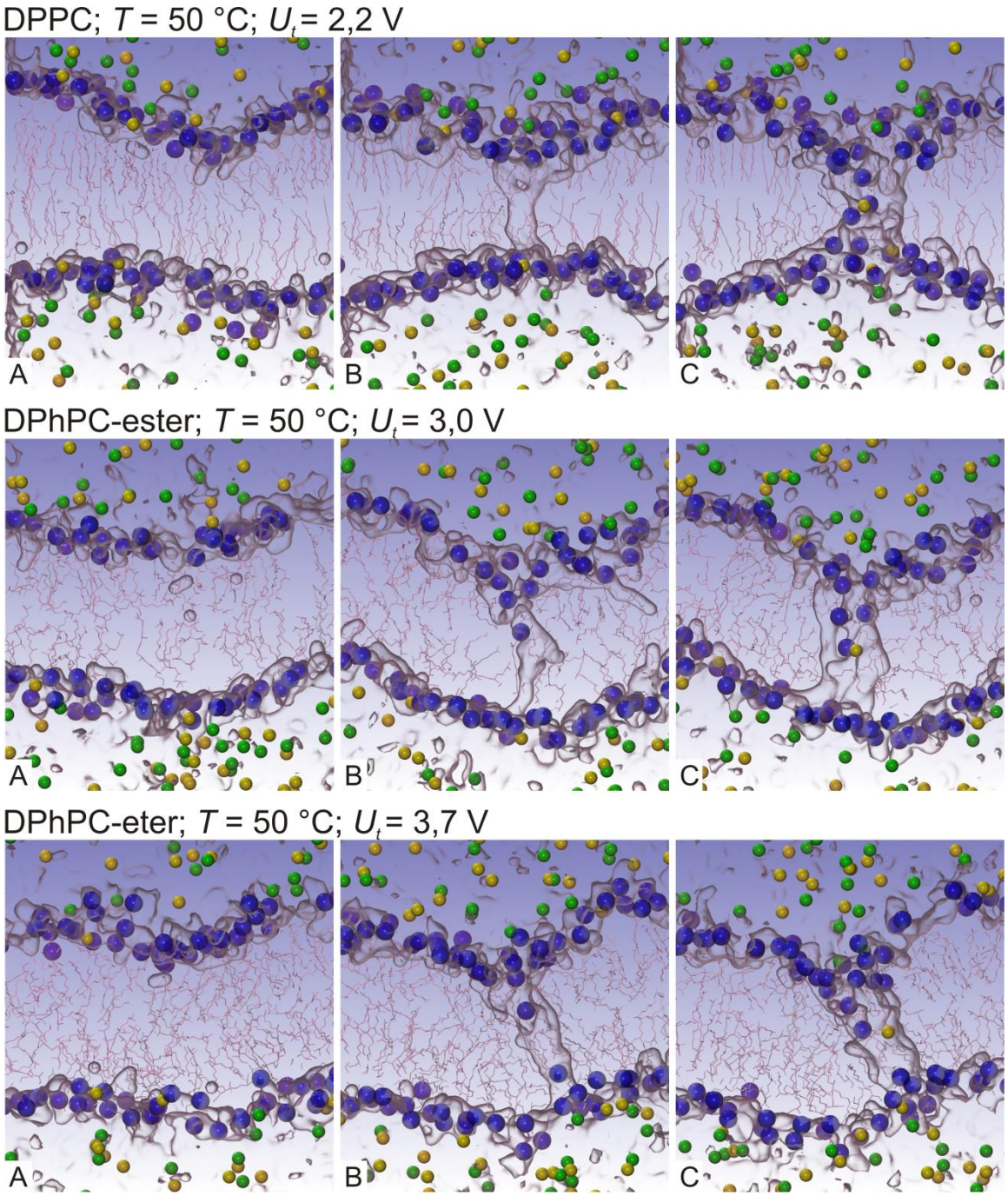

Slika 3: Proces elektroporacije v DPPC, DPhPC-ester and DPhPC-eter dvoslojih: A) dvosloj ob vzpostavitvi ionskega neravnovesja, B) tvorba vodne žice in C) tvorba prevodne hidrofilne pore (bela – lipidni repi (med lipidnimi glavami), modra – fosfor, rumena – kalijev ion, zelena – kloridni ion, siva površina - voda, *T* – temperatura, U_t – trasmembranska napetost).

Študija elektroporacije arhealnih lipidnih dvoslojev je pokazala, da se v njih pore tvorijo na poseben način (Slika 4). Elektroporacija se začne s formacijo vodnih prstov in nadaljuje z vodno žico preko dvosloja (Slika 4B), na enak način kot je opisano pri fosfolipidih. Hidrofobna vodna pora se nato razširi in omogoči prehod ionov preko dvosloja. Posebnost por arhealnih lipidnih dvoslojev je, da nismo nikoli opazili stabilizacije vodne pore z upogibom lipidov v notranjost lipidnega dvosloja. Takšno poro imenujemo hidrofobna pora (Slika 4). Stabilizacijo pore z upogibom lipidov v notranjost lipidnega dvosloja prav tako nismo opazili pri dvoslojih sestavljenih iz arheolipidov in DPPC molekul v enakem molarnem razmerju. Podobno tvorbo pore so opazili tudi v POPS dvoslojih (Dehez et al. 2014).

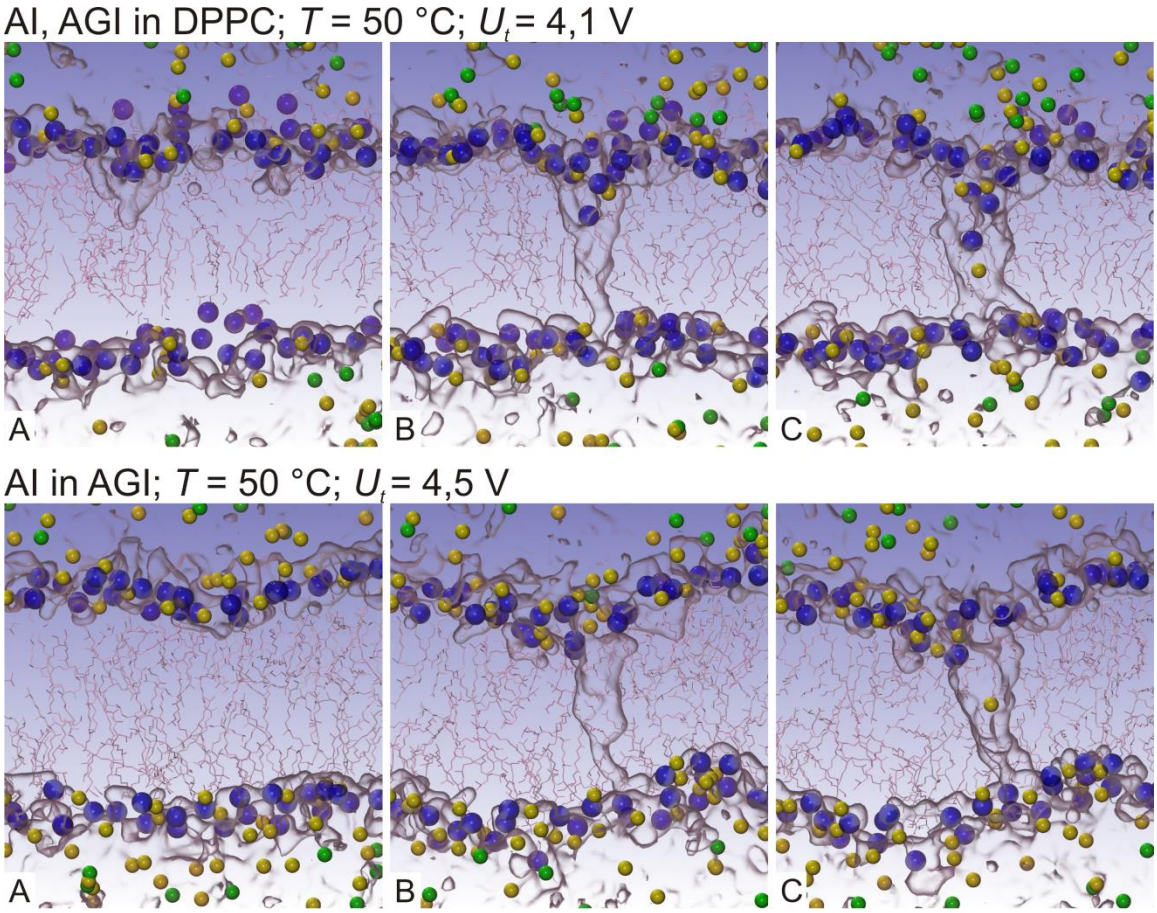

Slika 4: Proces elektroporacije v arhealnih dvoslojih in njihovih mešanicah z DPPC: A) dvosloj ob vzpostavitvi ionskega neravnovesja, B) tvorba vodne žice in C) tvorba prevodne hidrofobne pore (bela – lipidni repi (med lipidnimi glavami), modra – fosfor, rumena – kalijev ion, zelena – kloridni ion, siva površina – voda, T – temperatura, U_t – trasmembranska napetost).

Nastanek pore v POPC dvosloju z dodatkom surfaktanta $C_{12}E_8$ je nekoliko drugačen kot pri ostalih formacijah por (Slika 5). Najprej molekule $C_{12}E_8$ tvorijo skupek s svojimi hidrofilnimi deli v hidrofobnem delu lipidnega dvosloja. Nato voda prodre v hidrofilni del skupka molekul $C_{12}E_8$ v obliki vodnih prskov. Ko se vodni prsti z obeh strani dvosloja združijo, nastane vodna žica (Slika 5B), ki je že stabilizirana s hidrofilnimi glavami molekul $C_{12}E_8$. Vodna žica se nato razširi in dodatno stabilizira z upogibom lipidov v notranjost dvosloja. Nato gredo skozi poro tudi ioni (Slika 5C). Posebnost pore v POPC lipidnem dvosloju z dodatkom $C_{12}E_8$ je, da je že od začetka nastanka pore le-ta hidrofilna.

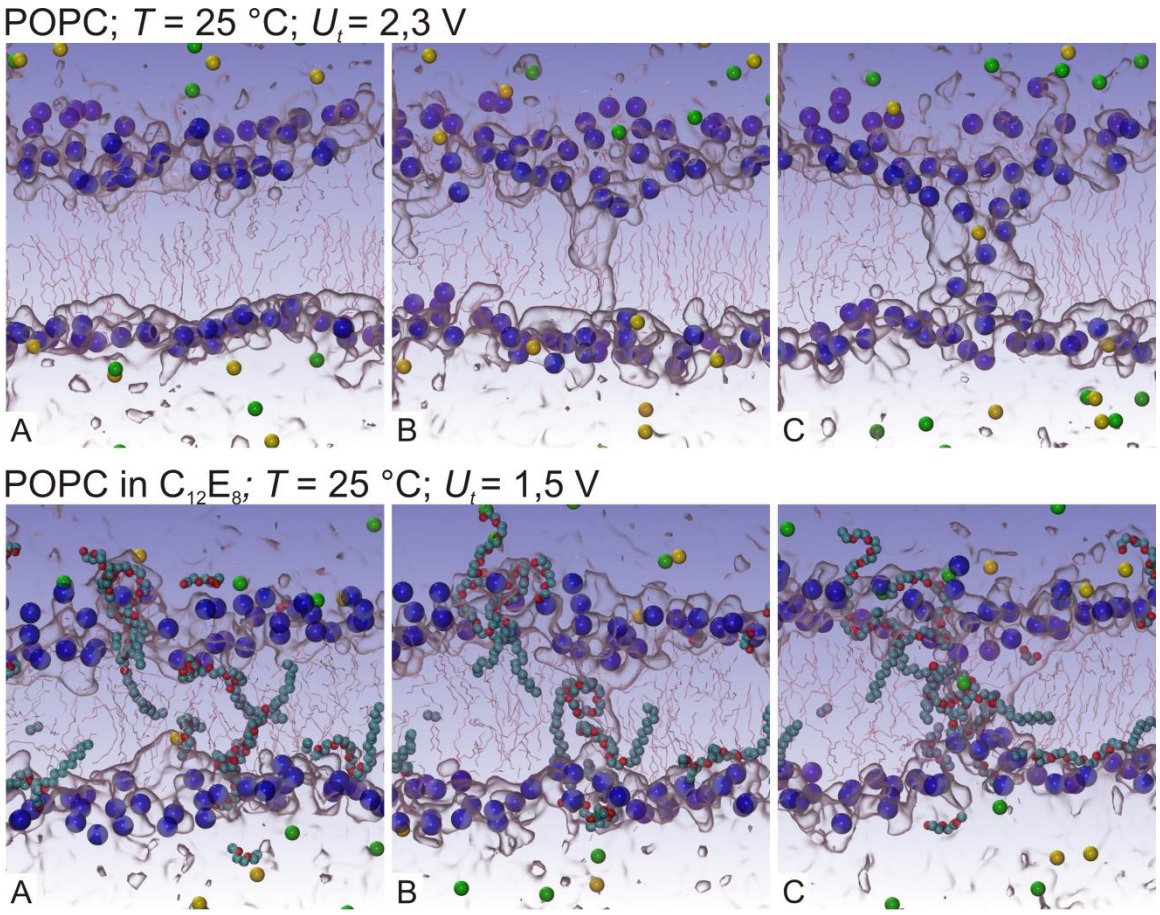

Slika 5: Proces elektroporacije v POPC dvosloju in POPC dvosloju z dodatkom surfaktanta $C_{12}E_8$: A) dvosloj ob vzpostavitvi ionskega neravnovesja, B) tvorba vodne žice in C) tvorba prevodne hidrofilne pore (bela – lipidni repi (med lipidnimi glavami), modra – fosfor, rumena – kalijev ion, zelena – kloridni ion, siva površina – voda, T – temperatura, U_t – trasmembranska napetost).

Zaključek

V okviru naloge smo izdelali sistem za merjenje lastnosti ravninskih lipidnih dvoslojev z različnimi metodami in regulacijo temperature. S tem sistemom smo izmerili lastnosti POPC ravninskih lipidnih dvoslojev in POPC ravninskih lipidnih dvoslojev z dodatkom surfaktanta $C_{12}E_8$. Sistem se uporablja tudi za druge raziskave, ki niso del te naloge. Eksperimentalno pridobljene podatke smo primerjali s simulacijami molekularne dinamike in dobili zelo dobro ujemanje. Z molekularno dinamiko smo sistematično proučili kateri deli molekul arheolipidov so vzrok visoki stabilnost na električni stres. Ugotovili smo, da se pore v arhealnih lipidnih dvoslojih ne tvorijo na enak način kot v ostalih PC-lipidih. Tako smo prvič opazili tvorbo hidrofobene prevodne pore. Tudi v POPC dvoslojih z vgrajenimi molekulami $C_{12}E_8$ smo opazili posebnost pri tvorjenju por. Tu molekule $C_{12}E_8$ tvorijo hidrofilni del v lipidnem dvosloju, preden voda prodre v notranjost. Menimo, da sta načina tvorjenja por ključna pri zvišanju oziroma znižanju praga elektroporacije.

Izvirni prispevki k znanosti

Na podlagi rezultatov doktorske disertacije smo ugotovili naslednje izvirne prispevke k znanosti:

Razvoj sistema za merjenje lastnosti ravninskih lipidnih dvoslojev

Izdelali smo sistem za merjenje lastnosti ravninskih lipidnih dvoslojev. Merilne metode smo povzeli iz drugih sistemov iz literature. Naš sistem omogoča merjenje z metodama vpete napetosti in vsiljenega toka. Ravninske lipidne dvosloje pa lahko tvorimo z metodo barvanja ali metodo dvigovanja gladine vode. Pri metodi dvigovanja gladine vode je omogočeno avtomatsko tvorjenje ravninskih lipidnih dvoslojev. Temperatura tvorjenih ravninskih lipidnih dvoslojev je regulirana na območju med 15 in 55 °C.

Razvoj modelov arhealnih lipidov za uporabo v simulacijah molekularne dinamike

Lipidi, ki jih najdemo v membranah arhej *Aeropyrum pernix*, še niso bili opisani v literaturi. V ta namen smo zgradili modela lipidov AI in AGI za uporabo v simulacijah molekularne dinamike. Modela sta bila zgrajena s kombinacijo različnih CHARMM knjižnic. Parametre eterskih vezi smo pa povzeli po Shinoda et al. (2004a). Modela sta bila preizkušena na nekaterih simulacijah lipidnih dvoslojev, kjer smo lastnosti primerjali z eksperimentalnimi podatki in dobili dobro ujemanje. Modela bosta tudi v prihodnje prosto dostopna na spletu za raziskovalce, ki delujejo na področju simulacij molekularne dinamike.

Analiza elektroporacije arhealnih lipidnih dvoslojev z uporabo molekularne dinamike

Ker sta molekuli AI in AGI, ki ju najdemo v arhejah *Aeropyrum pernix* zelo kompleksni, smo študijo razdelili na tri sklope. Najprej smo s primerjavo DPPC, DPhPC-ester in DPhPC-eter lipidnih dvoslojev ugotovili, da dodatne metilne skupine v lipidnih repih zvišajo prag elektroporacije. Zamenjava esterskih z eterskimi vezmi pa prag elektroporacije še zviša. V drugem delu smo ugotovili, da imajo arhealni lipidni dvosloji veliko višji prag elektroporacije kot dvosloji sestavljeni iz fosfolipidov. Ta prag lahko znižamo z dodatkom DPPC molekul. Pri procesu elektroporacije smo opazili posebno tvorbo prevodne hidrofobne pore. Podobna tvorba pore je bila opažena tudi v POPS dvosloju. Na koncu je dinamična analiza pokazala, da imajo arhealni lipidi veliko nižjo lateralno difuzijo kot fosfolipidi.

Analiza vpliva molekul $C_{12}E_8$ na elektroporacijo lipidnih dvoslojev iz palmitoil-oleoil-fosfatidilholina (POPC)

Z namenom boljšega razumevanja iz katerih molekul moramo sestaviti lipidni dvosloj z želenimi električnimi lastnostmi, smo proučili, kako surfaktant $C_{12}E_8$ vgrajen v POPC lipidni dvosloj vpliva na elektroporacijo. Z eksperimenti na ravninskih lipidnih dvoslojih smo potrdili navedbe v literaturi, da vgradnja surfaktanta $C_{12}E_8$ v POPC lipidni dvosloj zniža prag elektroporacije. S simulacijami molekularne dinamike smo znižanje praga potrdili in dobili vpogled, kaj se dogaja na molekularni

ravni. K znižanju praga elektroporacije prispevajo molekule $C_{12}E_8$ tako, da tvorijo skupek v hidrofobnem delu dvosloja s svojimi hidrofilnimi deli. V hidrofilni del voda lažje prodre in že na začetku nastanka pore je le-ta stabilizirana z $C_{12}E_8$ molekulami.

1 Introduction

Electroporation is a phenomenon in which biological membranes change their properties when they are exposed to high electric field. It is known that electroporation can be irreversible or reversible. Irreversible electroporation is known as a phenomenon when a cell dies due to membrane damage when exposed to the electric field (Goldman 1943). The changes in membrane exposed to the electric field can be reversible. This indicates that the cell membrane changes its properties when it is exposed to electric field. After exposure the cell membrane regains its properties from before the exposure (Stampfli 1958; Neumann et al. 1982). Both reversible and irreversible electroporation serve as basis for important applications in biology, medicine, food processing and biotechnology (Haberl et al. 2013). The best-known applications of reversible electroporation are electrochemotherapy (Sersa et al. 2012; Miklavčič et al. 2014), gene electrotransfection (C. Heller and Heller 2010), transdermal drug delivery (Zorec et al. 2013), cell electrofusion (Usaj et al. 2010) and insertions of proteins into membranes (Teissié 1998). Irreversible electroporation is used for food processing (Toepfl et al. 2007), tissue ablation (Al-Sakere et al. 2007; Rubinsky 2007) and water cleaning (Gusbeth et al. 2009).

Although electroporation is widely used, the principle of pore formation in biological membranes is still not fully elucidated. Therefore the research of electroporation goes in all directions, using experiments and modeling. Experiments are done on tissues, cells and membranes and are combined with modeling on different scales. This kind of research can provide a deeper understanding of electroporation phenomena (Kotnik et al. 2012). Modeling is also used to predict when the experiments or treatment by electroporation will be sufficient. Different modeling techniques are used: finite differential, finite element, molecular dynamics and quantum mechanics. First two techniques are used to simulate big models like tissue, cells and liposomes (Pavšelj and Miklavčič 2008; Corovic et al. 2013; Rems and Miklavčič 2014). Last two techniques are used to model liposomes and membranes at the molecular level. This kind of modeling is important, due to the fact that in experiments the processes in membranes at molecular level cannot be observed (Vries et al. 2003; Tarek 2005).

Synthetic liposomes are the simplest model of biological cell. They mimic the geometry of biological cell membrane but without the inner structures (Tekle et al. 2001). They can also be used as a drug delivery system. Drug can then be released from liposomes to selected intracellular target areas (Immordino et al. 2006; Elbayoumi and Torchilin 2010). Electroporation could be one of the methods for releasing the drug from synthetic liposomes (Napotnik et al. 2010). Electroporation of synthetic liposomes depends on the structure of the membrane and applied electric field (Portet et al. 2009). To study the drug release from liposomes, the structure of membrane and its behavior when exposed to

electric field has to be known. The planar lipid bilayer formed between two liquid solutions mimics a small fraction of liposome membrane which is however accessible from both sides; therefore the experiments are simpler compared to experiments on synthetic liposomes (Mueller et al. 1963; Huang et al. 1964; Benz et al. 1975; Ottova and Tien 2002).

1.1 Cell membrane

All living cells have a barrier, which separates the interior from the outside environment. The cells are divided into prokaryotes and eukaryotes. Not long ago archaea was classified as a new domain (Pace 2006). Prokaryotes are organisms without membrane bound nucleus or any other inner organelles. The cell membrane is strengthened by cell wall and capsule. Eukaryotes are cells with membrane bounded nucleus and other inner organelles. They do not have capsule over the cell membrane; however the plant eukaryotes have a cell wall. The cell membrane consists of lipids, proteins, carbohydrates and cytoskeleton. The basic structure of the membrane is a bilayer formed by lipids. The lipid head groups are forming two parallel layers. In between these two layers the acyl chains face each other. In the lipid bilayer, the proteins are inserted. The integral proteins are proteins which are permanently integrated into the membrane. Integral polytypic proteins span across the membrane (transmembrane proteins), on the other hand integral monotopic proteins are attached only to one of the membrane sides. Peripheral proteins are attached to the membrane temporally. Structures in the membrane are very dynamic. They move in lateral direction as well as in transverse direction.

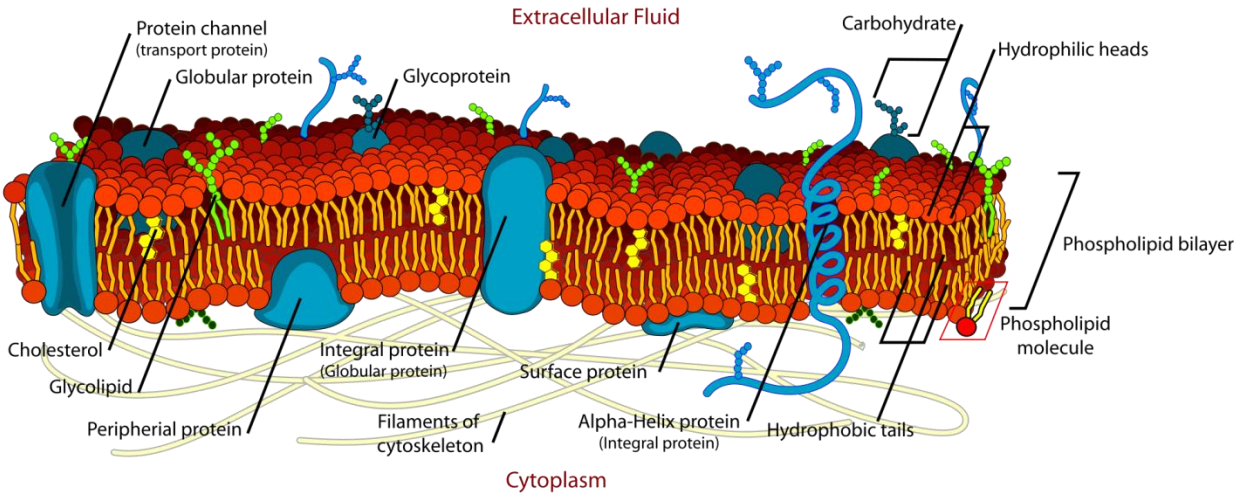

Figure 1: The structure of the cell membrane (Ruiz 2007).

1.2 Lipid bilayers

Lipid bilayer is the main structure of the plasma membrane. The bilayer is composed of two monolayers, which face each other by acyl chains. The bilayers' composition depends on the cell

species, temperature, pH ... Moreover, the membranes' inner leaflet differs in composition from the outer leaflet (Luckey 2008).

The complex lipids found in the membranes of prokaryotes and eukaryotes are glycerophospholipids, galactolipids, sphingolipids, and sterols. In membranes of archaea, special lipids can be found. Glycerophospholipids are composed of glycerol molecule, which is bonded to the phosphate. The fatty acyl chains are linked to carbon 1 and 2 with ester linkages. Several different moieties, such as phosphatydilcholine (PC), phosphatidylethanolamine (PE), phosphatidlyserine (PS), phosphatidylglcerol (PG), and phosphatidylinositol (PI) can also be phosphate bonded. The head groups and the phosphate form the hydrophilic part of the molecule and acyl chains are the hydrophobic part of molecule, also called polar and non-polar parts of molecule, respectively. This kind of molecule structure is called amphiphilic molecule. The acyl chains can be saturated or unsaturated. The polar head groups have negative charge (PS, PI, PG) or are zwitterionic (PE, PC) at physiological pH. The galactolipids are the type of glycolipids with galactose as a sugar group. Sphingosine is the main component of sphingolipids. A fatty acid phosphocoline, phosphoethanolamine head group and sugars or oligosaccharides are linked to the sphingosine. Sterols are molecules composed of five-carbon units called isoprene.

Archaeal lipids are special. They enable archaea to live in harsh environmental conditions. Archaea can be grouped based on the extreme environmental conditions into halophiles, which grow in high salt concentrations, acidophiles which grown at low pH, alcalophiles which grown at high pH, thermophiles which grow at high temperatures, psychrophilic which grow at low temperatures and many others (Benvegnu et al. 2004; Ulrih et al. 2007; Ulrih et al. 2009). The archaea membrane cells face the extreme outer environment and represent the first line of defense towards external factors. Therefore archaeal lipids which form these membranes need to have special moieties to increase their stability. In general they are composed of glycerophosphate head groups, ether linkages between glycerol moiety and hydrocarbon tails, methyl branching of hydrocarbon chains or hydrocarbon chains with cyclopentane rings. They are sometimes rather bipolar lipids with tetraether core and head group composed of carbohydrates (Ulrih et al. 2009).

Due to amphiphilic nature of lipids, they can form a diversity of structures. A typical lipid molecule has a hydrophilic head group and hydrophobic tails. In contrast to the polar part the hydrophobic tails do not have significant electrostatic interactions with water. In water media, the lipids assemble to form structures in which lipid tails face each other and lipid heads are faced to the water. Typical structures formed by lipids depend on the shape of the monomer (lipid) (Figure 2). The monomers can have the shape of a cylinder, cone or a wedge. When the monomers aggregate, they form bilayer, micelle or inverted micelle. Larger structures are called phases and are divided into lamerallar, hexagonal I and hexagonal II (Luckey 2008).

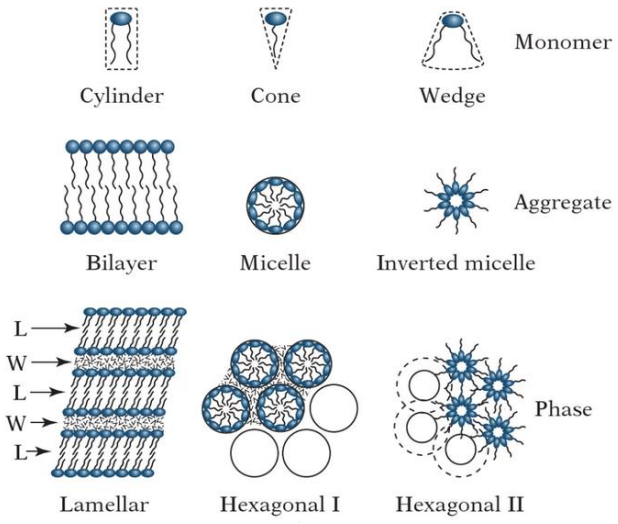

Figure 2: The amphiphile structures of lipids (Luckey 2008).

Organization of the lipids in the planar lipid bilayers depends on the temperature. In the bilayer, the lipids diffuse in lateral as well as in transverse direction. The dynamics of this motion depends on the structure and the temperature. The lipid bilayer structure exists in gel or liquid-crystalline phase. The phase is defined by the mobility of lipid molecules which changes with temperature. Mobility of the lipid molecules increases with temperature, resulting in the lipid bilayer being in the liquid-crystalline phase. Mobility of the lipid molecules decreases with a decrease in temperature; consequently the bilayer is in the gel phase. At a given temperature a lipid bilayer can exist in either liquid or gel phase. Also the thickness, capacitance and conductance of lipid bilayer change with the phase transition (Gutberlet and Katsaras 2001; Basu et al. 2001; Tokumasu et al. 2002; Luckey 2008). Figure 3 shows lipid phase transitions of the DPPC lipid bilayer. The main transition of this lipid bilayer is at 42 °C, but it also has a sub transition at lower temperature.

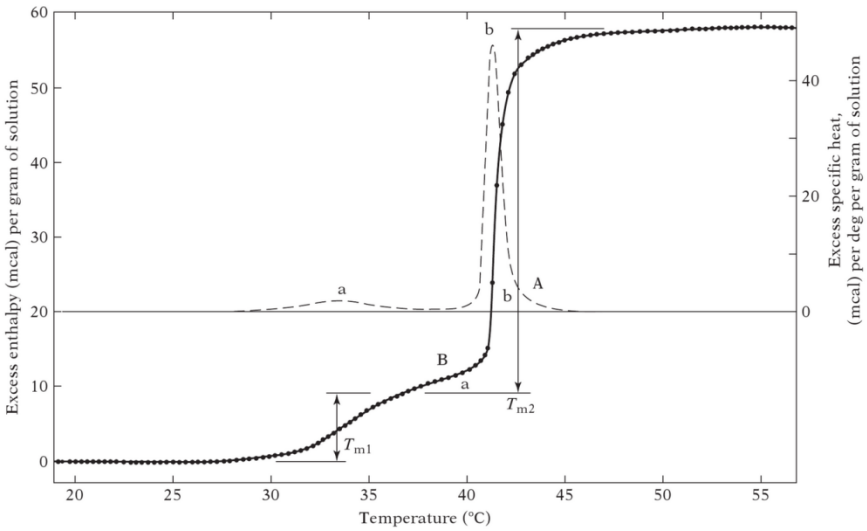

Figure 3: Differential scanning calorimetry of an aqueous dispersion of DPPC. The excess enthalpy (heat taken up) of the sample compared with a reference is measured as the temperature is raised. DPPC exhibits two phase transitions. The first is a pretransition called T_{m1}, which produce the ripple phase P_β followed by the transition T_{m2} to L_α (Luckey 2008)**.**

1.3 Planar lipid bilayers

Planar lipid bilayers are bilayers composed of two monolayers. They can be formed on the boundary between two different media (combination of bilayer and liquid, gel, substrate, air …) (Tien and Ottova 2003). Since cell membrane is surrounded with liquid solutions from both sides, the present research focused only on the bilayers formed between two liquid solutions.

1.3.1 Formation of planar lipid bilayers

The planar lipid bilayers' formation techniques between two liquid solutions have been developed throughout many decades: the painting method (Mueller et al. 1963), the folding method (Montal and Mueller 1972), the tip-dip method (Coronado and Latorre 1983), the double-well chip method (Funakoshi et al. 2006) and the cross- channel chip method (Funakoshi et al. 2006). Properties of the bilayers formed by these methods vary with the solvent preparation methods. DPPC lipid bilayers dissolved in *n*-decane/chloroform/methanol have lower specific capacitance compared to those dissolved in *n*-decane-dioxan (Antonov et al. 1990).

Painting method was the first method for planar lipid bilayers' formation between two liquids. It was proposed by Mueller and coworkers in 1963. The planar lipid bilayer is formed on a small aperture (1 mm), which connects two liquid reservoirs. Both reservoirs are filled with salt solution. A cluster of lipid molecules is added to the aperture. Lipid molecules slowly spread across the aperture and the rest of the lipids flow to the water solution surface (Mueller et al. 1963) (Figure 4). Formation of the planar lipid bilayers takes several minutes on average.

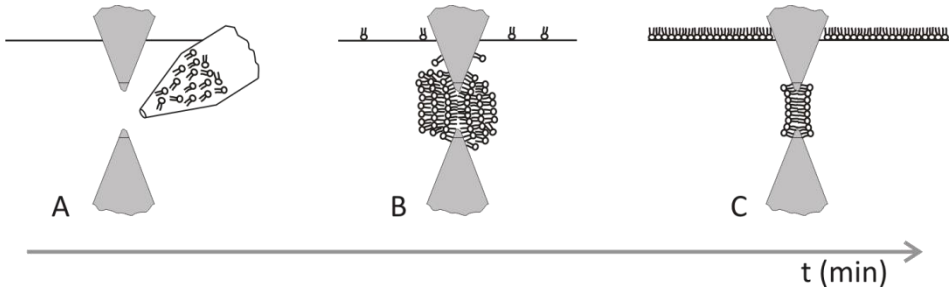

Figure 4: Painting method. A) Aperture and tip filled with lipid solution. B) Cluster of lipids on aperture. C) Planar lipid bilayer is formed.

For the folding method a similar chamber as for the paining method was used. At the folding method the aperture size is around 100 μm and made in thin Teflon sheet (25 μm), which is inserted between the two reservoirs. At the beginning, the salt solutions in both reservoirs are below the connecting aperture. Lipid molecules are spread on both surfaces of the solution. In the next step, both levels are raised above the connecting aperture. When levels reach and cross the connecting aperture, the planar lipid bilayer is formed (Montal and Mueller 1972) (Figure 5). The planar lipid bilayer is formed in a few seconds.

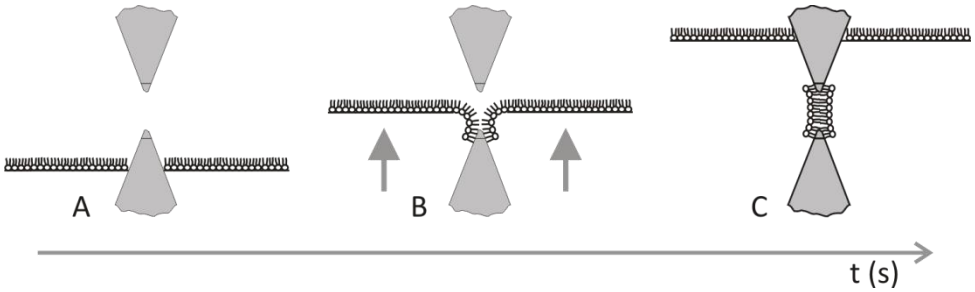

Figure 5: Folding method. A) The lipid monolayers on the surface of liquid solution below the aperture. B) The surfaces of liquid solutions are crossing the aperture and forming planar lipid bilayer. C) Planar lipid bilayer is formed.

Tip-dip method is a quick method to form planar lipid bilayers (Coronado and Latorre 1983). The chamber is filled with water solution. A lipid monolayer is on the surface of the water solution. The tip is first dipped into the water solution, and then pulled out. When the tip is pulled out, the lipid monolayer is formed at the top of the tip. Then the tip is dipped into the water solution again. This time the lipid bilayer is formed at the pick of the tip, (Figure 6). By this method, the planar lipid bilayer is formed in a few seconds.

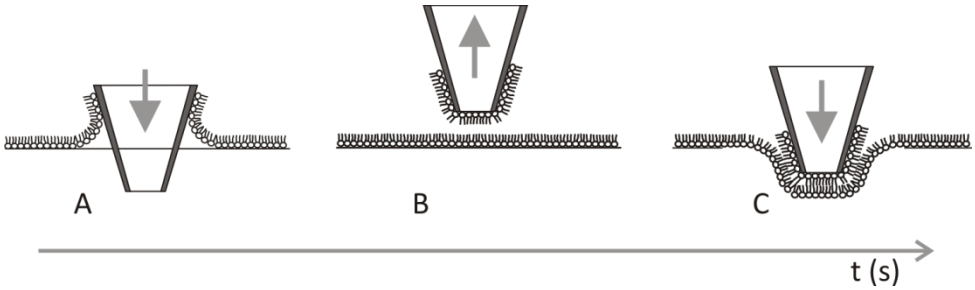

Figure 6: Tip-dip method. A) The tip is in the liquid solution. B) The tip is pulled out of the liquid solution. C) The tip is pushed back in the solution.

The double-well chip method uses simple fluidic control (Figure 7). The chamber contains two wells filled with lipid solution. As the water droplet is injected into each well, a lipid monolayer is formed at the interface between water and lipid solution. When two water droplets are driven together, the two interfaces (lipid monolayers) come together and form a bilayer (Funakoshi et al. 2006). The planar lipid bilayer is formed in a few minutes.

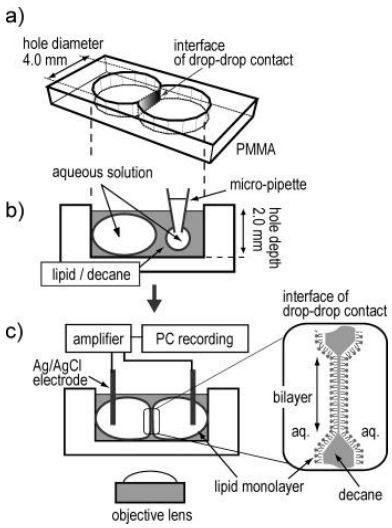

Figure 7: a) Overview of the double well chip, consisting of two wells connected. b) Procedure of the bilayer formation. Two droplets are injected in each well filled with lipid solution, forming a water/lipid solution/water interface at the section. c) Schematic diagram of the experimental setup. Electrodes are inserted in each droplet, and membrane current is measured using a patch clamp amplifier. (Funakoshi et al. 2006).

The cross-channel chip method also uses simple fluidic control. The chip has two inlet channels for water, one inlet channel for lipid solution and one outlet channel. First the lipid solution fills the junction of the channels, which is followed by the lipid monolayer formation at the interface between lipid solution and water, located at the water channels. In the next step the channel junction is filled with water through water channels, until two lipid monolayers face each other and form a bilayer (Funakoshi et al. 2006) (Figure 8). The planar lipid bilayer is formed in a few seconds.

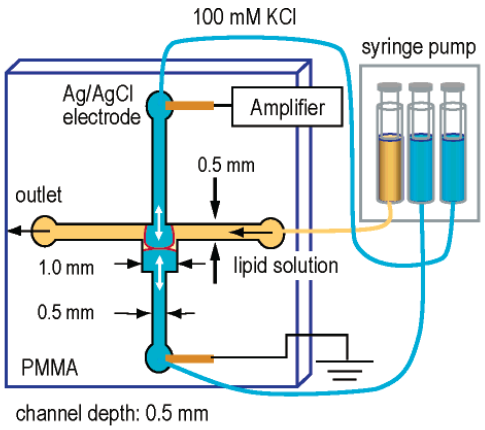

Figure 8: Schematic of the cross-channel chip. Two aqueous solutions with lipid solution in between make contact at the cross section to form a lipid bilayer (Funakoshi et al. 2006).

1.3.2 Electrical properties of planar lipid bilayer

From the electrical point of view, a planar lipid bilayer can be presented as capacitor and resistor in a parallel configuration. The capacitance of the lipid bilayer is 0.5–1.0 μF/cm^2. The resistance of planar lipid bilayer is very high since the hydrophobic core is impermeable to any charged atoms and molecules (Kramar et al. 2010). When strong electrical field is applied to the planar lipid membrane, it can change organization of molecules in the membrane and consequently lower the resistance of the planar lipid bilayer. When the electroporation is under consideration, voltage and current breakdown are the most important parameters. At high voltage and current breakdown values the planar lipid bilayers drastically change resistance and brake.

Many methods for measuring the capacitance of the planar lipid bilayers are known: a discharge method (Benz and Janko 1976; Benz et al. 1979; Chanturiya 1990; Sharma et al. 1996; Diederich et al. 1998; Meier et al. 2000a; Vargas et al. 2000; Kramar et al. 2007; Kramar et al. 2009), a capacitance to period conversion method (Kalinowski and Figaszewski 1995a), a capacitance to voltage conversion method, using bridges (Rosen and Sutton 1968; White 1970; Wobschall 1971; Darold 1972) and a method using LCR meter (Punnamaraju and Steckl 2010). The capacitance of the planar lipid bilayers also provides the information whether a planar lipid bilayer was properly formed. It is the indicator whether truly a bilayer rather than only a multilayer was formed. That explains why the capacitance is always measured before each experiment on any planar lipid bilayer.

The discharge method is the most common and simplest method for measuring the capacitance. First the planar lipid bilayer is charged by applied rectangular pulse of short duration 10–100 μs and amplitude up to 300 mV, not to overcome the planar lipid bilayer voltage breakdown. At the end of the pulse, the charge accumulated on planar lipid bilayer is discharged through resistor of known resistance. The shape of planar lipid bilayer discharge has an exponential decay shape whereas time constant is defined by capacitance and resistance of the measured system. Therefore the planar lipid

bilayer capacitance is obtained from discharge values of measured capacitance with and without planar lipid bilayer (Benz and Janko 1976; Sharma et al. 1996; Troiano et al. 1998; Diederich et al. 1998; Meier et al. 2000b; Vargas et al. 2000; Kramar et al. 2007; Kramar et al. 2009).

A capacitance to period conversion method is a continuous measurement method and it also enables capacitance measurement as a function of DC voltage across the planar lipid bilayer. The planar lipid bilayer is charged by a constant current. In the first step, the transmembrane voltage linearly increases to the certain threshold, at which the electronic circuit changes the direction of the current. Consequently the transmembrane voltage linearly decreases to a certain threshold, at which current changes the direction again. The frequency of the voltage and current signal is proportional to the measured capacitance of planar lipid bilayer (Kalinowski and Figaszewski 1995a).

The planar lipid bilayers' resistance and voltage breakdown are commonly measured using voltage-clamp method and current-clamp method. The voltage-clamp method applies voltage signal to the planar lipid bilayer and measures current response (Hanai et al. 1964; Rosen and Sutton 1968; White 1970; Wobschall 1971; Montal and Mueller 1972; Benz and Janko 1976; Benz et al. 1979; Yamaguchi and Nakanishi 1993a; Yamaguchi and Nakanishi 1993b; Kalinowski et al. 1998; Troiano et al. 1998; Hanyu et al. 1998; Weaver 2003). The current-clamp method applies current signal to the planar lipid bilayer and measures voltage response (Darold 1972; Robello and Gliozzi 1989; Kalinowski and Figaszewski 1995a; Kalinowski and Figaszewski 1995b; Koronkiewicz et al. 2002). The planar lipid bilayer's resistance is calculated from the voltage and current characteristics using Ohm's law or different bridges. The measuring systems use alternating signals or other arbitrary signals.

1.4 Molecular dynamics simulations

Molecular dynamics simulation is a computer simulation of a small system composed of atoms and molecules. The atoms are presented as points in the space. Atoms can be bounded to form a molecule. The atoms are moving in space and their positions are calculated by Newton's equation of motion:

$$m_i \frac{d^2\mathbf{r}_i}{dt^2} = \mathbf{F}_i = -\nabla_{\mathbf{r}_i} V(\mathbf{r}_i,...,\mathbf{r}_N), \tag{1}$$

where m_i and $\mathbf{r}_i$ are the mass and the position of particle i, respectively. $\mathbf{F}_i$ is the force and $V(\mathbf{r}_i,\ldots,\mathbf{r}_N)$ is the potential energy function of the system. The atoms' motion in the system is discrete; therefore the future positions of atoms are calculated from current position. The potential function is the sum of energies of non-bonded and bonded interactions:

$$\begin{aligned} V(\mathbf{r}_i,...,\mathbf{r}_N) = &\sum_{i<j} V_{Coulomb}(\mathbf{r}_{ij}) + \sum_{i<j} V_{Lennard-Jones}(\mathbf{r}_{ij}) + \sum_{Bonds} V_{Bond}(\mathbf{r}_{ij}) \\ &+ \sum_{Angles} V_{Angle}(\theta_{ijk}) + \sum_{Dihedrals} V_{Dihedrals}(\phi_{ijkl}) \end{aligned}, \tag{2}$$

The non-bonded interactions are divided into Coulomb interactions and Lennard-Jones interaction. The Coulomb potential is:

$$V_{Coulomb}(\mathbf{r}_{ij}) = \frac{q_i q_j}{4\pi\varepsilon\varepsilon_0 |\mathbf{r}_{ij}|}, \tag{3}$$

where q_i is the charge of an atom i, and ε and ε_0 are the relative dielectric constant and the dielectric constant of vacuum, respectively. The second function is Lennard-Jones potential:

$$V_{Lennard-Jones}(\mathbf{r}_{ij}) = \frac{A_{ij}}{\mathbf{r}_{ij}^{12}} - \frac{B_{ij}}{\mathbf{r}_{ij}^{6}}, \tag{4}$$

where A_{ij} and B_{ij} are constants which depend on the pair of atoms interacting with each other.

The bonded interactions are then divided into bonds, angle and dihedral interactions. These interactions are described with potential energy functions. The bond between two atoms is described by:

$$V_{Bond}(\mathbf{r}_{ij}) = \frac{1}{2} k_{ij}^{b} \left(r_{ij} - b_{ij}^{0}\right)^2 \quad , \tag{5}$$

where k_{ij}^{b} and b_{ij}^{0} describing the stiffness and the length of the bond between atom i and atom j.

The relation between two bonds is described by the angle potential:

$$V_{Angle}(\theta_{ijk}) = \frac{1}{2} k_{ijk}^{\theta} \left(\theta_{ijk} - \theta_{ijk}^{0}\right)^2 \quad , \tag{6}$$

where k_{ijk}^{θ} and θ_{ijk}^{0} depend on the bonds among three atoms. The torsional interaction among three atoms is described by dihedral potential function:

$$V_{Dihedrals}(\phi_{ijkl}) = k_{ijkl}^{\phi} \left(1 + \cos(n\phi_{ijkl} - \theta_{ijkl}^{0})\right) \quad , \tag{7}$$

where k_{ijkl}, Φ_{ijkl}^{0} and n depend on the atoms connected with these three bonds.

The parameters in potential energy function are gathered in the force fields. Nowadays we have different force fields like CHARMM (Brooks et al. 2009), AMBER (Salomon-Ferrer et al. 2013), GROMACS (Hess et al. 2008) and MARTINI (Marrink et al. 2007), which are used in different simulating programs to calculate the trajectories in parallel, *eg.* NAMD2 (Kalé et al. 1999; Phillips et al. 2005), GROMACS (Hess et al. 2008), AMBER (Salomon-Ferrer et al. 2013) and GROMACS (Hess et al. 2008).

The molecules in force fields can be described by all atom, united atoms or coarse grained models. At all atom models, each atom has its own parameters. At united atoms, the hydrogens are described together with aliphatic carbons. At coarse grained model, the group of atoms is described as one unit.

The molecular dynamics simulations are, due to high computational costs, used to simulate small systems. Using periodic boundary conditions, a small system is an imitation of a big system far from the edge of the big system (Figure 9). The elements in the system can move in and out from the unit cell. If they cross the boundary of the unit cell, they can return on the other side of it.

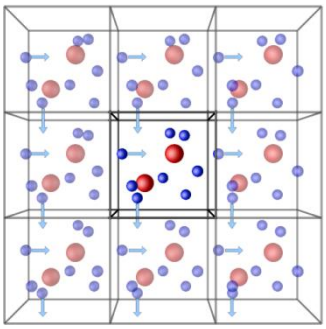

Figure 9: Scheme of periodic boundary conditions.

Molecular dynamics is used to simulate small systems at molecular level. Biological membranes' simulations were one of the fields of the present study. Biological membranes have very complex structure and are consisted of a large number of molecules. Due to high computation costs of molecular dynamics simulations, the simulations are done on a small patch of the membrane. This patch can contain lipids, proteins and other molecules. One of the interesting areas of research is the lipid bilayers' stability which is related to structural defects in the bilayer structure. Water pore structural defect was first observed at the lipid bilayer formation. When lipid and water molecules are randomly distributed in the simulation cell, they self-assemble into a bilayer due to affinity of the lipid molecules (Marrink et al. 2001). The water pores can be induced by tension, shock waves, surface active molecules, peptides, cationic polymers, lipid peroxsidation or electric field (Gurtovenko et al. 2010). The electric field can be applied to the lipid bilayer by attaching a force $q_i\mathbf{E}$ to each charged particle i in the system (Figure 10A) (Tieleman 2004). Another method is to induce electric filed across the membrane through a transmembrane ionic charge imbalance. To avoid the effect of periodic boundary conditions, two parallel lipid bilayers need to be simulated. They can independently control the ionic composition of water regions on both sides of the membrane (Figure 10B) (Sachs et al. 2004). Due to high computation costs of two bilayers simulation, Delemotte et al. have proposed a model of lipid bilayer with two water slabs, which are separated by vacuum slab. In these simulations the simulation cell needs to have a constant volume (Figure 10C) (Delemotte et al. 2008). Herrera and Pantano have proposed another method where the constant pressure is set and the restrictions for ions are defined. The ions can only be in the region close to the membrane interface and the charge

imbalance across the lipid bilayer is maintained (Herrera and Pantano 2009). Vernier et al. have shown that applications of electric field using force (Tieleman 2004) and charge imbalance method (Sachs et al. 2004) are comparable. There is no significant difference between these two methods (Vernier et al. 2006).

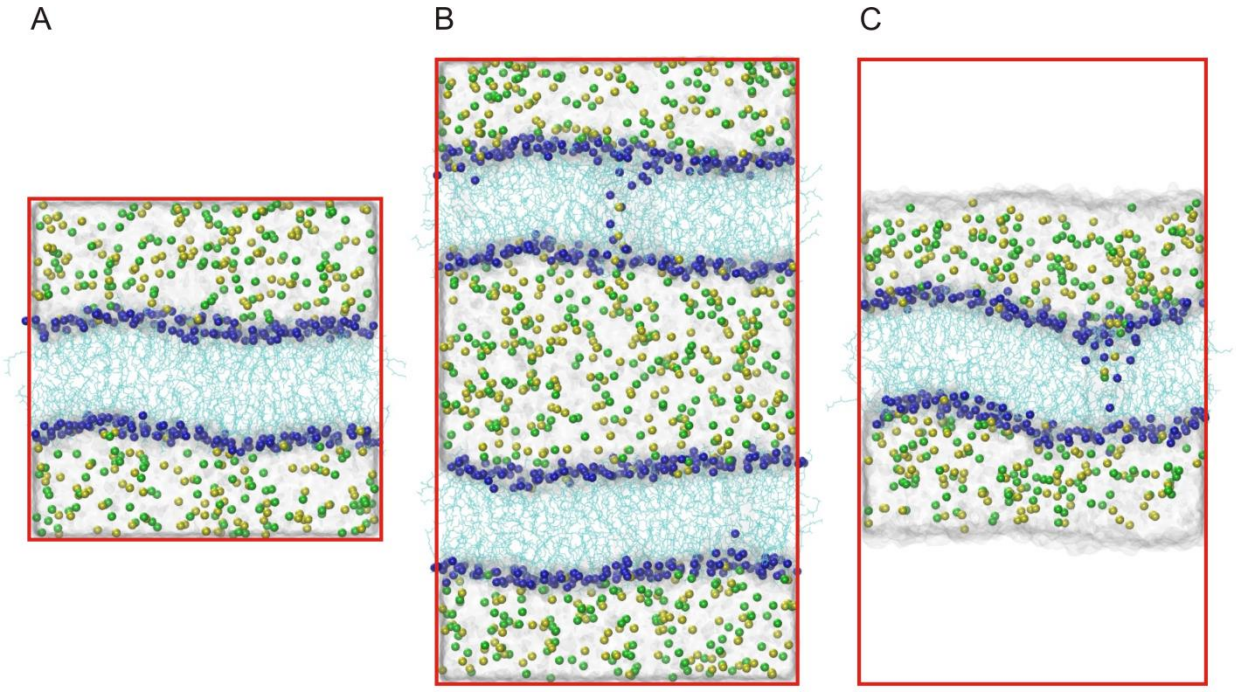

Figure 10: The MD electroporation methods: A) Method with applied electric field (to each charged atom the force q_iE is applied); B) Sach method (the charge imbalance across two lipid bilayers); C) Delemotte method (the charge imbalance method with vacuum slab) (blue – phosphorous atom, yellow – potassium ion, green – chloride ion, gray surface – water, cyan – lipid tails, red rectangle is the unit cell).

2 Aims of the thesis

The first aim of the doctoral thesis was to develop a system for measuring planar lipid bilayers' properties. The system is designed for a wide range of experiments, i.e. measuring properties using arbitrary shaped signals at different temperatures. Therefore a system which uses voltage and current-clamp method was developed, which enables the temperature of the planar lipid bilayers to be regulated between 15 and 55 °C.

The second aim was to measure the planar lipid bilayers' properties using the system developed for measuring these properties. We focused on capacitance and voltage breakdown measurements, since these two properties are the most important and can be directly related to the calculated values arising from molecular dynamics simulations.

The third aim was to study electroporation process using molecular dynamics simulations and correlate calculations results to experimentally measured values. Lipids which compose archaea *Aeropyrum pernix* membranes were studied. These lipids have very complex structure and were so far not described in any of the molecular dynamics force fields. Therefore, the effects of moieties on the electroporation were studied and later the models of archaeal lipids AI and AGI were built. The goal was also to research high stability of these bilayers, for this purpose a detailed analysis of their static and dynamics properties was performed.

The fourth aim was to obtain knowledge on how to construct lipid bilayers with certain chosen electrical properties. The study of archaeal lipids was extended to mixtures of archaeal lipids with DPPC lipids. Also a study on how $C_{12}E_8$ surfactant decreases the electroporation threshold of POPC bilayers was performed.

3 Research papers

The research papers are printed in chronological order. The first paper presents the hardware development for measuring planar lipid bilayers' properties. The other papers are molecular dynamics studies of bilayers with experimental result to support simulations.

In the first paper entitled **System for measuring planar lipid bilayer properties** the newly developed system for measuring planar lipid bilayers properties is described (Polak et al. 2012). The system is composed of a control unit, an output stage, an LCR meter, pumps for filling reservoirs, a bath with temperature regulation and a measurement chamber with four electrodes. The electrodes are connected to the Teflon chambers, where planar lipid bilayers are formed by painting or folding method. The system was evaluated by measuring the properties of lecithin and results were in good agreement with the results available in the literature.

The second paper entitled **On the electroporation thresholds of lipid bilayers: Molecular dynamics simulation investigations** is focused on the role of branched lipid tail, ester and ether linkages to the electrical stability of bilayers (Polak et al. 2013). This was a study in which the DPPC, DPhPC-ester and DPhPC-ether bilayers were simulated using molecular dynamics. The bilayers were first equilibrated. The properties of equilibrated bilayers were in agreement with those available in the literature. Also the values of the membrane dipole potential were in good agreement with the experimentally obtained results. The equilibrated bilayers were then exposed to charge imbalance. It was established that the addition of methyl groups to the lipid tails increases the electroporation threshold. In addition, changing the ester with the ether linkages was established to increase electroporation threshold even further.

The third paper entitled **Electroporation of Archaeal Lipid Membranes using MD Simulations** describes archaeal lipids' electroporation (Polak et al. 2014). Molecular dynamics models of lipids which compose the archaea *Aeropyrum pernix* membrane were built. The bilayers were composed of these lipids and mixed with DPPC in the same molar ratio. The electron density profiles of equilibrated membrane were compared to experimentally measured electron density profiles, using SAXS and good agreement among the compared values was obtained. The bilayers were then exposed to charge imbalance. It has been established that archaeal lipids have extremely high electroporation threshold and that it is a function of temperature. It has also been confirmed that the electroporation threshold can be changed (i.e. lowered) by adding DPPC lipids into the bilayer. A specific pore formation has been observed.

The forth paper entitled **Structural Properties of Archaeal Lipid Bilayers: Small-Angle X-Ray Scattering and Molecular Dynamics Simulation Study** is an extended study of the third paper. The

focus of the research was on the structure of pure archaeal lipids. Distributions, orientation, reorientation and diffusion of the bilayers were measured. The archaeal bilayers are thicker than other PC-lipids, due to long lipid tails. The head group moieties are large and interact with each other through hydrogen bond formation to form small clusters. The dynamics of moiety orientation in the lipid head group depends on the temperature. The diffusion of archaeal lipids is strongly related to temperature and is much lower compared to that of DPPC lipids.

In the fifth paper entitled **Polyoxyethylene glycol ($C_{12}E_8$) decreases the electroporation threshold of POPC lipid bilayers** the phenomenon of lowering electroporation threshold by adding surfactant $C_{12}E_8$ has been investigated. It has been experimentally observed that incorporation of $C_{12}E_8$ into the planar lipid bilayer lowers the electroporation threshold by 22%. A molecular dynamics simulation confirmed lowering of the electroporation threshold by $C_{12}E_8$ molecules incorporation into POPC bilayer. Also a specific pore formation was observed. Namely, first the $C_{12}E_8$ molecules move into the hydrophobic region and form hydrophilic structure. In the next stage the water and ions penetrate through this hydrophilic structure.

Paper 1

Title: System for measuring planar lipid bilayer properties

Authors: Polak A, Mulej B, Kramar P

Publication: The Journal of Membrane Biology

DOI: 10.1007/s00232-012-9476-9

Year: 2012

Volume: 245

Issue: 10

Pages: 625-632

J Membrane Biol (2012) 245:625–632
DOI 10.1007/s00232-012-9476-9

System for Measuring Planar Lipid Bilayer Properties

Andraž Polak · Boštjan Mulej · Peter Kramar

Received: 20 December 2011 / Accepted: 30 June 2012 / Published online: 19 July 2012

Abstract We present a system for measuring planar lipid bilayer properties. The system is composed of a control unit, an output stage, an LCR meter, pumps for filling reservoirs, a bath with temperature regulation and a measurement chamber with four electrodes. The planar lipid bilayer is automatically formed using a folding method on apertures of different sizes. The automatization is assured by two syringes, which are clamped in actuators. Actuators are driven and controlled by a control unit via RS-232 communication. The temperature of the planar lipid bilayer can be regulated between 15 and 55 °C. The regulation is assured by insertion of the measurement chamber into the temperature-regulated bath. Different shapes of voltage- or current-clamp signals can be applied to the planar lipid bilayer. By measuring the response of the planar lipid bilayer to the applied signal, the capacitance and breakdown voltage of the planar lipid bilayer can be determined. The cutoff frequencies of the system output stage for voltage- and current-clamp methods are 11 and 17 kHz, respectively.

Keywords Electroporation · Capacitance · Breakdown voltage · Temperature regulation

Introduction

Electroporation is a phenomenon that describes the occurrence of structural changes in biological membranes as a consequence of applied electric pulses (Chen et al. 2006; Kotnik et al. 1997; Weaver and Chizmadzhev 1996). These structural changes are most often named "pores" and present an increase in cell membrane permeability. Electroporation is nowadays used in different fields like biology, medicine and biotechnology. Electroporation is divided into two different fields: irreversible electroporation and reversible electroporation. In irreversible electroporation, the cell membrane does not reseal pores after applied voltage and the cell dies. Irreversible electroporation is used in food production and preservation (Golberg et al. 2010), water cleaning (Vernhes et al. 2002) and tissue ablation (Davalos et al. 2005; Maor et al. 2009). In reversible electroporation, the cell membrane pores are resealed after application of electric pulses. It can be used to introduce substances into the cell. The best-known applications of reversible electroporation are electrochemotherapy (Sersa et al. 2008), transdermal drug delivery (Denet et al. 2004; Prausnitz 1999), gene therapy (Daud et al. 2008), cell fusion (Mekid and Mir 2000; Ogura et al. 1994) and insertion of proteins into membranes (Ouagari et al. 1995; Teissié 1998). The principles of pore formation are not yet fully elucidated. Recently, studies based on molecular dynamics proved that pores are formed in a lipid bilayer (Tieleman et al. 2003). When a lipid bilayer is exposed to an electric field, water wires are formed across the membrane. Then, the water wires expand into the water-filled pores, which are stabilized by reorganization of lipid molecules in the lipid bilayer (Levine and Vernier 2010). It is believed that the general picture of electroporation is the same for the planar lipid bilayer and biological cell membrane (Tarek 2005). Therefore, the lipid bilayer is considered the most important part of the cell membrane for studying pore formation.

Synthetic liposomes and vesicles are the simplest model of the biological cell membrane. They mimic the geometry of the biological cell membrane, but they do not have inner

A. Polak (✉) · B. Mulej · P. Kramar
Faculty of Electrical Engineering, University of Ljubljana, Tržaška 25, 1000 Ljubljana, Slovenia
e-mail: andraz.polak@fe.uni-lj.si

P. Kramar
e-mail: peter.kramar@fe.uni-lj.si

structures (Tekle et al. 2001). In comparison to synthetic liposomes and vesicles, planar lipid bilayers can have trapped solvent between the two bilayer leaflets. These can lead to differences in measured electrical properties and influences on pore formation in the lipid bilayer (White 1974, 1978). The planar lipid bilayer formed between two liquid solutions mimics a small fraction of the cell membrane, and it is accessible from both sides; therefore, the experiments are simpler than experiments on synthetic liposomes and vesicles (Benz et al. 1975; Huang et al. 1964; Mueller et al. 1963; Ottova and Tien 2002). Moreover, due to similar geometry usually modeled in molecular dynamic simulations, the results of both research methods can be combined and compared. Electroporation on small vesicles can also be performed using the molecular dynamic simulation.

Through the years, many planar lipid bilayer formation techniques between two liquid solutions have been developed: the tip-dip method (Coronado and Latorre 1983), the double-well chip method (Funakoshi et al. 2006), the cross-channel chip method (Funakoshi et al. 2006), the painting method (Mueller et al. 1963) and the folding method (Montal and Mueller 1972). The folding method is faster than other methods and can be easily automated. In the folding method, the lipid solution is spread on the liquid solution surface at each reservoir. In a few minutes, monolayers on the liquid solution surfaces are formed. After monolayer formation, the liquid solution levels in both reservoirs are raised. When the liquid solution surfaces cross the aperture between the reservoirs, the planar lipid bilayer is formed. This method is simple and quick and formation can be automated by computer-controlled syringe pumps.

From the electrical point of view, the planar lipid bilayer is considered a capacitor and resistor in parallel configuration. The capacitance and resistance are the most frequently measured electrical properties of a planar lipid bilayer. An additional electrical property of a planar lipid bilayer is breakdown voltage. It is one of the most important properties of a lipid bilayer when electroporation is under consideration. The capacitance is also a reference that the planar lipid bilayer is formed. If the capacitance of the planar lipid bilayer is lower than the expected value, then either multiple layers are formed or the planar lipid bilayer is not formed at all. Electrical properties of planar lipid bilayers are usually measured by two types of methods: voltage clamp and current clamp (Kramar et al. 2010). In the voltage-clamp method, a voltage signal is applied to the planar lipid bilayer and current, which flows through planar lipid bilayer, is measured. In the current-clamp method, a current signal is applied to the planar lipid bilayer and the voltage across the planar lipid bilayer is measured. The two methods use different-shaped signals like pulses, linear rising signals, sinusoids or triangular signals. Planar lipid bilayer capacitance, for example, is mostly measured using a discharge method (Kramar et al. 2010), a capacitance to period conversion method (Kalinowski and Figaszewski 1995) or an LCR meter (Punnamaraju and Steckl 2010).

Lipid bilayers can exist in a gel or liquid phase. The phase is defined by the mobility of the lipid molecules, which changes with temperature. The mobility of lipid molecules is higher in the liquid phase than in the gel phase; therefore, a lipid bilayer is in liquid phase at higher temperatures and in gel phase at lower temperatures. At a given temperature, a lipid bilayer can exist in either a liquid or a gel phase. With the phase transition also the thickness of the lipid bilayer is changed (Katsaras and Gutberlet 2010; Luckey 2008; Tokumasu et al. 2002). Because the capacitance of the planar lipid bilayer is inversely proportional to its thickness, also changes of the planar lipid bilayer capacitance have been observed (Antonov et al. 2003; Boheim et al. 1980). Moreover, Basu et al. (2001) showed that the conductance of the planar lipid bilayer is temperature-dependent.

To study the phenomenon of electroporation at various temperatures and provoked by various electrical signals, we developed a new system for measuring the properties of planar lipid bilayers. In the system, the folding method for forming planar lipid bilayers is implemented. The folding method is automated by two syringes, which raise and lower liquid solution levels in the measurement chamber. The temperature in the measurement chamber can be maintained at a constant value, which can be changed during the experiment. The system can be used to determine the planar lipid bilayer capacitance and breakdown voltage. The breakdown voltage can be measured by the voltage- or current-clamp method using a broad spectrum of signal shapes.

System Architecture

The system is composed of a control unit, an output stage, an LCR meter, pumps for filling reservoirs, a bath with temperature regulation and a measurement chamber with four electrodes. The control unit consists of an embedded PC, a control circuit, a digital to analog converter and an analog to digital converter (Figs. 1, 2).

Control Unit

The control unit consists of an embedded PC, a control circuit, an analog to digital converter and a digital to analog converter. This part of the system controls all switches, actuators and generators and acquires signals from sensors.

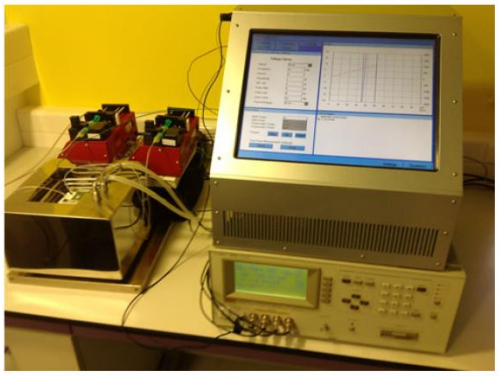

Fig. 1 The photography of the system for measuring the properties of planar lipid bilayers. On the left are two pumps for filling reservoirs and the bath with temperature regulation. The measurement chamber with four electrodes is inserted into the bath. The cables from the electrodes lead to the control unit, which is on the right. Below the control unit is the LCR meter

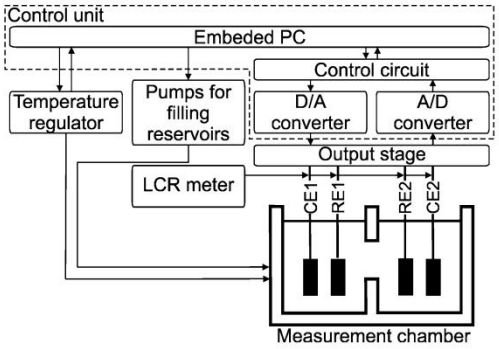

Fig. 2 The system for measuring the properties of planar lipid bilayer consists of the control unit, the LCR meter, the output stage, the pumps for filling reservoirs, the measurement chamber with four electrodes and the bath with temperature regulation. The control unit consists of the embedded PC, the control circuit, the digital to analog converter and the analog to digital converter

An embedded PC (Windows CE) is used as an interface between the human and the device. It has a graphical user interface, which allows setting of measurement method parameters and temperature. It also displays measured data and temperatures in both reservoirs and the bath. All acquired data are saved on a disc and can be accessible through Ethernet. By the press of a button, we can form planar lipid bilayers and start the measurement with the selected method.

The converters are a bridge between the analog and digital parts of the system. The digital to analog converter converts a digital signal from the control circuit to an analog signal, which is used by the output stage. The conversion is made at a frequency of 48 MHz with 14-bit resolution. It generates a bipolar signal between −2 and 2 V. These properties show that the generated signal is smooth and can contain high frequencies. The analog to digital converter converts an analog signal from the output stage to a digital signal, which is acquired by the control circuit. The conversion is made at a frequency of 150 kHz with 12-bit resolution. The analog voltage input can vary between −2 and 2 V. Both analog signals range between −2 and 2 V because the breakdown voltages of already measured planar lipid bilayers from the literature are in this range.

LCR Meter

The capacitance of a planar lipid bilayer is measured by an Agilent (Santa Clara, CA, USA) LCR meter 4284A. The LCR meter is connected directly to electrodes in the measurement chamber. The Agilent LCR meter 4284A can measure capacitance and resistance in different formations (parallel and serial). The LCR meter applies the sinus signal to the load and measures the response. We can set the parameters of the agitating sinus signal like frequency from 20 Hz to 1 MHz and the effective value from 0.005 to 2 V.

Output Stage

The output stage is a circuit, which combines the voltage- and current-clamp measuring circuits. The output stage has an input and an output that are connected to converters and four connectors for electrodes. Two of them are current electrodes (CE1 and CE2) and other two are reference electrodes (RE1 and RE2).

The voltage- and current-clamp methods that are implemented in our system are designed similarly. Both circuits have a current source and differential amplifier. The voltage-clamp method has closed-loop regulation, and the current-clamp method has open-loop regulation. The idea for the circuits was found in the literature (Kalinowski and Figaszewski 1995); our system has an additional resistor connected to the current electrodes for current source stabilization. The current source in our system generates current, which flows through an added resistor and planar lipid bilayer.

In the voltage-clamp method (Fig. 3a), the voltage is applied to the planar lipid bilayer and the current through the planar lipid bilayer and parallel resistor is measured. The differential amplifier measures the transmembrane voltage. The single-ended output of the differential amplifier is compared to the input voltage. The difference between the signals drives the current source, which forces

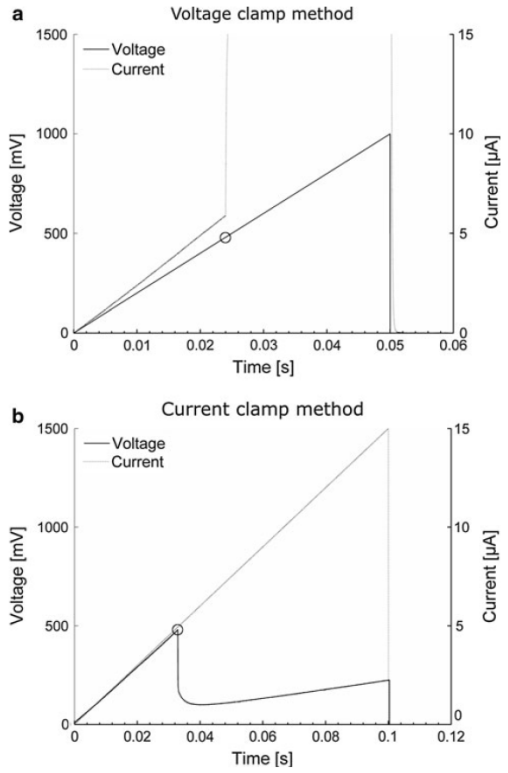

Fig. 3 The scheme of the circuit for the voltage-clamp method (**a**) and the scheme of the circuit for the current-clamp method (**b**). Both circuits consist of a differential amplifier and current source. The difference is only in the realization of the feedback loop. In the voltage-clamp method, the voltage is applied to the planar lipid bilayer and the current, which flows through the planar lipid bilayer and the resistor, is measured. In the current-clamp method, the current through the planar lipid bilayer and the resistor R_{I2} is forced and the voltage difference on the planar lipid bilayer is measured

current through the planar lipid membrane and resistor R_{I2}. The voltage at the output of the operational amplifier, which drives the current source, is proportional to the current which is forced through the planar lipid bilayer and resistor R_{I2}. The generated current is equal to the quotient between the driving voltage and resistor R_{I1}. The resistors R_{I1} and R_{I2} have a value of 100 kΩ. Capacitors C_{I1} and C_{I2} and resistor R_{I2} are added to the circuit to stabilize the current source and prevent oscillations. Capacitors C_{I1} and C_{I2} have a capacity of 33 and 100 pF, respectively.

The current-clamp method (Fig. 3b) is used to observe the transmembrane voltage response caused by forced current. The input voltage drives a current source, which forces current through the current electrodes and resistor R_{I2}. The voltage response on the planar lipid bilayer is measured by reference electrodes.

In both methods, different shapes of signals can be used, e.g., pulse, step change, linear rising signal or arbitrarily shaped signal. In the voltage-clamp method the output voltage range is between −1.5 and 1.5 V, with accuracy of 1 mV; the measured current ranges from −15 to 15 μA, with accuracy of 0.05 μA. In the current-clamp method, the output current range is between −15 and 15 μA, with accuracy 0.02 μA; the measured voltage ranges from −1.5 to 1.5 V, with accuracy 4 mV.

Pumps for Filling Reservoirs

The measurement chamber has two channels for filling reservoirs. Into each channel, a pipeline is inserted. Pipelines connect the reservoirs with the syringe filled with liquid solution. The syringes are clamped into actuators (Aladin-1000; World Precision Instruments, Sarasota, FL, USA). The Aladin-1000 is a syringe pump that can be driven via RS-232 communication. The syringe pumps are driven by an embedded PC, where we can set the volume which will be pumped into each reservoir. Each pump can be driven separately; therefore, we can avoid errors of liquid solution levels caused by asymmetry of the reservoirs. On the other hand, if asymmetric filing of the reservoirs is needed, the system allows setting this condition. Our system enables us to form planar lipid bilayers by the folding method by one press of a button.

Measurement Chamber

The measurement chamber is made of Teflon because it is highly resistant to chemicals and has a hydrophobic surface. The hydrophobic surface favors contact with lipid hydrophobic tails (Montal and Mueller 1972); therefore, the boundaries of the planar lipid bilayer can be linked to the edge of the aperture on the measurement chamber. The measurement chamber has two cubed reservoirs, which are connected with a round aperture. Each reservoir is made of a separate piece of Teflon. The round hole with a diameter of 3 mm connects the two reservoirs. Between the two reservoirs is a 25.40 μm-thin Teflon sheet with a round aperture of different sizes. The aperture is placed in the center of the connecting hole between the two reservoirs. The measurement chamber has two channels to each reservoir (Fig. 4a). In one channel the temperature probe is inserted, and in the other channel the pipe for filling the reservoir is inserted. The pipes are connected to the pumps, which fill or empty reservoirs.

Four electrodes made from Ag–AgCl (E255; IVM, Healdsburg, CA, USA) are inserted into the measurement chamber as shown in Fig. 4b. Two are current electrodes

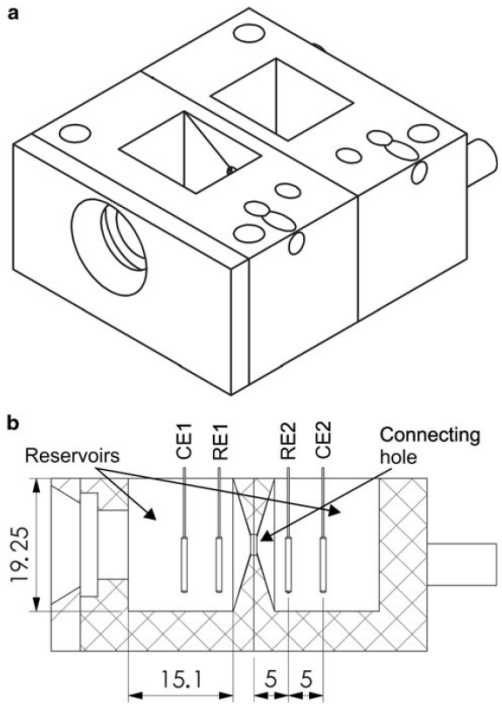

Fig. 4 The measurement chamber for formation of the planar lipid bilayer by the folding method. Perspective view reveals the construction of the measurement chamber (**a**). The Teflon sheet with aperture is inserted between the reservoirs. Lateral cut of the measurement chamber (**b**) reveals details and dimensions of the measurement chamber. *CE1*, *RE1*, *RE2* and *CE2* are Ag–AgCl electrodes. Chamber dimensions and electrode positions are in millimeters. The dimension of the reservoir perpendicular to the sketch is 17.8 mm. The hole, which connects the reservoirs, has a diameter of 3 mm

(CE1 and CE2), and the other two are reference electrodes (RE1 and RE2).

Temperature Regulation

The temperature of a planar lipid bilayer is ensured by a temperature-regulated bath. The bath is constructed of stainless steel. The inside dimensions of the bath are 150 × 150 × 100 mm. The bath is surrounded with 40-mm-thick insulation, and the bath cover has 20 mm of insulation. The coil, which is inserted into the bath, is used to heat or cool the medium and air in the bath. Through the coil flows medium with precisely regulated temperature. Regulation of the medium temperature is made by a Solid State (Wappingers Falls, NY, USA) ThermoCube 300. This

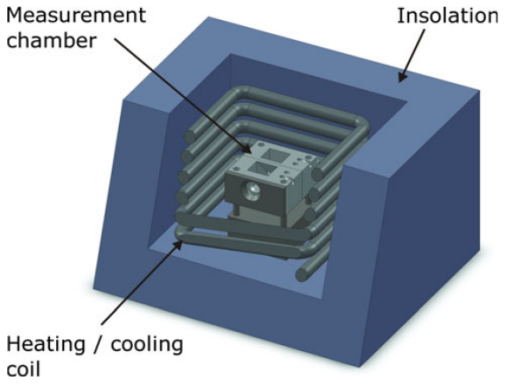

Fig. 5 The temperature-regulated bath with the measurement chamber. The bath is constructed of stainless steel and insolation. The heating coil and the measurement chamber are inserted into the bath

device can regulate medium temperature between 5 and 65 °C. The liquid solution that is in contact with the planar lipid bilayer can, however, achieve a temperature of 15–55 °C, which can be measured with an accuracy of 0.5 °C.

The measurement chamber is inserted in the temperature-regulated bath (Fig. 5). The temperature of the planar lipid bilayer is measured by two K-type thermocouple probes. They are inserted as close as possible to the planar lipid bilayer; therefore, the probes are inserted into reservoirs through the channels. One additional thermocouple probe is inserted into the bath. On the user interface, we set the temperature of the coil and measure the temperatures in the bath and both reservoirs.

System Evaluation

The system for measuring the properties of a planar lipid bilayer was evaluated using the frequency characteristic of the output stage, comparison of the measurement chambers with two sizes of the aperture and comparison of the voltage- and current-clamp measurement methods.

Chemicals

Lipids were prepared from 60 % lecithin (Fluka Analytical, Seelze, Germany), which was dissolved in a solution of hexane and ethanol at a ratio of 9:1. The mixture of hexadecane and pentane at a ratio of 3:7 was used for torus formation. The liquid solution consisted of 0.1 M KCl and 0.01 M HEPES in the same proportion. NaOH was added to obtain pH 7.4.

Methods

To evaluate the output stage, the electrode outputs, which lead into the same reservoir, were connected together (Fig. 4); the CE1 and RE1 outputs were connected together and the CE2 and RE2 outputs were connected together. On the input of the output stage, we applied the sinus signal with amplitude 1 V and frequencies from 1 Hz to 18 kHz generated by the Function/Arbitrary Waveform Generator 33250A. The input and output signals of the output stage were measured by a Tektronix (Beaverton, OR, USA) MSO4104 oscilloscope. We calculated gain and phase between output and input signals. Acquired data were analyzed using MATLAB software (Mathworks, Natick, MA, USA).

The parallel capacitance of the measurement chamber with and without formed lecithin planar lipid bilayers on two apertures with diameters of 126 and 197 μm was measured by the Agilent LCR meter 4284A. Measurements were done at 50 mV effective voltage, 1 kHz frequency and 25 °C temperature. The lecithin planar lipid bilayer is in liquid phase due to its mixture of unsaturated lipids, which have phase transition at low temperatures. At each aperture diameter, we performed 100 measurements. The difference between capacitances when the lecithin planar lipid bilayer was formed and when it was not present is the capacitance of the planar lipid bilayer. This value of the capacitance was divided by the area of the aperture. The result is specific capacitance of the lecithin planar lipid bilayer. At this point, it is not considered that the planar lipid bilayer has the Plateau-Gibbs border; therefore, the specific capacitance can be loaded with an error.

Voltage- and current-clamp methods to measure planar lipid bilayer breakdown voltage were tested on lecithin planar lipid bilayers formed on an aperture with a diameter of 126 μm at temperature 25 °C. During this test, we measured also the capacitance of each planar lipid bilayer to prove its correct formation. In the voltage-clamp method, we used linear rising voltage with slope 20 V/s. In the current-clamp method, we used a linear rising current with slope 150 μA/s. In each method, we performed three measurements. The mean values of breakdown voltage were calculated. Finally, the breakdown voltages obtained by the two methods were compared.

Results

Evaluation of the output stage has shown that, in the voltage-clamp and current-clamp methods, gain and phase between the output and input signals are close to 0 dB and 0° for frequencies from 1 Hz to 1 kHz. At higher frequencies, the gain and phase start to increase in the voltage-clamp method and decrease in the current-clamp method. This is expected because these two methods have inverted inputs and outputs. The voltage-clamp circuit reaches 3 dB gain at 11.0 kHz. The current-clamp circuit has −3 dB gain at 17 kHz. The phase of the circuits never reaches values of −45° or 45°. The frequency when the gain reaches −3 dB is called a "cutoff frequency." In our system, the voltage-clamp method has a lower cutoff frequency. The frequency characteristics for voltage and current clamp are shown in Fig. 6.

The lecithin planar lipid bilayer-specific capacitances were measured at 0.386 ± 0.027 and 0.381 ± 0.021 μF/cm^2 for apertures with diameters of 126 and 197 μm, respectively. The values are similar to the data reported in the literature (Naumowicz et al. 2003). The results also show that aperture size does not affect the specific capacitance.

The breakdown voltage was measured by applying linearly rising current or linearly rising voltage on the planar lipid bilayer. In the voltage-clamp method (Fig. 7a), planar lipid bilayer breakdown is detected by a dramatic increase of the current, while in the current-clamp method (Fig. 7b), planar lipid bilayer breakdown is detected by a sudden voltage drop. The breakdown voltage detected using the voltage-clamp method was 480.0 ± 5.0 mV. The breakdown voltage measured using the current-clamp method was 480.50 ± 6.5 mV. The specific capacitances of all formed planar lipid bilayers were 0.38 ± 0.01 μF/cm^2. The predominant species in lecithin is 1-palmitoyl-2-oleoyl-*sn*-glycero-3-phosphocholine (POPC). It was determined that the breakdown voltage of the POPC planar lipid membrane is 400 ± 6 mV in 100 mM KCl surrounding medium and use of voltage pulses (Meier et al. 2000). Using a linear rising signal to determine breakdown voltage can avoid multiple exposures to an applied signal. Kramar et al.

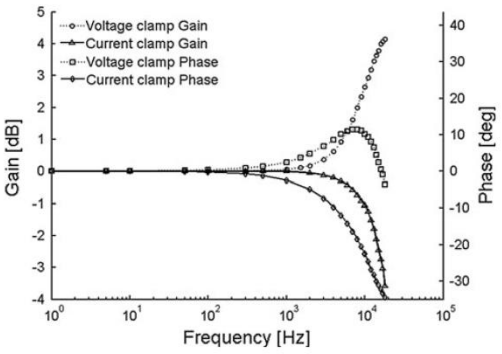

Fig. 6 Frequency characteristics for the voltage- and current-clamp circuits. The gain and phase for both circuits are shown for frequencies from 1 Hz to 18 kHz

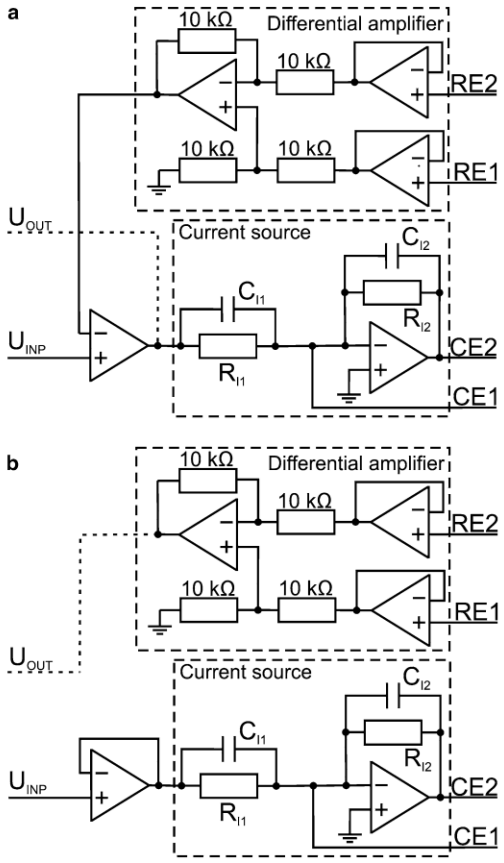

Fig. 7 The voltage and current signals acquired from the voltage- (**a**) and current- (**b**) clamp methods. In the voltage-clamp method, the rising voltage signal is applied. The current response is measured. At the beginning, the current rises proportionally to the applied voltage. When the current starts to increase more than before and goes out of the measured range, the planar lipid bilayer is broken. The value of voltage when this happens is voltage breakdown. In the current-clamp method the rising current signal is applied. The voltage response is measured, and it is proportional to the applied current. The planar lipid bilayer is broken when the measured voltage drops. The voltage value before the planar lipid bilayer is broken is breakdown voltage

(2007) found that breakdown voltage increases with increasing slope of the linear rising voltage signal. These measurements were performed using linear rising voltage signals with slopes from 4.8 to 48 kV/s. The minimum breakdown voltage of POPC in this study was 490 mV. In our experiment, we used a linear rising signal with slope of 20 V/s, due to expected lower values of the breakdown voltages. The measured breakdown voltages of the lecithin planar lipid bilayer using our new system are in the same range as the breakdown voltages of planar lipid bilayers using the other systems.

Discussion

We developed a system for formation of planar lipid bilayers and measuring planar lipid bilayer properties. The system allows the formation of planar lipid bilayers by the folding method. The electrical properties of a planar lipid bilayer which can be measured by this system are capacitance and breakdown voltage. Breakdown voltage can be determined by the voltage- and current-clamp methods. Using the voltage-clamp method we can generate voltage signals with 1 mV accuracy, while in the current-clamp method the system is able to measure voltage with 4 mV accuracy. The voltage and current signals can be generated as pulse, step change, linear rising signal or arbitrarily shaped signals. The cutoff frequencies of the system output stage are 11 and 17 kHz for the voltage-clamp and current-clamp methods, respectively. These two values show the dynamics of our system with open connectors. The voltage- and current-clamp methods were compared by measuring the breakdown voltage of lecithin planar lipid bilayers. In both cases, a linear raising signal was used to determine the breakdown voltage (Kramar et al. 2007). The results show that the two methods give similar breakdown voltages in similar conditions.

Planar lipid bilayers are automatically formed by the folding method. The automation is implemented by precise regulation of the liquid level in each reservoir. In this way, we are able to have the same hydrostatic pressure on both sides of the planar lipid bilayer, and each planar lipid bilayer is exposed to the same pressure conditions. This automation allows reproducible planar lipid bilayer formation and measurements at constant conditions. The measurement of planar lipid bilayer capacitance was tested on lecithin planar lipid bilayers at 25 °C. They were formed on apertures with diameters of 126 and 197 μm. The specific capacitances were 0.386 ± 0.027 and 0.381 ± 0.021 μF/cm^2, respectively. These values are similar to the literature data (Naumowicz et al. 2003). The results show that aperture size has no effect on measured specific capacitance.

The measurement chamber in our system is designed to form planar lipid bilayers by the folding method. The size of the aperture between the reservoirs, where the planar lipid bilayer is formed, is defined by the size of the aperture in the thin Teflon sheet which is inserted between the two parts of the chamber before experiments. Therefore, the size of the aperture can be easily changed by changing the Teflon sheet. The planar lipid bilayer can be formed on the aperture automatically. Moreover, we are able to have

the same pressure condition on a planar lipid bilayer at each formation by precisely regulating the liquid level in each reservoir.

Preliminary results confirm that the measuring system allows a broad spectrum of measurements. In particular, the temperature regulation can give new insights into planar lipid bilayer electroporation studies.

Acknowledgments This work was supported by the Slovenian Research Agency. The research was conducted in the scope of the EBAM European Associated Laboratory.

References

Antonov VF, Anosov AA, Norik VP et al (2003) Electrical capacitance of lipid bilayer membranes of hydrogenated egg lecithin at the temperature phase transition. Eur Biophys J 32:55–59

Basu R, De S, Ghosh D, Nandy P (2001) Nonlinear conduction in bilayer lipid membranes—effect of temperature. Phys A 292: 146–152

Benz R, Fröhlich O, Läuger P, Montal M (1975) Electrical capacity of black lipid films and of lipid bilayers made from monolayers. Biochim Biophys Acta 394:323–334

Boheim G, Hanke W, Eibl H (1980) Lipid phase transition in planar bilayer membrane and its effect on carrier- and pore-mediated ion transport. Proc Natl Acad Sci USA 77:3403–3407

Chen C, Smye SW, Robinson MP, Evans JA (2006) Membrane electroporation theories: a review. Med Biol Eng Comput 44:5–14

Coronado R, Latorre R (1983) Phospholipid bilayers made from monolayers on patch-clamp pipettes. Biophys J 43:231–236

Daud AI, DeConti RC, Andrews S et al (2008) Phase I trial of interleukin-12 plasmid electroporation in patients with metastatic melanoma. J Clin Oncol 26:5896–5903

Davalos RV, Mir LM, Rubinsky B (2005) Tissue ablation with irreversible electroporation. Ann Biomed Eng 33:223–231

Denet AR, Vanbever R, Préat V (2004) Skin electroporation for transdermal and topical delivery. Adv Drug Deliv Rev 56: 659–674

Funakoshi K, Suzuki H, Takeuchi S (2006) Lipid bilayer formation by contacting monolayers in a microfluidic device for membrane protein analysis. Anal Chem 78:8169–8174

Golberg A, Fischer J, Rubinsky B (2010) The use of irreversible electroporation in food preservation. In: Rubinsky B (ed) Irreversible electroporation. Springer, Berlin, pp 273–312

Huang C, Wheeldon L, Thompson TE (1964) The properties of lipid bilayer membranes separating two aqueous phases: formation of a membrane of simple composition. J Mol Biol 8:148–160

Kalinowski S, Figaszewski Z (1995) A 4-electrode potentiostat–galvanostat for studies of bilayer lipid membranes. Meas Sci Technol 6:1050–1055

Katsaras J, Gutberlet T (2010) Lipid bilayers: structure and interactions. Springer, Berlin

Kotnik T, Bobanovic F, Miklavcic D (1997) Sensitivity of transmembrane voltage induced by applied electric fields—a theoretical analysis. Bioelectrochem Bioenerg 43:285–291

Kramar P, Miklavcic D, Lebar AM (2007) Determination of the lipid bilayer breakdown voltage by means of linear rising signal. Bioelectrochemistry 70:23–27

Kramar P, Miklavcic D, Kotulska M, Lebar AM (2010) Voltage- and current-clamp methods for determination of planar lipid bilayer properties. Academic Press, San Diego, pp 29–69

Levine ZA, Vernier PT (2010) Life cycle of an electropore: field-dependent and field-independent steps in pore creation and annihilation. J Membr Biol 236:27–36

Luckey M (2008) Membrane structural biology: with biochemical and biophysical foundations. Cambridge University Press, New York

Maor E, Ivorra A, Rubinsky B (2009) Nonthermal irreversible electroporation: novel technology for vascular smooth muscle cell ablation. PLoS One 4:e4757

Meier W, Graff A, Diederich A, Winterhalter M (2000) Stabilization of planar lipid membranes: a stratified layer approach. Phys Chem Chem Phys 2:4559–4562

Mekid H, Mir LM (2000) In vivo cell electrofusion. Biochim Biophys Acta 1524:118–130

Montal M, Mueller P (1972) Formation of bimolecular membranes from lipid monolayers and a study of their electrical properties. Proc Natl Acad Sci USA 69:3561–3566

Mueller P, Rudin DO, Tien HT, Wescott WC (1963) Methods for the formation of single bimolecular lipid membranes in aqueous solution. J Phys Chem 67:534–535

Naumowicz M, Petelska A, Figaszewski Z (2003) Capacitance and resistance of the bilayer lipid membrane formed of phosphatidylcholine and cholesterol. Cell Mol Biol Lett 8:5–8

Ogura A, Matsuda J, Yanagimachi R (1994) Birth of normal young after electrofusion of mouse oocytes with round spermatids. Proc Natl Acad Sci USA 91:7460–7462

Ottova A, Tien H (2002) The 40th anniversary of bilayer lipid membrane research. Bioelectrochemistry 56:171–173

Ouagari KE, Teissié J, Benoist H (1995) Glycophorin A protects K562 cells from natural killer cell attack. J Biol Chem 270: 26970–26975

Prausnitz MR (1999) A practical assessment of transdermal drug delivery by skin electroporation. Adv Drug Deliv Rev 35:61–76

Punnamaraju S, Steckl AJ (2010) Voltage control of droplet interface bilayer lipid membrane dimensions. Langmuir 27:618–626

Sersa G, Miklavcic D, Cemazar M et al (2008) Electrochemotherapy in treatment of tumours. Eur J Surg Oncol 34:232–240

Tarek M (2005) Membrane electroporation: a molecular dynamics simulation. Biophys J 88:4045–4053

Teissié J (1998) Transfer of foreign receptors to living cell surfaces: the bioelectrochemical approach. Bioelectrochem Bioenerg 46:115–120

Tekle E, Astumian RD, Friauf WA, Chock PB (2001) Asymmetric pore distribution and loss of membrane lipid in electroporated DOPC vesicles. Biophys J 81:960–968

Tieleman DP, Leontiadou H, Mark AE, Marrink S-J (2003) Simulation of pore formation in lipid bilayers by mechanical stress and electric fields. J Am Chem Soc 125:6382–6383

Tokumasu F, Jin AJ, Dvorak JA (2002) Lipid membrane phase behaviour elucidated in real time by controlled environment atomic force microscopy. J Electron Microsc (Tokyo) 51:1–9

Vernhes MC, Benichou A, Pernin P et al (2002) Elimination of free-living amoebae in fresh water with pulsed electric fields. Water Res 36:3429–3438

Weaver JC, Chizmadzhev YA (1996) Theory of electroporation: a review. Bioelectrochem Bioenerg 41:135–160

White SH (1974) Temperature-dependent structural changes in planar bilayer membranes: solvent "freeze-out". Biochim Biophys Acta 356:8–16

White SH (1978) Formation of "solvent-free" black lipid bilayer membranes from glyceryl mono oleate dispersed in squalene. Biophys J 23:337–347

Paper 2

Title: On the electroporation thresholds of lipid bilayers: Molecular dynamics simulation investigations

Authors: Polak A, Bonhenry D, Dehez F, Kramar P, Miklavčič D, Tarek M

Publication: The Journal of Membrane Biology

DOI: 10.1007/s00232-013-9570-7

Year: 2013

Volume: 246

Issue: 11

Pages: 843-850

J Membrane Biol (2013) 246:843–850
DOI 10.1007/s00232-013-9570-7

On the Electroporation Thresholds of Lipid Bilayers: Molecular Dynamics Simulation Investigations

Andraž Polak · Daniel Bonhenry · François Dehez · Peter Kramar · Damijan Miklavčič · Mounir Tarek

Received: 4 February 2013 / Accepted: 31 May 2013 / Published online: 19 June 2013

Abstract Electroporation relates to the cascade of events that follows the application of high electric fields and that leads to cell membrane permeabilization. Despite a wide range of applications, little is known about the electroporation threshold, which varies with membrane lipid composition. Here, using molecular dynamics simulations, we studied the response of dipalmitoyl-phosphatidylcholine, diphytanoyl-phosphocholine-ester and diphytanoyl-phosphocholine-ether lipid bilayers to an applied electric field. Comparing between lipids with acyl chains and methyl branched chains and between lipids with ether and ester linkages, which change drastically the membrane dipole potential, we found that in both cases the electroporation threshold differed substantially. We show, for the first time, that the electroporation threshold of a lipid bilayer depends not only on the "electrical" properties of the membrane, i.e., its dipole potential, but also on the properties of its component hydrophobic tails.

Keywords Capacitance · Electroporation threshold · Membrane dipole potential · DPPC · DPhPC

A. Polak · P. Kramar · D. Miklavčič
Faculty of Electrical Engineering, University of Ljubljana, Tržaška cesta 25, 1000 Ljubljana, Slovenia
e-mail: andraz.polak@fe.uni-lj.si

P. Kramar
e-mail: peter.kramar@fe.uni-lj.si

D. Miklavčič
e-mail: damijan.miklavcic@fe.uni-lj.si

D. Bonhenry · F. Dehez · M. Tarek (✉)
CNRS, Unité Mixte de Recherche 7565, Université de Lorraine, Campus Science Grignard, Vandoeuvre-lés-Nancy, BP 239, 54506 Nancy Cedex, France
e-mail: mounir.tarek@univ-lorraine.fr

D. Bonhenry
e-mail: Daniel.bonhenry@univ-lorraine.fr

F. Dehez
e-mail: francois.dehez@univ-lorraine.fr

Introduction

Electroporation relates to a phenomenon in which cell membranes are permeabilized when they are exposed to high electric fields (Neumann and Rosenheck 1972). Several studies based on molecular dynamics (MD) simulations have shown that pores are formed when lipid bilayers, considered as simple models of cell membranes, are subject to such conditions. First, defects (water wires) penetrate the hydrophobic core of the bilayers; then, these expand to form water-filled pores spanning the whole bilayer, which are later stabilized by reorganization of lipid molecules (Levine and Vernier 2010; Tarek 2005; Tieleman 2004). Cell electroporation is used in several fields, like biology, biotechnology and medicine (Haberl et al. 2013). Electroporation is considered reversible if cells recover their initial state after the electric field is switched off; electroporation is considered irreversible if it leads to cell death. These two processes are used in electrochemotherapy (Sersa et al. 2008), transdermal drug delivery (Denet et al. 2004), gene therapy (Daud et al. 2008; Breton et al. 2012), water cleaning (Vernhes et al. 2002), food processing (Toepfl et al. 2007) and tissue ablation (Davalos et al. 2005).

Electroporation is also a potentially valuable method used to release drugs from uploaded synthetic liposomes (Napotnik et al. 2010), when these reach selected intracellular target areas (Elbayoumi and Torchilin 2010). Obviously, the electroporation of synthetic liposomes

depends on the structure of their constitutive lipids and on their response to an applied electric field (Portet et al. 2009). Accordingly, for efficient use of the protocol, the structure of the membrane and its behavior under an electric field have to be known.

Archaea membranes have high stability in harsh environments (Benvegnu et al. 2004; Ulrih et al. 2009) and as such are very good candidates for use as liposomes for drug delivery (Hanford and Peeples 2002; Ulrih et al. 2009). Their stability is probably due to several factors that directly relate to the peculiar chemical structure of the lipids of which they are composed. Compared to simple phosphatidylcholine lipids, archaeal lipids have a special headgroup formed of sugar moieties but also methyl branches in the lipid tails and ether linkages instead of ester linkages between the headgroup and the carbonyl region (Ulrih et al. 2009). Comparison between dipalmitoyl-phosphatidylcholine (DPPC)—, diphytanoyl-phosphocholine-ester (DPhPC-ester)—and diphytanoyl-phosphocholine-ether (DPhPC-ether)—based bilayers show, for instance, that branched chains increase the stability and decrease the permeability (Shinoda et al. 2003, 2004b) of the membrane, which are related to the slower conformational motion of the lipid tails. The difference in ester and ether linkage affects, on the other hand, the headgroup hydration and the membrane electrostatic potential. DPhPC-ester bilayers, for instance, have a dipole potential two times larger than DPhPC-ether bilayers (Shinoda et al. 2004a). We may therefore expect a direct effect on the stability of such bilayers under electrical stress, i.e., exposure to an electric field. Similar studies have reported effects on 1,2-dilauroyl-*sn*-phosphatidylcholine (DLPC), DPPC, palmitoyl-2-oleoyl-phosphatidylcholine (POPC), 1,2-dioleoyl-*sn*-phosphatidylcholine (DOPC), single-component lipid membranes (Ziegler and Vernier 2008) and POPC lipid membranes with incorporated cholesterol (Fernández et al. 2010). In both studies transmembrane voltages were induced by exposing the membranes to an external electric field. The results showed that different lipid tails have an effect on the electroporation threshold. In addition, the presence of increasing cholesterol amounts in simple lipid membranes was shown to increase the electroporation threshold (Needham and Hochmuth 1989).

In the present article, we propose specifically to evaluate the influence of branched lipid tails and headgroup linkage (ester and ether) on the electroporation of bilayers composed of archaeal-type lipids using atomistic MD simulations.

Materials and Methods

We studied three bilayers composed of DPPC, DPhPC-ester or DPhPC-ether lipids (Fig. 1). DPPC was modeled using the all-atom CHARMM 36 force field (Klauda et al. 2010). DPhPC-ester and DPhPC-ether are not described in this force field topology database; the former was therefore built by adding four methyl groups to each tail of DPPC lipid, while the latter was subsequently built by changing the ester bond to an ether bond in the DPhPC-ester molecules. The force field parameters of ether linkage were adopted from Shinoda et al. (2004a).

The MD simulations presented here were carried out using the program NAMD (Kalé et al. 1999). The systems were examined in the NPT (constant number of atoms, pressure and temperature) and NVT (constant number of atoms, volume and temperature) ensembles employing

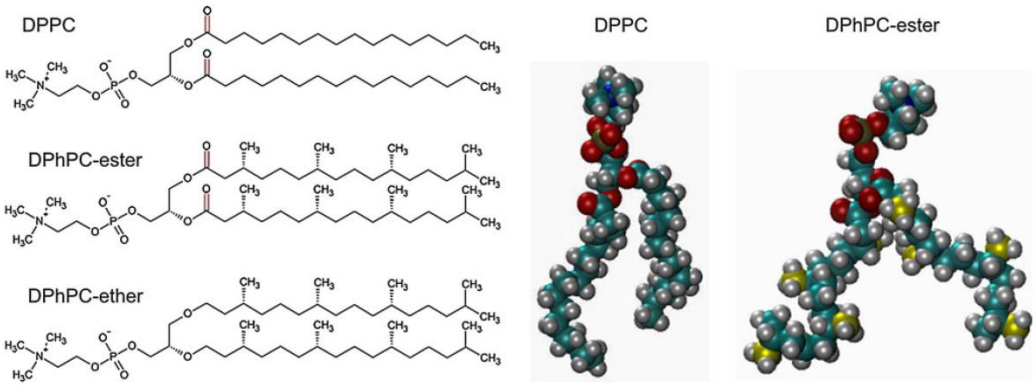

Fig. 1 *Left* Sketches of the studied lipid molecules (DPPC, DPhPC-ester and DPhPC-ether). *Right* MD models of the studied lipid molecules (DPPC and DPhPC-ester, the DPhPC-ether is not shown due to similarity to the DPhPC-ester). The atoms in the models are color-labeled (O, *red*; C, *cyan* and *yellow*; H, *gray*; N, *blue*; P, *brown*)

Langevin dynamics and the Langevin piston method. The time step for integrating the equations of motion was set at 2.0 fs. Short- and long-range forces were calculated every one and two time steps, respectively. Bonds between hydrogen and heavy atoms were constrained to their equilibrium value. Long-range, electrostatic forces were taken into account using the particle mash Ewald (PME) approach (Darden et al. 1993; Essmann et al. 1995).

All systems were considered at a ~0.45 M KCl solution and contained enough lipids to form large patches. The DPPC bilayer was hence composed of 256 lipid molecules, 20,174 water molecules, 153 potassium (K^+) ions and 153 chloride (Cl^-) ions. The DPhPC-ester and DPhPC-ether membranes were composed each of 256 DPhPC molecules, 25,888 water molecules, 196 K^+ ions and 196 Cl^- ions. The numbers of ions and water molecules differ among systems, but the chosen salt molar concentration was the same for all systems. For further calculation, systems without ions were also considered and constructed by removing the ions from the equilibrated DPhPC-ester/ether systems with ions. These were mainly used to compare our results to existing data in order to check the validity of the force field and the protocols used.

Equilibrations of the bilayers were performed at constant pressure (1 atm.) and constant temperatures (50 and 25 °C) for tens of nanoseconds. The last 15 ns of each simulation had a stable area per lipid; therefore, these intervals were assumed to be equilibrated runs and were used for the analyses.

The electrostatic potential profiles along the membrane normal was derived from MD simulations using Poisson's equation and expressed as the double integral of the molecular charge density distributions, $\rho(z)$: $\Phi(z) = -\varepsilon_0^{-1} \iint \rho(z'')dz''dz'$, z being the position of the charge in the direction along the normal to the bilayer.

The capacitance of the simulated membranes was calculated using the charge imbalance method (Delemotte et al. 2008; Sachs et al. 2004). Selected configurations from the equilibrated NPT runs were used to set new systems, where the simulation box size was extended in the direction perpendicular to the membrane to create an air–water interface. For these runs, the temperature was maintained at 50 °C and the volume was maintained constant. Systems with charge imbalances of 0, 2, 4, 6 and 8e were simulated for over 10 ns each. The last 5 ns of simulation were analyzed for electrostatic potential distribution, from which the transmembrane voltages (U_t) were calculated. For all simulations, U_t was found in a linear correlation with q, the charge imbalance normalized to the membrane area. Accordingly, the capacitance of the bilayers was estimated as $c = q/U_t$.

Electroporation of the lipid bilayers was induced by applying high transmembrane voltages created by means of the charge imbalance method. All MD simulations were run at several voltages. The electroporation threshold ($U_{EPthres}$) is reported as the interval between the highest U_t at which lipid bilayers are not electroporated in the 100-ns timescale and the lowest U_t at which pores are created in the membrane.

Results

The time evolutions of the surface area per lipid for DPPC, DPhPC-ester and DPhPC-ether bilayers in 0.45 M KCl at 50 °C and in no-salt solutions at 50 and 25 °C show that the membranes were well equilibrated within few tens of nanoseconds (data not shown). The average areas per lipid for both DPhPC-ester and DPhPC-ether (respectively, 80.1 ± 0.6 and 74.6 ± 0.7 Å^2) are much higher than for the DPPC bilayer (60.0 ± 0.9 Å^2) (Table 1). Note here that the average DPPC area/molecule value found here is similar to that reported by Klauda et al. (2010) (59.1 ± 0.4 Å^2) and smaller than the experimentally reported one, 63.0 ± 1.0 Å^2 (Kucerka et al. 2008), with no ions. The areas per molecule for the DPhPC-ester and DPhPC-ether bilayers slightly change in the absence of salt and as the temperature is further lowered to 25 °C (Table 1). At 25 °C the values found here for DPhPC-ester

Table 1 Properties of the equilibrated DPPC, DPhPC-ester and DPhPC-ether bilayers from MD simulations

Bilayers	Buffer (M KCl)	T (°C)	Area per lipid (Å^2)	Dipole potential (V)
DPPC	0.45	50	60.0 ± 0.9 (59.1,[a] 63.0[c])	0.70 (0.7,[a] 0.24[f,g])
DPhPC-ester	0.45	50	80.1 ± 0.6	0.62
	–	50	79.9 ± 0.6	0.58
		25	78,6 ± 0.6 (77.7,[b] 76[d])	0.62 (1.00,[b] 0.51[e])
DPhPC-ether	0.45	50	74.6 ± 0.7	0.36
	–	50	75.7 ± 0.6	0.38
		25	73.6 ± 0.4 (74.1[b])	0.36 (0.57,[b] 0.26[e])

Simulation data: [a] Klauda et al. (2010) and [b] Shinoda et al. (2004a). Experimental data: [c] Kucerka et al. (2008), [d] Wu et al. (1995), [e] Wang et al. (2006), [f] Gawrisch et al. (1992) and [g] Peterson et al. (2002)

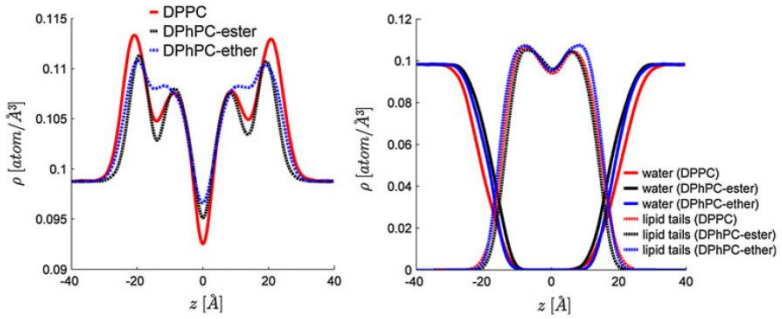

Fig. 2 *Left* Total density profiles of DPPC, DPhPC-ester and DPhPC-ether bilayers in 0.45 M KCl and at 50 °C. *Right* Water and lipid tail density profiles of DPPC, DPhPC-ester and DPhPC-ether bilayers in 0.45 M KCl and 50 °C

and DPhPC-ether (78.6 ± 0.6 and 73.6 ± 0.4 Å^2) match quite nicely those reported by others (Shinoda et al. 2004a) (77.7 and 74.1 Å^2). Finally, as a comparison, the experimentally determined area per molecule for DPhPC-ester is 76 Å^2 (Wu et al. 1995), which provides some confidence in the force field and protocol used here. The density profiles across the DPPC, DPhPC-ester and DPhPC-ether bilayers in KCl solution are reported in Fig. 2.

The electrostatic potential profiles across the DPPC, DPhPC-ester and DPhPC-ether bilayers were estimated from the distribution of charges in the systems using the Poisson equation. The presence of ions in the systems does not modify the electrostatic potential profiles much (data not shown). Also, the lipid bilayers at temperatures of 50 and 25 °C have similar overall electrostatic potential profiles; therefore, these profiles are shown only for systems with ions (Fig. 3). Because of the similarity of their headgroups, DPPC and DPhPC-ester electrostatic profiles are very close. There is, in contrast, a large difference between the profiles of ester and ether DPhPCs. The so-called membrane dipole potentials (measure of the difference between voltages between the outside and the hydrophobic core of the membrane) of DPPC, DPhPC-ester and DPhPC-ether measured from the corresponding electrostatic profiles are, respectively, 0.70, 0.62 and 0.36 V.

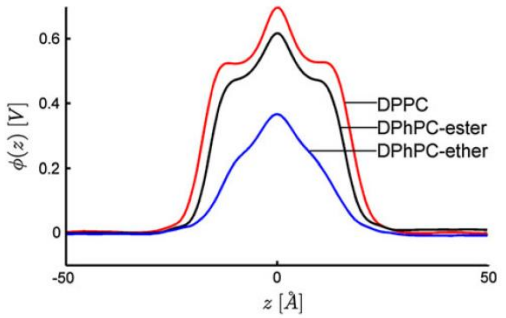

Fig. 3 Electrostatic potential profiles of DPPC, DPhPC-ester and DPhPC-ether bilayers in 0.45 M KCl and 50 °C. Average estimated dipole potentials of DPPC, DPhPC-ester and DPhPC-ether bilayers are 0.70, 0.62 and 0.36 V, respectively

For DPPC, there is a large difference between the experimental dipole potential values [using the charge relaxation method 0.23 V (Gawrisch et al. 1992) and 0.24 V (Peterson et al. 2002)] and those derived from our MD simulations, which are consistent with the 0.7 V found using a similar force field (Klauda et al. 2010). However, for DPhPC, the simulation data are in good agreement with those derived using cryo-EM, where the dipole potentials for DPhPC-ester and DPhPC-ether were, respectively, 0.51 and 0.26 V (Wang et al. 2006).

Similar analyses were performed for the systems with no salt concentration and at lower temperature. These changes, as previously mentioned, had little effect on the shape of the electrostatic profiles; and accordingly, the magnitudes of the dipole potentials were quite similar (Table 1).

Lipid bilayers behave as capacitors (Delemotte et al. 2008). Hence, by imposing a charge imbalance across the lipid bilayers (DPPC, DPhPC-ester and DPhPC-ether), one may create a transmembrane voltage across these bilayers. These transmembrane voltages are found to be proportional to the charge imbalance normalized to the lipid bilayer area (Fig. 4). By imposing charge imbalances (0, 2, 4, 6 and 8e) to the modeled systems at 0.45 M KCl, we have estimated their capacitances. There is only a mild difference (0.94, 0.93 and 0.90 μF cm^{-2}) between the values found, respectively, for DPPC, DPhPC-ester and DPhPC-ether. Again, there is a discrepancy between these values and those determined experimentally: ∼0.38 μF cm^{-2} of DPPC (Antonov et al. 1990) and DPhPC-ester bilayers found by others to range from 0.5 to 0.6 μF cm^{-2} (Ridi et al. 1998). Consistent with previous studies on POPC (Kramar et al. 2012), all capacitance values determined from atomistic simulations were much higher than those determined experimentally.

Having hence characterized the electrostatic properties of the three bilayers, we performed additional simulations

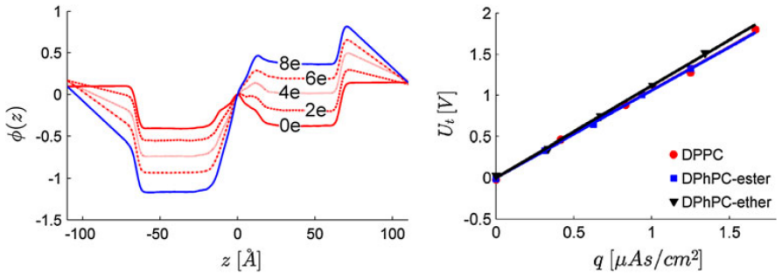

Fig. 4 *Left* Electrostatic potential profiles across the DPhPC-ether bilayers for simulations performed at different net charge imbalances Q (0–8e) between the upper and lower electrolytes. *Right* Transmembrane potentials across the DPPC, DPhPC-ester and DPhPC-ether bilayers as a function of the charge imbalance (Q) normalized to the area of membranes. The *slopes* represent linear fits to the data that permit estimates of bilayer capacitance

in order to determine U_{EPthres}, i.e., their electroporation thresholds. Simulations of DPPC, DPhPC-ester and DPhPC-ether lipid bilayers at several applied transmembrane voltages were performed. The times the hydrophobic pore is created and the first ion goes through the pore are shown in Table 2. In all simulations, above the threshold, the pores are created in the 30-ns timescale. For voltages where no pore was created, the simulations were extended for more than 60 ns. Hence, electroporation of DPPC, DPhPC-ester and DPhPC-ether lipid bilayers did not occurr at, respectively, $\sim$1.8, 2.3 and 3.0 V for extended-length simulations. On the contrary, electroporation (creation of pores) of the lipid bilayers occurred in less than 30 ns for DPPC, DPhPC-ester and DPhPC-ether bilayers at, respectively, $\sim$2.3, 3.0 and 3.7 V.

Discussion

In this MD simulations study, we compared DPPC-, DPhPC-ester- and DPhPC-ether-based lipid bilayers characteristics and responses to electrical stress. Analyses of the simulations of the bilayers showed that the electrostatic potentials across the DPPC, DPhPC-ester and DPhPC-ether bilayers are independent of the surrounding solvent salt concentration and only slightly change for temperatures varying from 25 to 50 °C. These electrostatic potentials depend, however, on the membrane's lipid composition, in particular, the nature of the tails and to a much greater extent the nature of the linkages (ester and ether) from headgroup to tail.

We investigated the stability of DPPC, DPhPC-ester and DPhPC-ether bilayers under an electric stress. Comparison of the electroporation thresholds obtained from MD simulations under conditions mimicking the effect of low-magnitude millisecond electric pulses (Delemotte and Tarek 2012) suggests that both the nature of the lipid tails and the type of linkages (ester and ether) have an effect. Changing the lipid from DPPC to DPhPC, i.e., addition of methyl groups in the hydrophobic tails, stabilizes the lipid bilayer and increases the electroporation threshold, U_{EPthres}. Changing the ester linkage with an ether when going from DPhPC-ester to DPhPC-ether stabilizes even more the bilayer and increases further the U_{EPthres}. Hence, the U_{EPthres} values for DPPC, DPhPC-ester and DPhPC-ether bilayers were between 1.8 and 2.2 V, between 2.3 and 2.7 V and between 3.0 and 3.4 V, respectively. Note that fine-tuning these ranges can be achieved if the systems modeled were much larger lipid patches. The ranges nonetheless indicate here clearly a threshold increase.

These "absolute values" of the U_{EPthres} increase are probably overestimated, as are so far all the electroporation thresholds determined from MD simulations. It is not yet clear to us what are the reasons behind such large discrepancies between electroporation thresholds found in simulations and those determined experimentally. Considering the electrical properties of the membranes, the dipole potential of DPPC-based membranes is in agreement with other MD simulations but is much higher than experimental results measured by invasive methods (Table 1). On the other hand, the membrane dipole potentials of DPhPC-ester and -ether membranes are only slightly higher than those determined experimentally using noninvasive methods (e.g., cryo-EM). Quite interestingly, the ratio between membrane dipole potentials of DPhPC-ester and -ether determined from MD simulations ($\sim$2) is the same as that found in experiments. We also considered the link to the lipid tail properties via the permittivity of the membrane, ε, and therefore the capacitance, C, of the bilayer: $C = \varepsilon A/d$. The capacitances of the membranes measured using the charge imbalance method for all three lipids are around 0.9 μF cm^{-2}, which is about two times higher than those obtained experimentally. A similar discrepancy was obtained for POPC bilayers (Kramar et al. 2012).

Table 2 Characteristics of DPPC, DPhPC-ester and DPhPC-ether lipid bilayers under various transmembrane voltages created by a net charge imbalance

Bilayers	Charge imbalance (e)	Transmembrane voltage (V)	Simulation (ns)	Water wire formed (ns)	First ion through (ns)
DPPC	8	1.8	63	–	–
	10	2.2	14	2.5	2.7
			18	16.5	16.9
			10	–	–
			10	–	–
	12	2.6	10	1.5	1.8
DPhPC-ester	14	2.3	67	–	–
	16	2.7	38	12.5	13.3
			37	–	–
	18	3.0	27	12.0	12.6
	20	3.3	10	4.1	5.2
			10	1.9	2.9
			10	2.0	2.4
			10	4.5	5.2
DPhPC-ether	16	3.0	66	–	–
	18	3.4	51	26.8	28.0
	20	3.7	26	15.9	17.5
	22	4.1	10	6.1	7.0
			10	6.5	6.7
			10	3.5	4.0
			10	–	–
	24	4.5	10	2.0	2.7
	26	4.9	4	2.3	2.7

We performed a few analyses seeking to relate the reason for changes in the electroporation threshold between the lipid bilayers to their structural and physical properties. The profiles of the three bilayers indicate only a mild change in the density profiles between the three components and, therefore, do not provide strong evidence of variability that can be directly correlated with the changes in U_{EPthres}. The correspondence between U_{EPthres} and the lipid bilayer capacitance is also weak since the force fields used do not provide for a large change in the lipid bilayer capacitances, while there is a significant change in their U_{EPthres}.

We have also estimated the local pressure profiles (Lindahl and Edholm 2000) along z, the bilayer normal, at various system configurations. The pressure profiles may be calculated from simulations as $p(z) = \frac{1}{\Delta V}\left[\sum_i m_i v_i \otimes v_i - \sum_{i<j} F_{ij} \otimes r_{ij} f\left(z, z_i, z_j\right)\right]$, where $p(z)$ is the local pressure tensor in the slab centered on the coordinate z, the sum over the kinetic term running over all atoms in the slab and $f\left(z, z_i, z_j\right)$ a weighting function. All calculations were performed on the fly (Kalé et al. 1999) from the simulations performed at constant temperature and constant pressure. In a lipid bilayer, pressure profiles arise due to the amphipathic nature of the lipids composing it: the hydrophilic headgroups are squeezed together to prevent exposure of the hydrophobic tails to the solvent leading to a negative lateral pressure, while the attractive dispersion forces and entropic repulsion between the lipid tails result mainly in a positive lateral pressure.

Comparison of the pressure profiles of DPPC and DPhPC-ester (Fig. 5) showed again only a mild increase for the branched chain lipid bilayer in the upper region of the hydrophobic tails. It is unlikely that such an increase in the local membrane lateral tension affects greatly the U_{EPthres}.

Shinoda et al. (2004b) performed an extensive study of water permeability in both membranes that may provide a rationale for the increased electroporation threshold as we go from DPPC to DPhPC. Indeed, the authors show from analyses of local diffusion coefficients that water molecules have considerably reduced mobility in the DPhPC membrane interior compared with the DPPC membrane interior. As a result of reduced water diffusion in the branch chained membrane, the water permeability of the DPhPC bilayer was less than that of the DPPC bilayer by about 30 %. As such permeability or diffusion toward the

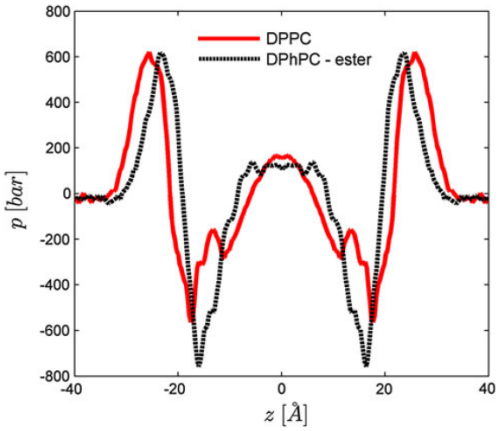

Fig. 5 Lateral pressure profile of DPPC and DPhPC-ester bilayers in 0.45 M KCl and at 50 °C

interior of the membrane is the very initial key step in electroporation (Delemotte and Tarek 2012; Tockman et al. 2013), we expect that this has a direct impact on U_{EPthres}.

Evidently, more studies comparing different lipid bilayers are needed in order to understand and determine the link between the electroporation threshold and the specificities of the lipid components of a membrane. The present results, however, show clearly that the electroporation threshold of a lipid bilayer depends not only on the "electrical" properties of the membrane, i.e., its dipole potential, but also on the properties of its components' hydrophobic tails.

Acknowledgments This work was in part supported by the Slovenian Research Agency. Research was conducted in the scope of the EBAM European Associated Laboratory. The article is a result of the networking efforts of COST Action TD1104. Part of the calculations and the finalization of the article was performed during the Short-Term Scientific Mission (Grant 070113-021794, to A. P.). Simulations were performed using HPC resources from GENCI-CINES (Grant 2012-076434). The authors thank the ANR Intcell program (ANR-10-BLAN-096).

References

Antonov VF, Smirnova EY, Shevchenko EV (1990) Electric field increases the phase transition temperature in the bilayer membrane of phosphatidic acid. Chem Phys Lipids 52:251–257

Benvegnu T, Brard M, Plusquellec D (2004) Archaeabacteria bipolar lipid analogues: structure, synthesis and lyotropic properties. Curr Opin Colloid Interface Sci 8:469–479

Breton M, Delemotte L, Silve A, Mir LM, Tarek M (2012) Nanosecond pulsed electric field driven transport of siRNA molecules through lipid membranes: an experimental and computational study. J Am Chem Soc 134:13938–13941

Darden T, York D, Pedersen L (1993) Particle mesh Ewald: an N·log(N) method for Ewald sums in large systems. J Chem Phys 98:10089

Daud AI, DeConti RC, Andrews S et al (2008) Phase I trial of interleukin-12 plasmid electroporation in patients with metastatic melanoma. J Clin Oncol 26:5896–5903

Davalos RV, Mir LM, Rubinsky B (2005) Tissue ablation with irreversible electroporation. Ann Biomed Eng 33:223–231

Delemotte L, Tarek M (2012) Molecular dynamics simulations of lipid membrane electroporation. J Membr Biol 245:531–543

Delemotte L, Dehez F, Treptow W, Tarek M (2008) Modeling membranes under a transmembrane potential. J Phys Chem B 112:5547–5550

Denet A-R, Vanbever R, Préat V (2004) Skin electroporation for transdermal and topical delivery. Adv Drug Deliv Rev 56:659–674

Elbayoumi TA, Torchilin VP (2010) Current trends in liposome research. Methods Mol Biol 605:1–27

Essmann U, Perera L, Berkowitz ML et al (1995) A smooth particle mesh Ewald method. J Chem Phys 103:8577

Fernández ML, Marshall G, Sagués F, Reigada R (2010) Structural and kinetic molecular dynamics study of electroporation in cholesterol-containing bilayers. J Phys Chem B 114:6855–6865

Gawrisch K, Ruston D, Zimmerberg J et al (1992) Membrane dipole potentials, hydration forces, and the ordering of water at membrane surfaces. Biophys J 61:1213–1223

Haberl S, Miklavcic D, Sersa G et al (2013) Cell membrane electroporation—part 2. The applications. IEEE Electr Insulation Mag 29:29–37

Hanford MJ, Peeples TL (2002) Archaeal tetraether lipids: unique structures and applications. Appl Biochem Biotechnol 97:45–62

Kalé L, Skeel R, Bhandarkar M et al (1999) NAMD2: greater scalability for parallel molecular dynamics. J Comput Phys 151:283–312

Klauda JB, Venable RM, Freites JA et al (2010) Update of the CHARMM all-atom additive force field for lipids: validation on six lipid types. J Phys Chem B 114:7830–7843

Kramar P, Delemotte L, Lebar AM et al (2012) Molecular-level characterization of lipid membrane electroporation using linearly rising current. J Membr Biol 245:651–659

Kucerka N, Nagle JF, Sachs JN et al (2008) Lipid bilayer structure determined by the simultaneous analysis of neutron and X-ray scattering data. Biophys J 95:2356–2367

Levine ZA, Vernier PT (2010) Life cycle of an electropore: field-dependent and field-independent steps in pore creation and annihilation. J Membr Biol 236:27–36

Lindahl E, Edholm O (2000) Spatial and energetic–entropic decomposition of surface tension in lipid bilayers from molecular dynamics simulations. J Chem Phys 113:3882

Napotnik TB, Rebersek M, Kotnik T et al (2010) Electropermeabilization of endocytotic vesicles in B16 F1 mouse melanoma cells. Med Biol Eng Comput 48:407–413

Needham D, Hochmuth RM (1989) Electro-mechanical permeabilization of lipid vesicles. Role of membrane tension and compressibility. Biophys J 55:1001–1009

Neumann E, Rosenheck K (1972) Permeability changes induced by electric impulses in vesicular membranes. J Membr Biol 10:279–290

Peterson U, Mannock DA, Lewis RNA et al (2002) Origin of membrane dipole potential: contribution of the phospholipid fatty acid chains. Chem Phys Lipids 117:19–27

Portet T, Camps I, Febrer F, Escoffre J-M et al (2009) Visualization of membrane loss during the shrinkage of giant vesicles under electropulsation. Biophys J 96:4109–4121

Ridi A, Scalas E, Robello M, Gliozzi A (1998) Linear response of a fluctuating lipid bilayer. Thin Solid Films 327–329:796–799

Sachs JN, Crozier PS, Woolf TB (2004) Atomistic simulations of biologically realistic transmembrane potential gradients. J Chem Phys 121:10847–10851

Sersa G, Miklavcic D, Cemazar M et al (2008) Electrochemotherapy in treatment of tumours. Eur J Surg Oncol 34:232–240

Shinoda W, Mikami M, Baba T, Hato M (2003) Molecular dynamics study on the effect of chain branching on the physical properties of lipid bilayers: structural stability. J Phys Chem B 107:14030–14035

Shinoda K, Shinoda W, Baba T, Mikami M (2004a) Comparative molecular dynamics study of ether- and ester-linked phospholipid bilayers. J Chem Phys 121:9648–9654

Shinoda W, Mikami M, Baba T, Hato M (2004b) Molecular dynamics study on the effects of chain branching on the physical properties of lipid bilayers: 2. Permeability. J Phys Chem B 108:9346–9356

Tarek M (2005) Membrane electroporation: a molecular dynamics simulation. Biophys J 88:4045–4053

Tieleman DP (2004) The molecular basis of electroporation. BMC Biochem 5:10

Tockman M, Lee JH, Levine ZA, Ho M-C, Colvin ME, Vernier PT (2013) Electric field-driven water dipoles: nanoscale architecture of electroporation. PLoS One 8(4):e61111

Toepfl S, Heinz V, Knorr D (2007) High intensity pulsed electric fields applied for food preservation. Chem Eng Process 46:537–546

Ulrih NP, Gmajner D, Raspor P (2009) Structural and physicochemical properties of polar lipids from thermophilic Archaea. Appl Microbiol Biotechnol 84:249–260

Vernhes M, Benichou A, Pernin P et al (2002) Elimination of free-living amoebae in fresh water with pulsed electric fields. Water Res 36:3429–3438

Wang L, Bose PS, Sigworth FJ (2006) Using cryo-EM to measure the dipole potential of a lipid membrane. Proc Natl Acad Sci USA 103:18528–18533

Wu Y, He K, Ludtke SJ, Huang HW (1995) X-ray diffraction study of lipid bilayer membranes interacting with amphiphilic helical peptides: diphytanoyl phosphatidylcholine with alamethicin at low concentrations. Biophys J 68:2361–2369

Ziegler MJ, Vernier PT (2008) Interface water dynamics and porating electric fields for phospholipid bilayers. J Phys Chem B 112:13588–13596

Paper 3

Title: Electroporation of Archaeal Lipid Membranes using MD Simulations

Authors: Polak A, Tarek M, Tomšič M, Valant J, Ulrih N P, Jamnik A, Kramar P, Miklavčič D

Publication: Bioelectrochemistry

DOI: 10.1016/j.bioelechem.2013.12.006

Year: 2014

Volume: 100

Issue: /

Pages: 18-26

Bioelectrochemistry 100 (2014) 18–26

Contents lists available at ScienceDirect

Bioelectrochemistry

journal homepage: www.elsevier.com/locate/bioelechem

Electroporation of archaeal lipid membranes using MD simulations

Andraž Polak [a], Mounir Tarek [b,c], Matija Tomšič [d], Janez Valant [e], Nataša Poklar Ulrih [e], Andrej Jamnik [d], Peter Kramar [a], Damijan Miklavčič [a,*]

[a] University of Ljubljana, Faculty of Electrical Engineering, Tržaška cesta 25, SI-1000 Ljubljana, Slovenia
[b] Université de Lorraine, UMR 7565, F-54506 Vandoeuvre-lés-Nancy, France
[c] CNRS, UMR 7565, F-54506 Vandoeuvre-lés-Nancy, France
[d] University of Ljubljana, Faculty of Chemistry and Chemical Technology, Aškerčeva c. 5, SI-1000 Ljubljana, Slovenia
[e] University of Ljubljana, Biotechnical Faculty, Jamnikarjeva 101, SI-1000 Ljubljana, Slovenia

ARTICLE INFO

Article history:
Received 25 September 2013
Received in revised form 24 December 2013
Accepted 31 December 2013
Available online 9 January 2014

Keywords:
Transmembrane voltage
X-ray scattering
Aeropyrum pernix
Lipid bilayers
Charge imbalance

ABSTRACT

Molecular dynamics (MD) simulations were used to investigate the electroporation of archaeal lipid bilayers when subjected to high transmembrane voltages induced by a charge imbalance, mimicking therefore millisecond electric pulse experiments. The structural characteristics of the bilayer, a 9:91 mol% 2,3-di-O-sesterterpanyl-sn-glicerol-1-phospho-myo-inositol (AI) and 2,3-di-O-sesterterpanyl-sn-glicerol-1-phospho-1′(2′-O-α-D-glucosyl)-myo-inositol (AGI) were compared to small angle X-ray scattering data. A rather good agreement of the electron density profiles at temperatures of 298 and 343 K was found assessing therefore the validity of the protocols and force fields used in simulations. Compared to dipalmitoyl-phosphatidylcholine (DPPC), the electroporation threshold for the bilayer was found to increase from ~2 V to 4.3 V at 323 K, and to 5.2 V at 298 K. Comparing the electroporation thresholds of the archaeal lipids to those of simple diphytanoyl-phosphatidylcholine (DPhPC) bilayers (2.5 V at 323 K) allowed one to trace back the stability of the membranes to the structure of their lipid head groups. Addition of DPPC in amounts of 50 mol% to the archaeal lipid bilayers decreases their stability and lowers the electroporation thresholds to 3.8 V and 4.1 V at respectively 323 and 298 K. The present study therefore shows how membrane compositions can be selected to cover a wide range of responses to electric stimuli. This provides new routes for the design of liposomes that can be efficiently used as drug delivery carriers, as the selection of their composition allows one to tune in their electroporation threshold for subsequent release of their load.

1. Introduction

Archaea are extremophile organisms that optimally grow in extreme environments. They are grouped into halophiles that grow in high salt concentration, methanogens that grow under anaerobic condition, thermophiles that grow at high temperatures and psychrophilic that grow at low temperatures. The cell membranes of these archaea have a unique composition, a high chemical and a high physical stability [1–3]. Compared to simple phosphatidyl-choline (PC) lipids, archaeal lipids have head-groups formed by sugar moieties, ether linkages instead of ester linkages between the head group and the carbonyl region, and methyl-branched lipid tails [2]. *Aeropyrum pernix* is an aerobic hyperthermophilic archaea organism that grows in a coastal solfataric vent at Kodakara, Juma Island, Japan. Its optimal growth environment is at temperatures between 363 K and 368 K, pH 7.0 and salinity of ~3.5%. *A. pernix* cells are spherical with diameters ranging from 0.8 to 1.2 μm [4]. Their membrane is composed of two lipids: 2,3-di-O-sesterterpanyl-sn-glicerol-1-phospho-myo-inositol (AI) and 2,3-di-O-sesterterpanyl-sn-glicerol-1-phospho-1′(2′-O-α-D-glucosyl)-myo-inositol (AGI) at a molar ratio of 9:91 mol% [5]. The core of both lipids is a 2,3-di-o-sesterterpanyl-sn-glycerol ($C_{25,25}$-archaeol) while the polar heads are inositol for AI and glucose for AGI (Fig. 1).

The lipids forming the membranes of such organisms are as such very good candidates as components of liposomes for drug delivery [2,6]. For such applications however, the drug should be ultimately released when the carrier (liposome) reaches the intracellular milieu [7]. One of the methods that can be used to enhance the drug release from the synthetic liposomes is electroporation [8,9]. Electroporation is a phenomenon that affects the stability of lipid membranes since it disturbs transiently or permanently their integrity when these are subject to high voltages (electric fields) [10]. Such a technique is now routinely used in fields as diverse as biology, biotechnology and medicine [11]. For simple membranes, molecular dynamics (MD) simulations have shown that the main effect of high electric fields is to enhance the membrane permeability due to the formation of

* Corresponding author at: Laboratory of Biocybernetics, University of Ljubljana, Faculty of Electrical Engineering, Trzaska 25, SI-1000 Ljubljana, Slovenia. Tel.: +386 1 4768 456; fax: +386 1 426 46 58.
E-mail addresses: andraz.polak@fe.uni-lj.si (A. Polak), mounir.tarek@univ-lorraine.fr (M. Tarek), matija.tomsic@fkkt.uni-lj.si (M. Tomšič), janez.valant@bf.uni-lj.si (J. Valant), natasa.poklar@bf.uni-lj.si (N.P. Ulrih), andrej.jamnik@fkkt.uni-lj.si (A. Jamnik), peter.kramar@fe.uni-lj.si (P. Kramar), damijan.miklavcic@fe.uni-lj.si (D. Miklavčič).

1567-5394/$ – see front matter © 2014 Elsevier B.V. All rights reserved.
http://dx.doi.org/10.1016/j.bioelechem.2013.12.006

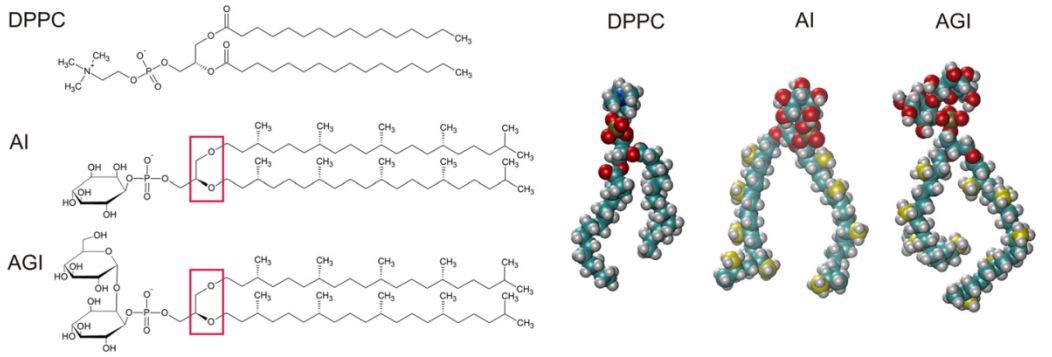

Fig. 1. Representations of archaeal lipids which compose the membrane of Archaea *Aeropyrum pernix* (AI and AGI) and the DPPC lipid.

hydrophilic pores that can be wide enough to transport ions and small molecules [12–17]. When exposed long enough to high fields, lipid bilayers and liposomes can undergo irreversible breakdown [18–20].

Obviously, electroporation of membranes depends on their lipid composition [21]. A molecular level insight about the phenomena has been gathered from MD simulations of lipid bilayers subject to large transmembrane voltages. Most studies concerned the electroporation of phosphatidylcholine (PC) based lipid bilayers [22–26] and the large body of data showed that the electroporation thresholds depend on the type of lipid considered. The presence of increasing cholesterol amounts in lipid membranes was also shown to increase the electroporation threshold [27,28]. Recently, we considered dipalmitoyl-PC (DPPC), and diphytanoyl-PC (DPhPC)-ester and -ether based bilayers [24], comparing therefore lipids with acyl chains and methyl branched chains, and lipids with ether or ester linkages, which changes drastically the membrane dipole potential. We have shown that the electroporation thresholds of these bilayers depend not only on the properties of their component hydrophobic tails but also on the "electrical" properties of the membrane, i.e. its dipole potential.

Archaeal lipids from *A. pernix* present an additional feature: their head group possesses either inositol or glucose moieties. It is unknown how such lipids when forming bilayers would behave under high voltages. It is also interesting to determine how their stability can be modulated by changing the lipid composition, e.g. by adding a third component. This is precisely what we are investigating in the present paper. We first determine the structural characteristics of archaeal lipid bilayers by confronting small angle X-ray scattering data performed on unilamellar vesicles to MD simulations of bilayers of the same composition. We proceed then to study these bilayers electroporation.

2. Material and methods

2.1. Growth of A. pernix K1

The optimum conditions for maximizing *A. pernix* biomass were obtained when $Na_2S_2O_3 \times 5H_2O$ (1 g of per liter) (Alkaloid, Skopje, Macedonia) added Marine Broth 2216 (Difco™, Becton, Dickinson and Co., Sparks, USA) at pH 7.0 (20 mM HEPES buffer) was used as a growing medium in 1 L flask at 365 K (for details see [29]). After growth, the cells were harvested by centrifugation, washed and lyophilized.

2.2. Isolation and purification of lipids, and vesicle preparation

The polar lipid methanol fraction composed of approximately 91% AGI and 9% AI [5] (average molecular mass, 1181.42 g mol^{-1}) was purified from lyophilized *A. pernix* cells, as described previously [30]. After isolation, the lipids were fractioned using adsorption chromatography [31], and the polar lipid methanol fraction was used for further analysis. Organic solvents were removed under a stream of dry nitrogen, followed by the removal of the last traces under vacuum. For mixed lipid liposomes, the appropriate mass of archaeal $C_{25,25}$ lipids and DPPC were dissolved in chloroform and mixed together in glass round-bottomed flasks. The lipid film was prepared by drying the sample on a rotary evaporator. For preparation of a pure DPPC lipid film, chloroform/methanol (7/3, v/v) was used as solvent. The dried lipid films were then hydrated with warm (~318 K) 20 $mmol.l^{-1}$ HEPES buffer, pH 7.0 or deionized water (milliQ). The mol% of the archaeal $C_{25,25}$ lipids in the mixed archaeal-DPPC liposomes was: 100, 95, 90, 75 and 50. Multilamellar vesicles (MLV) were prepared by vortexing the lipid suspensions vigorously for 10 min. MLV were further transformed into large unilamellar vesicles (LUV). After six freeze (liquid nitrogen) and thaw (warm water) cycles, the liposomes were pressure-extruded 21 times through 400-nm polycarbonate membranes on an Avanti polar mini-extruder (Avanti Polar Lipids, Alabastr, Alabama, USA), at between 323 and 333 K. The total lipid concentration in all SAXS experiments was 10 mg/ml.

2.3. Small-angle X-ray scattering measurements

Small-Angle X-Ray Scattering (SAXS) measurements were performed on the Kratky compact camera (Anton Paar KG, Graz, Austria) [32], which was modified to enclose the focusing multilayer optics for X-rays (Göbel mirror; Osmic). The camera was attached to a conventional X-ray generator Kristalloflex 760 (Bruker AXS GmbH, Karlsruhe, Germany) equipped with a sealed X-ray tube (Cu K_α X-rays with a wavelength $\lambda = 0.154$ nm) and operating at 40 kV and 35 mA. The samples were measured in a standard quartz capillary with an outer diameter of 1 mm and wall thickness of 10 μm. The scattering intensities were detected with the position sensitive detector PSD-50 M (M. Braun GmbH, Garching, Germany) in the small-angle regime of scattering vectors $0.1 < q < 7.5$ nm^{-1}, where $q = 4\pi/\lambda \cdot \sin(\vartheta/2)$, ϑ representing the scattering angle. In order to get reliable measuring statistics, each sample was measured for a period of 20 h. Prior to the data analysis by the inverse Fourier transformation method, the scattering data were corrected for the empty capillary and solvent scattering, and put on the absolute scale using water as a secondary standard [33].

2.4. Evaluation of SAXS data

SAXS data were evaluated using the Indirect Fourier Transformation (IFT) technique [34,35]. Even through the overall dimension of the lipid

bilayer is much above the resolution of the SAXS measurements, we can still extract information about the thickness of the lipid bilayer using such an approach. For this purpose the function $I(q)\ q^2$, $I(q)$ being the scattering intensity, is cosine transformed into the real space yielding the thickness pair distance distribution function $p_t(r)$ [35–37], which is in the next step transformed into the profile $\Delta\rho_e(z)$ by a convolution square root operation [38–40].

The profile $\Delta\rho_e(z)$ represents the local scattering contrast, i.e. the difference between the local electron density at a distance z from the center of symmetry (central plane in the middle of bilayer) and the average electron density of the sample $\overline{\rho}_e$. Further in the text, the scattering contrast profile $\Delta\rho_e(z)$ will be referred to simply as the electron density profile and denoted as $\rho_e(z)$. In this paper we present only the final SAXS electron density profiles. Details of the evaluation of these SAXS data and other structural SAXS results will be presented elsewhere.

2.5. MD simulations

Morii et al. suggested that two stereo-structures of phospho-myo-inositol (1D and 1L) of AGI may compose the membrane of *A. pernix* [5]. For simplicity we have chosen here to model only the 1D conformation. The AGI and AI molecules were modeled by combining of CHARMM 36 lipids force field (FF) [41] and that of carbohydrates. The FF parameters of ether linkage were adopted from [42].

We considered hydrated bilayers of AI and AGI at a 9:91 molar ratio, and mixed bilayers composed of archaeal lipids + DPPC at 50:50 molar ratio. The MD simulations were carried out using NAMD [43]. The systems were examined at constant pressure ($P = 98$ kPa) and constant temperature (T), or at constant volume (V) and constant T employing Langevin dynamics and the Langevin piston method. The time step for integrating the equations of motion was set to 2.0 fs. Short- and long-range forces were calculated every one and two time steps, respectively. Bonds between hydrogen and heavy atoms were constrained to their equilibrium value. Long-range, electrostatic forces were taken into account using the Particle Mesh Ewald (PME) approach [44,45].

First, a small hydrated bilayer patch (64 lipid molecules spread equally on both leaflets and 10,283 water molecules, 144 potassium (K^+) and 80 chloride (Cl^-) ions) was equilibrated at 323 K for 120 ns. The system was then replicated four times and further equilibrated for tens of ns at 298, 323, 343 and 363 K. These bilayers were composed of 232 AGI and 24 AI molecules. The systems composed of mixtures of archaeal lipids and DPPC in the same ratio were set by replacing half of the archaeal lipids by DPPC molecules (and deleting 128 potassium ions). The latter were equilibrated for tens of ns at 298, 323, 343 K. All the systems were modeled at an ~0.45 mol.l^{-1} KCl solution. In the systems studied at 298 and 343 K, the potassium and chloride ions were removed and replaced by Na^+ counter ions to neutralize the overall charge. These systems were used to compare electron density profile determined from simulations to the data derived from SAXS experiments.

The last 15 ns of each simulation had stable average area per lipid; therefore these intervals were assumed as equilibrated runs and were used for the analyses.

The electrostatic potential profiles along the membrane normal was derived from MD simulations using Poisson's equation and expressed as the double integral of the molecular charge density distributions $\rho(z)$:

$$\Phi(z) = -\varepsilon_0^{-1} \iint \rho(z'')dz''dz', \tag{1}$$

z being the position of the charge in the direction along the normal to the bilayer. The dipole potential (U_d) of the bilayers was defined as the electrostatic potential difference between the middle of the bilayer (hydrophobic core) and the bulk (solvent). The transmembrane voltage (U_t) on the other hand was defined as the electrostatic potential difference between the two bulk regions surrounding the bilayer. The electron density profiles, along the bilayer normal were derived directly from the MD simulations.

The capacitances of the membranes were calculated using the charge imbalance method [46,47]: Selected configurations from the equilibrated NPT (constant pressure and temperature) runs were used to set new systems, where the simulation box size was extended in direction (z) perpendicular to the membrane to create two air water interfaces. For these runs, the temperature was maintained at 298 and 323 K and the volume was maintained constant. Systems with charge imbalances of 0e, 2e, 4e, 6e and 8e were simulated for over 1 ns each. The last 0.5 ns of simulation were used to determine the electrostatic potential distribution, from which the transmembrane voltages (U_t) were calculated. For all simulations, U_t was found in a linear correlation with Q_{im} the charge imbalance normalized to the membrane area. Accordingly the capacitance of the bilayers was estimated as $C_{sp} = Q_{im}/U_t$.

The electroporation of the lipid bilayers was induced by applying high transmembrane voltages using the charge imbalance method. This method mimics the effect of low magnitude microsecond electric pulses [25,47]. The MD simulations of the systems at 298 and 323 K were run at several voltages. The electroporation threshold ($U_{EPthres}$) was reported as interval between the highest U_t at which lipid bilayers are not electroporated in the 100 ns time scale and the lowest U_t at which pores are created in the membrane.

Additional simulations at constant temperature (298 and 323 K) and constant pressure (98 kPa) were performed to estimate the pressure profiles $p(z)$ across the lipid bilayers [48]:

$$p(z) = \frac{1}{\Delta V}\left[\sum_i m_i \mathbf{v}_i \otimes \mathbf{v}_i - \sum_{i<j} \mathbf{F}_{ij} \otimes \mathbf{r}_{ij} f\left(z, z_i, z_j\right)\right], \tag{2}$$

Here $p(z)$ is the local pressure tensor in the slab centered on z, the sum over the kinetic term running over all atoms in the slab and $f(z, z_i, z_j)$ a weighting function. The calculations were all performed on the fly [43].

3. Results and discussion

3.1. Structural characteristics of the bilayers

The time evolutions of the average surface area per lipid molecule (A_m) for archaeal lipid bilayers and their mixtures with DPPC in

Table 1
Properties of the equilibrated archaeal lipids and their mixtures with DPPC bilayers from MD simulations.

Buffer	Bilayer	T/K	t_{sim}/ns	A_m/Å^2	U_d/V	C_{sp}/μF cm^{-2}
0.45 mol l^{-1} KCl	Archaeal lipids	298	53	82.5 ± 0.3	0.23	0.67
		323	31	86.0 ± 0.6	0.23	0.72
		343	25	86.8 ± 0.6	0.20	–
		363	31	90.4 ± 0.7	0.18	–
	Archaeal lipids + DPPC	298	26	69.1 ± 0.7	0.42	0.68
		323	31	72.0 ± 0.9	0.42	0.68
		343	21	73.8 ± 0.7	0.42	–
Na^+ counter ions	Archaeal lipids	298	18	83.4 ± 0.4	–	–
		343	33	86.7 ± 0.7	–	–
	Archaeal lipids + DPPC	298	34	68.9 ± 0.4	–	–
		343	23	74.6 ± 0.9	–	–

For comparison the capacitance of DPPC bilayers at 323 K is 0.9 μF cm^{-2} [51] (– not calculated).
T – temperature.
t_{sim} – simulation time.
A_m – area per lipid molecule.
U_d – membrane dipole potential.
C_{sp} – specific capacitance of bilayer.

0.45 mol l^{-1} KCl and in water with Na^+ counter ions extracted from the MD simulations performed at different temperatures show that the bilayers were well equilibrated within few tens of ns (data not shown). The obtained molecular and electrical properties of equilibrated membranes are shown in Table 1. The values of A_m are somewhat larger in the archaeal lipid membranes compared with the membranes with mixtures of archaeal lipids and DPPC. They increase with increasing temperature in all studied bilayers. Quite interestingly, the presence of buffer in the systems has practically no effect on A_m.

We have computed the electron density profiles from MD simulations and compared them to those extracted from SAXS data on vesicle samples of the same composition determined at 298 and 343 K to evaluate the quality of the time averaged structure from our simulations. These electron densities (Fig. 2) of each bilayer were found to be in very good agreement. The comparison of profiles of the bilayer in two different buffers estimated from the simulations (data not presented) shows that the buffer has practically no effect on the electron densities of the membrane.

3.2. Dipole potentials

The electrostatic potential profiles across the archaeal lipid bilayers and their mixtures with DPPC were estimated from the charge distribution of their components (cf. methods). The analyses indicate that varying the temperature does not modify the electrostatic potential profiles (data not shown). It is also noticeable that regardless of composition, changes in the temperatures of the systems do not seem to affect much the dipole potential (U_d) of the bilayers (cf. Table 1). However, U_d changes moderately with the lipid composition in particular as DPPC is added. Indeed, archaeal lipid bilayers have a dipole potential of ~0.2 V and this values almost doubles when DPPC is added at 50 mol%. This dipole potential remains though much smaller than that obtained under similar conditions (force fields and simulation protocols) for pure DPPC bilayers (0.7 V) [24].

3.3. Membrane capacitances

The lipid bilayers were subject to transmembrane voltages (U_t) created using the charge imbalance method. As previously shown, this protocol mimics the effect of low magnitude microsecond electric pulses [25,47]. As depicted in Fig. 3, U_t were found to be proportional to (Q_{im}), the charge imbalance per lipid unit area as found for a variety of other lipid bilayers [24,47,49]. By imposing charge imbalances ranging from 0e to 8e to the modeled systems at 0.45 mol l^{-1} KCl, we have estimated their capacitances [24,47,49]. At 323 K, the latter amount to 0.7 μF cm^{-2} for all lipid bilayers studied here. These values are lower than those of pure DPPC bilayers (0.9 μF cm^{-2}) [24]. This difference is probably mainly rooted in the fact that archaeal lipids, having longer tails, form thicker bilayers. Finally, we found no difference in the capacitances of the bilayers composed of archaeal lipids and their mixtures with DPPC estimated at 298 and 323 K.

3.4. Electroporation thresholds and pores morphologies

We have performed additional simulations at higher charge imbalances and consequently higher transmembrane voltages to trigger electroporation of the bilayers under investigation (cf. Table 2).

Several authors have described MD simulations of zwitterionic (mostly PC based) lipid membranes subject to high transmembrane voltages [12–16]. When the TM voltage is above a threshold value

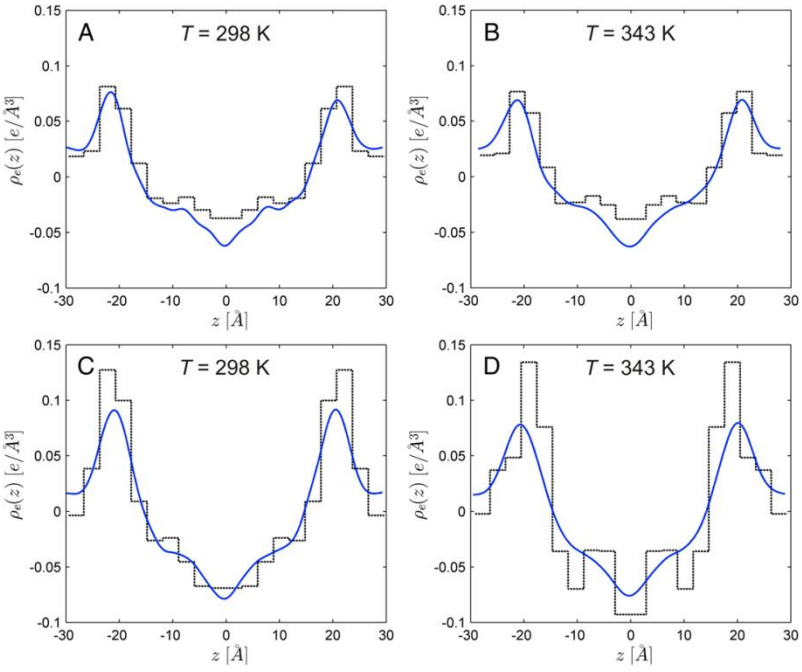

Fig. 2. SAXS derived electron density profiles of liposomes composed of archaeal lipids (A and B) and their mixtures with DPPC (C and D) at 298 and 343 K (dashed black line) and density profiles derived from the MD simulations (blue full line).

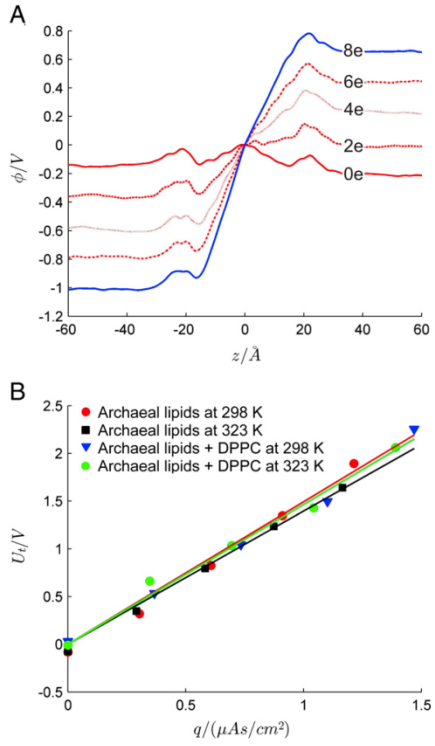

Fig. 3. A) Electrostatic potential profiles (ϕ) across the archaeal lipid bilayers at 323 K (as a function of z distance from the bilayer center) for simulations performed at different net charge imbalances Q (0e to 8e) between the upper and lower electrolytes. B) Transmembrane potentials (U_t) across the archaeal lipids and their mixtures with DPPC bilayers as a function of q, the charge imbalance normalized to the area of bilayers. The slopes represent linear fits to the data that permits estimates of the bilayers capacitances.

Table 2
Electrical and pore characteristics of the archaeal lipids and their mixtures with DPPC in bilayers under various transmembrane voltages created by a net charge imbalance.

Bilayer	T/K	Q_{im}/e	U_t/V	t_{sim}/ns	t_{water}/ns	t_{ion}/ns
Archaeal lipids	298	22	5.0	60	–	–
		24	5.4	59	50.0	58.1
		26	5.9	25	22.1	23.0
		28	6.3	10	7.8	8.4
		30	6.8	3	–	–
	323	20	4.1	61	–	–
		22	4.5	38	26.0	27.4
		24	4.9	10	5.0	6.3
		26	5.3	10	1.2	1.4
Archaeal lipids + DPPC	298	14	3.9	61	–	–
		16	4.3	57	50.5	55.0
		18	4.8	10	5.6	8.7
		20	5.4	10	4.6	5.8
		22	5.9	10	6.1	6.7
		24	6.5	10	1.4	1.6
	323	14	3.6	66	–	–
		16	4.1	23	20.8	22.1
		18	4.6	10	2.8	3.7
		20	5.1	7	2.1	3.3
		22	5.6	10	1.5	1.6

T – temperature.
Q_{im} – charge imbalance.
U_t – transmembrane voltage.
t_{sim} – simulation time.
t_{water} – time when first water wire is formed.
t_{ion} – time when first ions goes through the pore.

characteristic of the lipid composition, the membrane loses its integrity. This enables to increase substantially the ionic and molecular transport through the otherwise impermeable membranes [17]. Electroporation starts with the formation of water fingers that protrude inside the hydrophobic core of the membrane. Within nanoseconds, water wires bridging the two sides of the lipid bilayer appear. If the simulations are further extended, few lipid head-groups migrate along one water wire and form a hydrophilic connected pathway; if the voltage is maintained the ions present in solution start to flow through this pathway from one side of the membrane to the other. If the TM voltage is lowered, or is reduced due to ionic flow across the membrane, the pores collapse to reach a non-solvated and non-conductive state [13,24,25]. It was shown that the full recovery of the membrane integrity (migration of the lipid head groups back to the lipid water interface) requires few tens of nanoseconds.

In the present case (cf Fig. 4), for archaeal lipid bilayers, as reported for zwitterionic membranes, the process of electroporation starts with the protrusion of water fingers from either one or both sides of the membrane. Water defects appear within few nanoseconds then merge to form a complete transmembrane wire. Such a defect, hereafter called a "hydrophobic pore" to indicate that the water columns are in contact with the hydrophobic lipid tails, then expands in width. Surprisingly, in all the trajectories, the pores remained "hydrophobic" i.e. no lipid head groups moved toward the interior of the lipid hydrophobic core along these water wires. Regardless of this nature of the pore, ions were then driven along the electrical gradient (cf Fig. 4). Hence, in contrast to previously reported behavior of PC based lipids, the archaeal lipids forming the bilayer did not migrate toward the interior of the hydrophobic core to stabilize the water conducting pores. A similar behavior was also noted for the systems containing a fraction of DPPC. The series of simulations performed along with the characteristic times: t_{water} (time when the first water wire was created in the lipid bilayer) and t_{ion} time at which the first ions went through the pore created are reported in Table 2.

In the cases where test voltages did not lead to the creation of the pore (for simulation times (t_{sim}) exceeding 60 ns), we concluded that the electroporation threshold $U_{EPthres}$ was higher. We defined therefore the latter as lying between the U_t values where the pores have not occurred and the U_t values where we observed the pore creation. The $U_{EPthres}$ intervals found for archaeal lipids are reported in Fig. 5 and compared to those DPPC, DPhPC-ester and -ether derived from a previous study [24].

4. Discussion

In the present study we investigated the properties and electroporation thresholds of bilayers formed by archaeal lipids (AI and AGI) and their mixtures with DPPC using MD simulations. Prior to the examination of the response to electrical stress of these bilayers, we have compared their structural characteristics to those determined by small angle X-ray scattering. The electron density profiles derived from MD simulations were found to agree very well with the ones determined from SAXS measurements providing therefore some confidence in the force fields and protocols adopted in the simulations.

The configurational sampling of the lipids partitioning in a mixed composition bilayer is a very slow process, and there is always a nagging question whether the results of finite time simulations depend on the initial membrane configuration. One possibility to overcome this

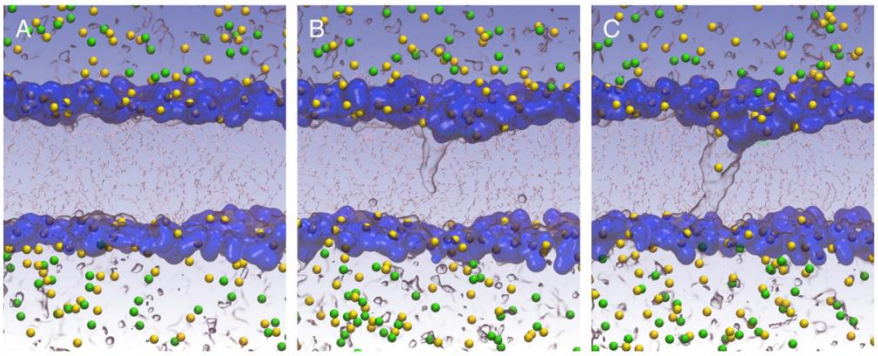

Fig. 4. Electroporation of archaeal lipid bilayers (snapshots at successive times after imposing a transmembrane voltage above the threshold): A) initial configuration, B) formation of water wire and C) formation of conducting 'hydrophobic' pore (white — lipid tails (between lipid headgroups), blue — lipid headgroups, yellow — potassium ion, green — chloride ion, water — gray surface).

would be to perform MD simulations using coarse grain models [50], but today, there are not yet robust force-fields to represent archaeal lipids. Here we have assumed that the AI at this concentration (10 mol% lipid content) does not aggregate but partition uniformly in the bilayer. We have then mainly relied on the comparison of the structural features to SAXS data to gain some confidence in the membrane model.

Before proceeding with the study of the archaeal lipids electroporation we have sought to determine and check some key properties of the bilayers. Among these, the dipole potential and capacitance as we have previously shown can be directly estimated from simulations and compared to experiments. The charge and molecular dipole distributions in the anisotropic lipid bilayers are at the origin of an intrinsic electrostatic profile (EP) across the membrane. In their pioneering work [51], from the measurements of the partition coefficients of fat-soluble tetraphenylboron anions and fat-soluble triphenylphosphonium cations between the membrane and aqueous phases, Liberman and Topaly hypothesized that the inner part of the bilayer membrane must be initially positively charged. The absolute value of this "dipole potential" has been very difficult to measure or predict [52–54], and estimates obtained from various methods and for various lipids range from 200 to 1000 mV. More recent and direct measurement based on Cryo-EM imaging [54] and atomic force microscopy (AFM) [55] techniques showed that the dipole potential can be "measured" in a noninvasive manner and estimate its value to few 100 mV. The large body of data from the simulations of fully hydrated lipid bilayers is found in qualitative agreement with experiments, showing that the EP profile monotonically increases across the membrane–water interface [41,42,54,56,57]. Given the diversity of the lipids studied and more significantly of the force fields used, values of dipole potentials ranging from 500 to 1200 mV have been reported [46,53,54,58–60]. The dipole potential measured here for archaeal lipids were found in this range (~200 mV). Though direct estimates from experiments for membranes of this composition are not available, it is worth to note that the results we obtained in a recent study for diphytanoyl-PC (DPhPC) [24], a lipid with tails similar to those of the archaeal lipids amount to 700 mV and 360 mV for the ester and ether forms which matches very well the data from [54] 510 mV and 260 mV, respectively. In particular the force fields used are good enough to reproduce the 50% decrease in the dipole potential from ester to ether lipids.

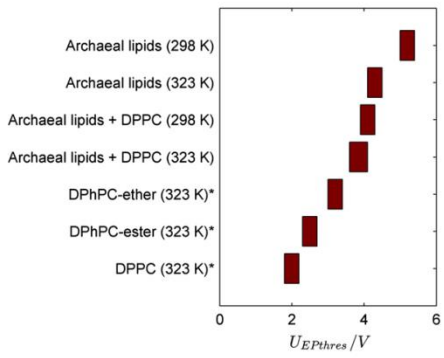

Fig. 5. Electroporation thresholds ($U_{EPthres}$) intervals determined from the MD simulations for the archaeal lipids and their mixtures with DPPC at 298 and 323 K. $U_{EPthres}$ of DPPC, DPhPC-ester and DPhPC-ether were adopted from [24]*.

The MD protocols used here allow one also to estimate the capacitance of the bilayer at specific ionic strength and for a given salt composition. Here, the value found for the archaeal lipids, to the best of our knowledge not determined yet experimentally amounts to 0.7 μF cm^{-2}, which is in within the magnitude of the capacitances found in similar systems (DPhPC). Taken together, these initial analyses of the MD simulations strengthen our confidence in the force fields used as far as the electrostatic properties of the membranes modeled here are concerned.

Accordingly, these protocols were further used to study the stability of archaeal lipids bilayers and their mixtures with DPPC when subject to transmembrane voltages using a method mimicking the effect of low magnitude microsecond electric pulses [25,47]. The electroporation thresholds ($U_{EPthres}$) found here are probably overestimated as are all the electroporation thresholds determined so far from MD simulations [25,49]. Indeed, the $U_{EPthres}$ of planar lipid bilayers formed of phospholipids estimated using simulations are above 1.5 V [24,25,61] while the experimentally measured voltage breakdown of planar lipid bilayers ranges rather from 200 mV to 600 mV [62]. The reasons behind such large discrepancies are to date unclear.

At any rate, our calculations show that the archaeal lipid membranes have a much higher $U_{EPthres}$ than all other bilayers composed of simple phospholipids studied so far. The properties of lipids which contribute to the stability of membranes might be numerous and diverse, but include at least (a) the structure of the lipid tails, (b) the chemical nature of the head group and (c) the nature of the head to tail linkage

(ester or ether). The studied archaeal lipids have special head groups carrying inositol and glucose functions. In comparison to simple phosphatidylcholine (PC) head groups these carbohydrates are larger moieties that move much more slowly. Furthermore and as importantly, the carbohydrates in the lipid head groups are packed and are involved in hydrogen bonds. As clearly evident from the data (Fig. 5) and comparing $U_{EPthres}$ between DPhPC and archaeal lipids, these special head group moieties contribute substantially to the increase of these bilayers electroporation thresholds.

More so the head-group/head-group and tail/tail moieties interactions in a membrane composed of lipid mixtures play a key, yet not evident role in their electrical stability. Uitert et al. [63] showed for instance that stability of lipid membranes composed of two types of lipids is not necessarily linearly dependent on the concentration of one species, highlighting the fact that the behavior of mixtures cannot easily be predicted. Other examples are found in the literature. For instance, the electrical stability of POPC membranes increases with the addition of cholesterol up to 50% [64], while the stability of DPhPC membranes increases with addition of cholesterol only up to 10%, then decreases at higher concentration: at cholesterol ratios of ~50%, the electrical stability of DPhPC is even lower than stability of pure DPhPC [63].

The archaeal lipids studied here have very complex structure in comparison to the DPPC or even DPhPC. It is very hard to predict, how the electrical stability of their mixtures with a second component (here DPPC) vary with the lipid composition. The DPPC lipid tails are not as long as those of archaeal lipids and they are formed of simple acyl chains. It is unclear how their zwittterionic and smaller head groups affect the bilayer electrical stability. Both characteristics namely influence the packing of the lipids in the bilayer.

Shinoda et al. have performed an extensive study of water permeability [65] in DPPC and DPhPC bilayers that may perhaps provide a rationale for the increased electroporation threshold, due to branched lipid tails. The authors show from analyses of local diffusion coefficients that water molecules have considerably reduced mobility in the DPhPC membrane interior as compared with the DPPC membrane interior. As a result of reduced water diffusion in the branch-chained membrane, the water permeability of the DPhPC bilayer was less than that of the DPPC bilayer by about 30%. As such permeability or diffusion toward the interior of the membrane is the very initial and key step in electroporation, we expect that this has a direct incidence on $U_{EPthres}$. One note along these lines that our previous study of bilayers composed of DPhPC-ester showed the increase of $U_{EPthres}$ compared to DPPC bilayers due to change in the lipid tails composition [24].

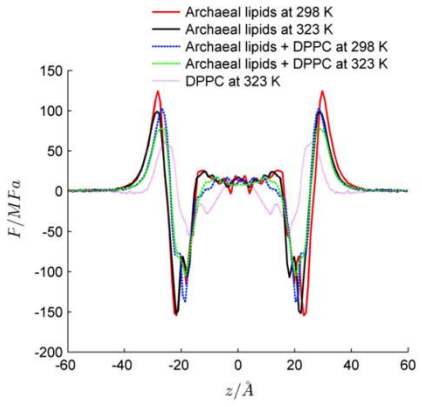

Fig. 6. The lateral pressure profile of archaeal lipid bilayers and their mixtures with DPPC in 0.45 mol l^{-1} KCl and at 298 and 323 K and the DPPC bilayers at 323 K.

Seeking to identify how such characteristics can change in the electroporation thresholds, we have computed the lateral pressure profiles of the archaeal lipid membranes and their mixtures with DPPC and pure DPPC (Fig. 6). The profiles show higher peaks in hydrophilic head group region as well as in the hydrophobic core region. The same effect was observed at comparison of DPPC and DPhPC lipids [24]. One may speculate in line with our previous finding that a direct implication of such characteristics is also to lower the permeability of water and therefore to increase the electroporation threshold. Similarly, the temperature, another key factor in the lipid chains mobility is shown here to affect $U_{EPthres}$.

In contrast, the capacitances of the bilayers studied here do not seem to correlate to any extent with the electroporation thresholds, since these were found essentially unchanged with bilayers composition. Counter intuitively also to what was expected, the bilayers dipole potentials magnitudes are not directly correlated with the value of $U_{EPthres}$. These dipole potentials are proportional to the strength of the electric field at the bilayer headgroup/water interfaces. The one of archaeal lipid bilayers is much lower than that of pure PC lipids and increases with increasing concentration of DPPC lipids in the mixtures, while the thresholds of electroporation subsequently decrease.

5. Conclusion

In this study we showed that archaeal lipids with their special moieties i.e. methyl groups in tails, ether linkages instead of ester linkages and carbohydrates in the head groups have much higher stability than other simple lipids studied so far. We also showed that by mixing the archaeal lipids with phospholipids, one can lower their stability. Tuning in the electroporation threshold by lipid composition provides new routes for the design of liposomes composition that can be efficiently used as drug delivery carriers, and for which quantitatively monitored electroporation can serve for subsequent release of the drug when the carrier has reached proper location.

Abbreviations

T	temperature
t_{sim}	simulation time
A_m	area per lipid molecule
U_d	membrane dipole potential
C_{sp}	specific capacitance of bilayer
Q_{im}	charge imbalance
U_t	transmembrane voltage
t_{sim}	simulation time
t_{water}	time when first water wire is formed
t_{ion}	time when first ions goes through the pore

Acknowledgment

Research was conducted within the scope of the EBAM European Associated Laboratory. This work was in part supported by the Slovenian Research Agency (J2-3639, P1-0201 and P2-0249). The manuscript is a result of the networking efforts of COST Action TD1104 (www.electroporation.net). Part of the calculations and finalization of the paper was performed during the Short Term Scientific Mission Grant STSM [070113-021794] to Andraž Polak. Simulations were performed by using HPC resources from GENCI-CINES (Grant 2012–2013 [076434]).

References

[1] T. Benvegnu, M. Brard, D. Plusquellec, Archaeabacteria bipolar lipid analogues: structure, synthesis and lyotropic properties, Curr. Opin. Colloid Interface Sci. 8 (2004) 469–479.
[2] N.P. Ulrih, D. Gmajner, P. Raspor, Structural and physicochemical properties of polar lipids from thermophilic archaea, Appl. Microbiol. Biotechnol. 84 (2009) 249–260.
[3] N.P. Ulrih, U. Adamlje, M. Nemec, M. Sentjurc, Temperature- and pH-induced structural changes in the membrane of the hyperthermophilic archaeon *Aeropyrum pernix* K1, J. Membr. Biol. 219 (2007) 1–8.
[4] Y. Sako, N. Nomura, A. Uchida, Y. Ishida, H. Morii, Y. Koga, et al., *Aeropyrum pernix* gen. nov., sp. nov., a novel aerobic hyperthermophilic archaeon growing at temperatures up to 100 °C, Int. J. Syst. Bacteriol. 46 (1996) 1070–1077.
[5] H. Morii, H. Yagi, H. Akutsu, N. Nomura, Y. Sako, Y. Koga, A novel phosphoglycolipid archaetidyl(glucosyl)inositol with two sesterterpanyl chains from the aerobic hyperthermophilic archaeon *Aeropyrum pernix* K1, Biochim. Biophys. Acta, Mol. Cell. Biol. Lipids 1436 (1999) 426–436.
[6] M.J. Hanford, T.L. Peeples, Archaeal tetraether lipids: unique structures and applications, Appl. Biochem. Biotechnol. 97 (2002) 45–62.
[7] T.A. Elbayoumi, V.P. Torchilin, Current trends in liposome research, Methods Mol. Biol. 605 (2010) 1–27.
[8] T.B. Napotnik, M. Rebersek, T. Kotnik, E. Lebrasseur, G. Cabodevila, D. Miklavcic, Electropermeabilization of endocytotic vesicles in B16 F1 mouse melanoma cells, Med. Biol. Eng. Comput. 48 (2010) 407–413.
[9] L. Retelj, G. Pucihar, D. Miklavcic, Electroporation of intracellular liposomes using nanosecond electric pulses—a theoretical study, IEEE Trans. Biomed. Eng. 60 (2013) 2624–2635.
[10] E. Neumann, K. Rosenheck, Permeability changes induced by electric impulses in vesicular membranes, J. Membr. Biol. 10 (1972) 279–290.
[11] S. Haberl, D. Miklavcic, G. Sersa, W. Frey, B. Rubinsky, Cell membrane electroporation-Part 2: the applications, IEEE Electr. Insul. Mag. 29 (2013) 29–37.
[12] M. Tarek, Membrane electroporation: a molecular dynamics simulation, Biophys. J. 88 (2005) 4045–4053.
[13] Z.A. Levine, P.T. Vernier, Life cycle of an electropore: field-dependent and field-independent steps in pore creation and annihilation, J. Membr. Biol. 236 (2010) 27–36.
[14] D.P. Tieleman, The molecular basis of electroporation, BMC Biochem. 5 (2004) 10.
[15] H. Leontiadou, A.E. Mark, S.-J. Marrink, Ion transport across transmembrane pores, Biophys. J. 92 (2007) 4209–4215.
[16] A. Cordomí, O. Edholm, J.J. Perez, Effect of ions on a dipalmitoyl phosphatidylcholine bilayer. A molecular dynamics simulation study, J. Phys. Chem. B 112 (2008) 1397–1408.
[17] M. Breton, L. Delemotte, A. Silve, L.M. Mir, M. Tarek, Transport of siRNA through lipid membranes driven by nanosecond electric pulses: an experimental and computational study, J. Am. Chem. Soc. 134 (2012) 13938–13941.
[18] E. Tekle, H. Oubrahim, S.M. Dzekunov, J.F. Kolb, K.H. Schoenbach, P.B. Chock, Selective field effects on intracellular vacuoles and vesicle membranes with nanosecond electric pulses, Biophys. J. 89 (2005) 274–284.
[19] T. Portet, C. Favard, J. Teissié, D.S. Dean, M.-P. Rols, Insights into the mechanisms of electromediated gene delivery and application to the loading of giant vesicles with negatively charged macromolecules, Soft Matter 7 (2011) 3872.
[20] P. Kramar, D. Miklavcic, A.M. Lebar, Determination of the lipid bilayer breakdown voltage by means of linear rising signal, Bioelectrochemistry 70 (2007) 23–27.
[21] T. Portet, F. Camps i Febrer, J.-M. Escoffre, C. Favard, M.-P. Rols, D.S. Dean, Visualization of membrane loss during the shrinkage of giant vesicles under electropulsation, Biophys. J. 96 (2009) 4109–4121.
[22] M.J. Ziegler, P.T. Vernier, Interface water dynamics and porating electric fields for phospholipid bilayers, J. Phys. Chem. B 112 (2008) 13588–13596.
[23] P.T. Vernier, Z.a. Levine, M.a. Gundersen, Water bridges in electropermeabilized phospholipid bilayers, Proc. IEEE 101 (2013) 494–504.
[24] A. Polak, D. Bonhenry, F. Dehez, P. Kramar, D. Miklavčič, M. Tarek, On the electroporation thresholds of lipid bilayers: molecular dynamics simulation investigations, J. Membr. Biol. 246 (2013) 843–850.
[25] L. Delemotte, M. Tarek, Molecular dynamics simulations of lipid membrane electroporation, J. Membr. Biol. 245 (2012) 531–543.
[26] R. a Böckmann, B.L. de Groot, S. Kakorin, E. Neumann, H. Grubmüller, Kinetics, statistics, and energetics of lipid membrane electroporation studied by molecular dynamics simulations, Biophys. J. 95 (2008) 1837–1850.
[27] D. Needham, R.M. Hochmuth, Electro-mechanical permeabilization of lipid vesicles. Role of membrane tension and compressibility, Biophys. J. 55 (1989) 1001–1009.
[28] M.L. Fernández, G. Marshall, F. Sagués, R. Reigada, Structural and kinetic molecular dynamics study of electroporation in cholesterol-containing bilayers, J. Phys. Chem. B 114 (2010) 6855–6865.
[29] I. Milek, B. Cigic, M. Skrt, G. Kaletunç, N.P. Ulrih, Optimization of growth for the hyperthermophilic archaeon Aeropyrum pernix on a small-batch scale, Can. J. Microbiol. 51 (2005) 805–809.
[30] D. Gmajner, A. Ota, M. Sentjurc, N.P. Ulrih, Stability of diether C(25,25) liposomes from the hyperthermophilic archaeon *Aeropyrum pernix* K1, Chem. Phys. Lipids 164 (2011) 236–245.
[31] E.G. Bligh, W.J. Dyer, A rapid method of total lipid extractin and purification, Can. J. Biochem. Physiol. 37 (1959) 911–917.
[32] O. Kratky, H. Stabinger, X-ray small angle camera with block-collimation system an instrument of colloid research, Colloid Polym. Sci. 262 (1984) 345–360.
[33] D. Orthaber, A. Bergmann, O. Glatter, SAXS experiments on absolute scale with Kratky systems using water as a secondary standard, J. Appl. Crystallogr. 33 (2000) 218–225.
[34] O. Glatter, A new method for the evaluation of small-angle scattering data, J. Appl. Crystallogr. 10 (1977) 415–421.
[35] O. Glatter, Evaluation of small-angle scattering data from lamellar and cylindrical particles by the indirect transformation method, J. Appl. Crystallogr. 13 (1980) 577–584.
[36] D.J. Iampietro, L.L. Brasher, E.W. Kaler, A. Stradner, O. Glatter, Direct analysis of SANS and SAXS measurements of catanionic surfactant mixtures by Fourier transformation, J. Phys. Chem. B 102 (1998) 3105–3113.
[37] T. Sato, H. Sakai, K. Sou, M. Medebach, O. Glatter, E. Tsuchida, Static structures and dynamics of hemoglobin vesicle (HBV) developed as a transfusion alternative, J. Phys. Chem. B 113 (2009) 8418–8428.
[38] O. Glatter, Convolution square root of band-limited symmetrical functions and its application to small-angle scattering data, J. Appl. Crystallogr. 14 (1981) 101–108.
[39] O. Glatter, B. Hainisch, Improvements in real-space deconvolution of small-angle scattering data, J. Appl. Crystallogr. 17 (1984) 435–441.
[40] R. Mittelbach, O. Glatter, Direct structure analysis of small-angle scattering data from polydisperse colloidal particles, J. Appl. Crystallogr. 31 (1998) 600–608.
[41] J.B. Klauda, R.M. Venable, J.A. Freites, J.W. O'Connor, D.J. Tobias, C. Mondragon-Ramirez, et al., Update of the CHARMM all-atom additive force field for lipids: validation on six lipid types, J. Phys. Chem. B 114 (2010) 7830–7843.
[42] K. Shinoda, W. Shinoda, T. Baba, M. Mikami, Comparative molecular dynamics study of ether- and ester-linked phospholipid bilayers, J. Chem. Phys. 121 (2004) 9648–9654.
[43] L. Kalé, R. Skeel, M. Bhandarkar, R. Brunner, A. Gursoy, N. Krawetz, et al., NAMD2: greater scalability for parallel molecular dynamics, J. Comput. Phys. 151 (1999) 283–312.
[44] U. Essmann, L. Perera, M.L. Berkowitz, T. Darden, H. Lee, L.G. Pedersen, A smooth particle mesh Ewald method, J. Chem. Phys. 103 (1995) 8577.
[45] T. Darden, D. York, L. Pedersen, Particle mesh Ewald: an N·log(N) method for Ewald sums in large systems, J. Chem. Phys. 98 (1993) 10089.
[46] J.N. Sachs, P.S. Crozier, T.B. Woolf, Atomistic simulations of biologically realistic transmembrane potential gradients, J. Chem. Phys. 121 (2004) 10847–10851.
[47] L. Delemotte, F. Dehez, W. Treptow, M. Tarek, Modeling membranes under a transmembrane potential, J. Phys. Chem. B 112 (2008) 5547–5550.
[48] E. Lindahl, O. Edholm, Spatial and energetic–entropic decomposition of surface tension in lipid bilayers from molecular dynamics simulations, J. Chem. Phys. 113 (2000) 3882.
[49] P. Kramar, L. Delemotte, A. Maček Lebar, M. Kotulska, M. Tarek, D. Miklavčič, Molecular-level characterization of lipid membrane electroporation using linearly rising current, J. Membr. Biol. 245 (2012) 651–659.
[50] H.I. Ingólfsson, C.a. Lopez, J.J. Uusitalo, D.H. de Jong, S.M. Gopal, X. Periole, et al., The power of coarse graining in biomolecular simulations, Wiley Interdiscip. Rev. Comput. Mol. Sci. 00 (2013).
[51] E. Liberman, V. Topaly, Permeability of bimolecular phospholipid membranes for fat-soluble ions, Biophysics (1968) 477–487.
[52] R.J. Clarke, The dipole potential of phospholipid membranes and methods for its detection, Adv. Colloid Interface Sci. 89–90 (2001) 263–281.
[53] A.P. Demchenko, S.O. Yesylevskyy, Nanoscopic description of biomembrane electrostatics: results of molecular dynamics simulations and fluorescence probing, Chem. Phys. Lipids 160 (2009) 63–84.
[54] L. Wang, P.S. Bose, F.J. Sigworth, Using cryo-EM to measure the dipole potential of a lipid membrane, Proc. Natl. Acad. Sci. U. S. A. 103 (2006) 18528–18533.
[55] Y. Yang, K.M. Mayer, N.S. Wickremasinghe, J.H. Hafner, Probing the lipid membrane dipole potential by atomic force microscopy, Biophys. J. 95 (2008) 5193–5199.
[56] K. Gawrisch, D. Ruston, J. Zimmerberg, V. a Parsegian, R.P. Rand, N. Fuller, Membrane dipole potentials, hydration forces, and the ordering of water at membrane surfaces, Biophys. J. 61 (1992) 1213–1223.
[57] U. Peterson, D. a Mannock, R.N.A.H. Lewis, P. Pohl, R.N. McElhaney, E.E. Pohl, Origin of membrane dipole potential: contribution of the phospholipid fatty acid chains, Chem. Phys. Lipids 117 (2002) 19–27.
[58] M.L. Berkowitz, D.L. Bostick, S. Pandit, Aqueous solutions next to phospholipid membrane surfaces: insights from simulations, Chem. Rev. 106 (2006) 1527–1539.
[59] R.J. Mashl, H.L. Scott, S. Subramaniam, E. Jakobsson, Molecular simulation of dioleoylphosphatidylcholine lipid bilayers at differing levels of hydration, Biophys. J. 81 (2001) 3005–3015.
[60] A.M. Smondyrev, M.L. Berkowitz, Structure of dipalmitoylphosphatidylcholine/cholesterol bilayer at low and high cholesterol concentrations: molecular dynamics simulation, Biophys. J. 77 (1999) 2075–2089.
[61] P.T. Vernier, M.J. Ziegler, Y. Sun, M. a Gundersen, D.P. Tieleman, Nanopore-facilitated, voltage-driven phosphatidylserine translocation in lipid bilayers—in cells and in silico, Phys. Biol. 3 (2006) 233–247.
[62] M. Kotulska, P. Kramar, D. Miklavc, Voltage- and current-clamp methods for determination of planar lipid bilayer properties, in: A. Iglič (Ed.), Adv. Planar Lipid Bilayers Liposomes, vol. 11, Elsevier, Amsterdam, 2010, pp. 29–69.
[63] I. van Uitert, S. Le Gac, A. van den Berg, The influence of different membrane components on the electrical stability of bilayer lipid membranes, Biochim. Biophys. Acta 1798 (2010) 21–31.
[64] M. Naumowicz, Z.A. Figaszewski, Pore formation in lipid bilayer membranes made of phosphatidylcholine and cholesterol followed by means of constant current, Cell Biochem. Biophys. 66 (2013) 109–119.
[65] W. Shinoda, M. Mikami, T. Baba, M. Hato, Molecular dynamics study on the effects of chain branching on the physical properties of lipid bilayers: 2. Permeability, J. Phys. Chem. B 108 (2004) 9346–9356.

Andraž Polak was born in 1986. He received his B.Sc. degree in Electrical Engineering from the University of Ljubljana, Slovenia, in 2010. He is currently a Ph.D. student in the Department of Biomedical Engineering at the Faculty of Electrical Engineering of the University of Ljubljana. His current research interests include electroporation of planar lipid bilayers on experimental and modeling level.

Nataša Poklar Ulrih was born in 1965. She received a Ph.D. in Physical Chemistry from the University of Ljubljana, Slovenia, in 1994. She is a full professor of Biochemistry, head of the Chair of Biochemistry and Food Chemistry, and vice-dean of the Department of Food Science and Technology at the Biotechnical Faculty, University of Ljubljana. During the last few years she is interested in the molecular mechanism of adaptation of archaea to extreme environmental conditions.

Mounir Tarek was born in 1964. He received a Ph.D. (1994) in Physics from the University of Paris. He is currently a senior research scientist (Directeur de Recherches) of the CNRS at the University of Lorraine, France. He joined the CNRS after 3 years as a postdoctoral scientist at the University of Pennsylvania, and a 4-year tenure at the National Institute of Standards and Technology, Gaithersburg, Maryland. During the last few years, he has worked on large-scale, state-of-the-art molecular simulations of lipid membranes and transmembrane proteins, probing their structure and dynamics.

Andrej Jamnik was born in 1961. He received his Ph.D. in Chemistry from the University of Ljubljana, Slovenia, in 1992. Currently he is a full professor of Physical Chemistry in the Faculty of Chemistry and Chemical Technology at the University of Ljubljana. His research focuses on the investigations of thermodynamic and structural properties of simple fluids, solutions and colloidal dispersions using theoretical methods based on principles of statistical mechanics (integral equation theories and computer simulations) and complementing experimental techniques based on scattering of light and X-rays.

Matija Tomšič was born in 1976. He received a Ph.D. on the Faculty of Chemistry and Chemical Technology (FKKT UL), University of Ljubljana, Slovenia, in 2004. He is currently a lecturer on the Chair of Physical Chemistry on the FKKT UL. After his studies he specialized in the field of light scattering methods and their application in structural research of various colloidal systems. His current research interests include structural aspects of bacterial polysaccharide systems, calculating small-wide-angle X-ray scattering (SWAXS) data of modeled liquids and their validation by experimental SWAXS results.

Peter Kramar was born in 1977. He received a Ph.D. in Electrical Engineering from the University of Ljubljana, Slovenia, in 2010. He is currently a teaching assistant in the Faculty of Electrical Engineering at the University of Ljubljana. His current research interests include electroporation of planar lipid bilayers.

Janez Valant was born in 1979. He received his Ph.D. in biochemistry and molecular biology at University of Ljubljana in 2010. He is currently employed as a postdoctoral scientist at University of Ljubljana, Biotechnical faculty. His current research interest includes toxicological aspects of nanoparticles, especially interactions of nanoparticles with lipid membranes.

Damijan Miklavčič was born in 1963. He received a Ph.D. in Electrical Engineering from the University of Ljubljana, Slovenia in 1993. He is currently a full professor, head of the Laboratory of Biocybernetics, and head of the Department of Biomedical Engineering at the Faculty of Electrical Engineering of the University of Ljubljana. During the last few years his research has been focused on electroporation-based gene transfer and drug delivery, development of electronic hardware, and numerical modeling of biological processes.

Paper 4

Title: Structural Properties of Archaeal Lipid Bilayers: Small-Angle X-Ray Scattering and Molecular Dynamics Simulation Study

Authors: Polak A, Tarek M, Tomšič M, Valant J, Poklar Ulrih N, Jamnik A, Kramar P, Miklavčič D

Publication: *Langmuir*

DOI: 10.1021/la5014208

Year: 2014

Volume: 30

Issue: 28

Pages: 8308-8315

Langmuir

Article

pubs.acs.org/Langmuir

Structural Properties of Archaeal Lipid Bilayers: Small-Angle X-ray Scattering and Molecular Dynamics Simulation Study

Andraž Polak,[†] Mounir Tarek,*[,‡,§] Matija Tomšič,[∥] Janez Valant,[⊥] Nataša Poklar Ulrih,[⊥] Andrej Jamnik,[∥] Peter Kramar,[†] and Damijan Miklavčič*[,†]

[†]Faculty of Electrical Engineering, University of Ljubljana, Tržaška cesta 25, SI-1000 Ljubljana, Slovenia

[‡]Université de Lorraine, UMR 7565, F-54506 Vandoeuvre-lès-Nancy, France

[§]CNRS, UMR 7565, F-54506 Vandoeuvre-lès-Nancy, France

[∥]Faculty of Chemistry and Chemical Technology, University of Ljubljana, Aškerčeva c. 5, SI-1000 Ljubljana, Slovenia

[⊥]Biotechnical Faculty, University of Ljubljana, Jamnikarjeva 101, SI-1000 Ljubljana, Slovenia

ABSTRACT: *Aeropyrum pernix* is an aerobic hyperthermophilic archaeon that grows in harsh environmental conditions and as such possesses unique structural and metabolic features. Its membrane interfaces with the extreme environment and is the first line of defense from external factors. Therefore, lipids composing this membrane have special moieties that increase its stability. The membrane of *A. pernix* is composed predominantly of two polar lipids 2,3-di-*O*-sesterterpanyl-*sn*-glicerol-1-phospho-1′(2′-*O*-α-D-glucosyl)-*myo*-inositol (AGI) and 2,3-di-*O*-sesterterpanyl-*sn*-glicerol-1-phospho-*myo*-inositol (AI). Both have methyl branches in their lipid tails and ether linkages and carbohydrates in their headgroup. These moieties significantly affect the structure and dynamics of the bilayer. To provide a molecular level insight into these characteristics, we used here Molecular Dynamics (MD) simulations of lipid bilayers of composition similar to those of the archaeal membranes. First, we show that the electron density profiles along the normal to the bilayers derived from the simulations are in good agreement with the profiles obtained by the small-angle X-ray scattering (SAXS) technique, which provides confidence in the force fields used. Analyses of the simulation data show that the archaeal lipid bilayers are less hydrated than conventional phosphatidylcholine (PC) lipids and that their structure is not affected by the salt present in the surrounding solution. Furthermore, the lateral pressure in their hydrophobic core, due to the presence of the branched tails, is much higher than that at PC-based lipid bilayers. Both the methyl branched tails and the special headgroup moieties contribute to slow drastically the lateral diffusion of the lipids. Furthermore, we found that the lipid head groups associate via hydrogen bonding, which affects their reorientational dynamics. All together, our data provide links between the microscopic properties of these membranes and their overall stability in harsh environments.

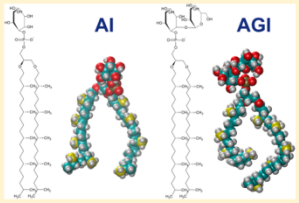

1. INTRODUCTION

Archaea are microorganisms that survive and grow at harsh environmental conditions and as such possess unique structural and metabolic features. They can be grouped on the basis of the extreme environmental conditions as follows: into halophiles that grow in high salt concentration, acidophiles that grow at low pH, alcalophiles that grow at high pH, thermophiles that grow at high temperatures, psychrophilic that grow at low temperatures, and many others.[1−3] The membranes of archaea cells interface with the extreme environment and are the first line of defense against external factors. Therefore, archaeal lipids that form these membranes have special moieties that increase their stability. They are composed in general by glycerophosphate head groups, ether linkages between glycerol moiety and hydrocarbon tails, methyl branching of hydrocarbon chains or hydrocarbon chains with cyclopentane rings, and sometimes are rather bipolar lipids with tetraether core and headgroup composed of carbohydrates.[2]

Aeropyrum pernix K1 is an aerobic hyperthermophilic archaea that grows in a coastal solfataric vent at Kodakara, Juma Island, Japan. It can live in temperatures up to 100 °C. The optimal growth conditions of *A. pernix* are temperature between 90 and 95 °C, pH 7.0, and salinity of 3.5%. The shape of the cells is spherical with a diameter from 0.8 to 1.2 μm.[4] The membranes of these archaea are composed of two lipids: 2,3-di-*O*-sesterterpanyl-*sn*-glicerol-1-phospho-1′(2′-*O*-α-D-glucosyl)-*myo*-inositol (AGI) and 2,3-di-*O*-sesterterpanyl-*sn*-glicerol-1-phospho-*myo*-inositol (AI) with molar ratio of AI and AGI as 9:91 mol %.[5] It has been shown that vesicles composed of AI and AGI lipids are very stable, capable of encapsulating potential substances, and may be uptaken into cells endocytotically.[6,7] It was also found that these lipids are nontoxic to CACO-2 and Hep G2 cells, only mildly toxic to B1-6F1 and CHO cells, and very toxic to EA.hy926 cells.[7]

In this Article, we investigate the structural properties of archaeal lipid bilayer, composed of polar lipids isolated from *A. pernix*, at different temperatures. The bilayers were first investigated using the small-angle X-ray scattering (SAXS) technique, which provided corresponding thickness pair-distance

Received: April 14, 2014
Revised: June 20, 2014
Published: June 25, 2014

dx.doi.org/10.1021/la5014208 | Langmuir 2014, 30, 8308−8315

distribution functions and the electron density profiles. These were then compared to the electron density profiles derived from MD simulations. From the equilibrated bilayers in the MD simulation, we fully characterized the structural and electrostatic properties of these bilayers. This study is an extension of our previous study entitled "Electroporation of Archaeal Lipid Membranes using MD Simulations".[8]

2. MATERIALS AND METHODS

2.1. Growth of *Aeropyrum pernix* K1. *A. pernix* was grown in a 1 L flask at 92 °C. The maximal biomass was obtained by adding $Na_2S_2O_3 \times 5H_2O$ (1 g of per liter) (Alkaloid, Skopje, Macedonia) to Marine Broth 2216 (Difco, Becton, Dickinson and Co., Sparks, U.S.) at pH 7.0 (20 mM HEPES buffer) as described before.[9] After growth, the cells were harvested by centrifugation, washed, and lyophilized.

2.2. Isolation and Purification of Lipids, and Vesicle Preparation. The total polar lipid methanol fraction composed of 91 mol % AGI and 9 mol % AI[5] (average molecular mass, 1181.42 g mol^{-1}) was purified from lyophilized *A. pernix* cells, as described previously.[6] After isolation, the lipids were fractionated with adsorption chromatography.[10] The liposomes were prepared by thin lipid film formation by drying the lipid sample on a rotary evaporator. The dried lipid films were then hydrated by 20 mM HEPES buffer pH 7.0 or deionized water (Milli-Q), temperature 45 °C. Multilamellar vesicles (MLV) were prepared by vortexing the lipid suspensions vigorously for 10 min. MLV were further transformed into large unilamellar vesicles (LUV) by six freeze (liquid nitrogen) and thaw (warm water) cycles and by pressure-extruded 21 times through 400 nm polycarbonate membranes on an Avanti polar mini-extruder (Avanti Polar Lipids, Alabastr, AL), at temperature between 50 and 60 °C. The lipid concentration in the samples for SAXS experiments was 10 mg/mL.

2.3. Small-Angle X-ray Scattering (SAXS) Measurements. SAXS measurements were performed on the modified Kratky compact camera (Anton Paar KG, Graz, Austria)[11] equipped with the focusing multilayer optics for X-rays (Osmic, Max-Flux). The camera was attached to a conventional X-ray generator Kristalloflex 760 (Bruker AXS GmbH, Karlsruhe, Germany) with a sealed X-ray tube (Cu K_α X-rays with a wavelength $\lambda = 0.154$ nm) operating at 40 kV and 35 mA. The samples were measured in a standard quartz capillary with an outer diameter of 1 mm and wall thickness of 10 μm. Position-sensitive detector PSD-50 M (M. Braun GmbH, Garching, Germany) was used for detection of the scattered x-rays in the small-angle regime of scattering vectors $0.1 < q < 7.5$ nm^{-1}, where, $q = 4\pi/\gamma \cdot \sin(\vartheta/2)$, ϑ representing the scattering angle. To get sufficient measuring statistics, each sample was measured for a period of 20 h. Prior to the detailed data analysis, the scattering data were corrected for the empty capillary and solvent scattering, and put on the absolute scale using water as a secondary standard.[12]

2.4. Evaluation of SAXS Data. Experimental SAXS data were evaluated utilizing the Generalized Indirect Fourier Transformation (GIFT) software package.[13−18] There were no interlamellar interference peaks observed in the scattering curves in our case. Similarly, the maximum dimension of the scattering particles (large unilamellar vesicles) was much bigger than the size resolution of the SAXS method; therefore, solely the basic part of the GIFT, that is, the Indirect Fourier Transformation (IFT) technique, was used.[19,20] In such cases, one can still extract the structural information on the thickness of the lipid bilayer from the scattering curves, because the thickness of the bilayer is usually still well within the experimental resolution of the SAXS method. For this purpose, the IFT technique is used in a special mode, where $I(q)q^2$ is cosine transformed into the real space yielding the thickness pair distance distribution function $p_t(r)$.[20−22] In this procedure, a considerable cutoff must be applied to the scattering curves in the regime of very low q values to exclude the part of the scattering curve that is strongly affected by the scattering contribution originating from the large dimensions of the lipid bilayer; in this way, solely the structural information related to the thickness of the lamellar bilayer can be extracted. Such an approach is based on the thickness form factor, $I_t(q)$, which represents the scattering due to the structure in perspective of the bilayer thickness and is completely model-free. The thickness form factor can be written as the cosine transformation of the thickness pair-distance distribution function $p_t(r)$:[20−22]

$$I(q)q^2 = 2\pi A I_t(q) = 4\pi A \int_0^\infty p_t(r)\cos(qr)\,dr \quad (1)$$

where r is the distance between two scattering centers within the particle. The resulting $p_t(r)$ function serves as a tool for the determination of the scattering particles geometry.[19−23] At distances r bigger than the thickness of the bilayer, the $p_t(r)$ function adopts the value of zero and in this way provides a useful tool for the determination of the bilayer thickness. In addition, the scattering contrast profile across the bilayer in direction perpendicular to its plane, which provides valuable information on the bilayer internal structure, can be calculated from the $p_t(r)$ function by a convolution square root operation utilizing the DECON program:[24−26]

$$p_t(r) = \int_{-\infty}^{\infty} \Delta\rho_e(z)\cdot\Delta\rho_e(z-r)\,dr \quad (2)$$

with $\Delta\rho_e(z)$ representing the local scattering contrast, that is, the difference between the local electron density at distance z from the center of symmetry (central plane in the middle of bilayer) and the average electron density of the sample $\overline{\rho}_e$. To facilitate comparison of MD and SAXS results, in further text the scattering contrast profile $\rho_e(z)$ will be referred to simply as the electron density profile and denoted with the symbol $\rho_e(z)$. Note that r in $p_t(r)$ corresponds to the distance in real space (information on the overall bilayer thickness), but z in the electron density profile is determined with respect to the central plane of the bilayer.

2.5. MD Simulations. The molecular dynamics (MD) models and simulations were adopted from our previous study.[8] The MD simulations presented here were carried out using the program NAMD.[27] The systems were examined in the NPT (constant number of atoms, pressure, and temperature) ensembles employing Langevin dynamics and the Langevin piston method. The time step for integrating the equations of motion was set at 2.0 fs. Short- and long-range forces were calculated every one and two time steps, respectively. Bonds between hydrogen and heavy atoms were constrained to their equilibrium value. Long-range, electrostatic forces were taken into account using the particle mash Ewald (PME) approach.[28,29] The structures of AI and AGI molecules, which compose the membrane of *A. pernix*, were suggested by Morii et al.[5] The MD models were built by combining the CHARMM 36 lipid force field and the CHARMM 36 carbohydrate force field. The parameters for ester linkages were adopted from Shinoda et al.[30]

First, the bilayer was composed of 64 lipids (6 AI and 58 AGI). The composition of the bilayer was a molar ratio of 9:91, which was measured experimentally.[5] The bilayer was surrounded by 10 283 water molecules, 144 potassium (K^+), and 80 chloride (Cl^-) ions (~0.45 M KCl). That system was equilibrated for 120 ns at constant numbers of atoms, constant pressure (1 atm), and constant temperature (50 °C) (NPT). The system then was replicated twice in the X and Y directions of the bilayer plane to afford a large membrane patch and equilibrated again at 90, 70, and 25 °C (NPT) for 30 ns. After the equilibration of systems at 70 and 25 °C, the potassium (K^+) and chloride (Cl^-) ions were removed, and then the counterions (Na^+) were added to neutralize the systems and equilibrated again for the 30 ns. The systems with counterions (Na^+) mimicked the situation during the SAXS experiments. The electron density profiles of these two systems were compared to electron density profiles obtained by experimental SAXS. These SAXS data were measured for the systems containing ~0.45 M KCl.

In all of the simulated systems, the average area per lipid was estimated by dividing the total area of the bilayer by the number of lipids in each leaflet. The thickness of the bilayer was defined as the distance between the two highest peaks of the electron density profile. The positions of these peaks correspond to the location of the lipid phosphate groups in bilayer. The radial distribution functions (RDFs) were calculated using the VMD GofRGUI Plugin. The in-plane lateral diffusion coefficients (D) of the lipids were estimated from the slopes of the mean squared displacements (MSDs) of the center of the molecules in the interval from 5 to 15 ns according to

$$D = \frac{1}{2d}\lim_{t\to\infty}\frac{1}{t}\langle|r(t-t_0) - r(t_0)|^2\rangle_z \quad (3)$$

dx.doi.org/10.1021/la5014208 | *Langmuir* 2014, 30, 8308−8315

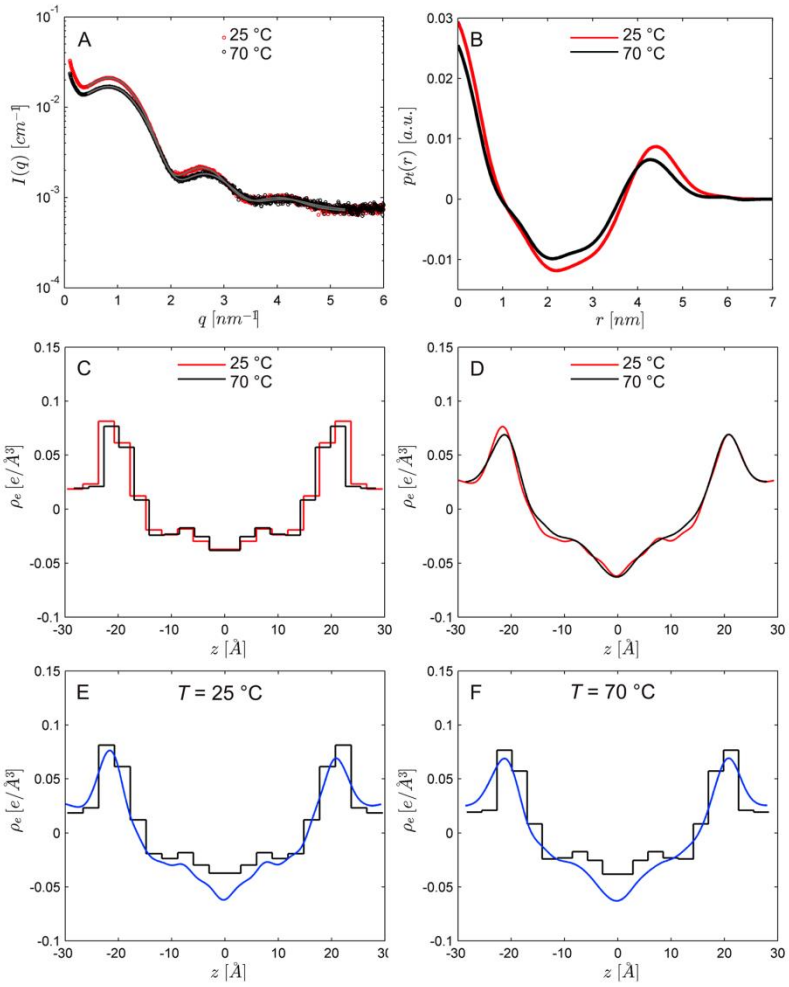

Figure 1. (A) Experimental SAXS curves of liposomes composed of archaeal lipids at 25 °C (red ○) and 70 °C (○) on absolute scale and IFT fits for the lamellar symmetry (gray lines). (B) The corresponding results of the IFT evaluation for lamellar symmetry−thickness pair-distance distribution functions $p_t(r)$. (C) Electron density profiles $\rho_e(z)$ determined on the basis of the experimental SAXS results obtained from the $p_t(r)$ functions by a convolution square root operation. (D) Electron density profiles of archaeal lipid bilayers derived from MD simulations. The electron density profiles of liposomes composed of archaeal lipids at 25 °C (E) and 70 °C (F). The profiles are derived from MD simulations (archaeal lipids in water with counterions Na^+) (blue) and electron density profiles $\rho_e(z)$ determined on the basis of the experimental SAXS results (black). These comparisons of electron density profiles between SAXS measurements and MD simulations have already been published by Polak et al.[8]

where $d = 2$ is the number of translational degrees of freedom and $t_0 = 5$ ns.

The rotational motion of the head groups moieties was calculated using the second rank reorientational autocorrelation function:

$$C(t) = \frac{1}{2}\langle 3[\vec{V}(t)\cdot\vec{V}(0)]^2 - 1\rangle \quad (4)$$

where **V** is unit vector defined in Figure 5A.

All tof he analyses were performed on the data of the last 15 ns of each simulation run.

We have also estimated the local pressure profiles[31] along z, the bilayer normal, at various system configurations. The pressure profiles may be calculated from simulations as

$$p(z) = \frac{1}{\Delta V}[\sum_i m_i \mathbf{v}_i \otimes \mathbf{v}_i - \sum_{i<j} \mathbf{F}_{ij} \otimes \mathbf{r}_{ij} f(z, z_i, z_j)] \quad (5)$$

where $p(z)$ is the local pressure tensor in the slab centered on the coordinate z, the sum over the kinetic term running over all atoms in the slab, and $f(z,z_i,z_j)$ is a weighting function. The calculations were all

dx.doi.org/10.1021/la5014208 | *Langmuir* 2014, 30, 8308−8315

performed on the fly[27] from the simulations performed at constant temperature and constant pressure. The lateral pressure profiles were calculated using built-in function in NAMD. The simulation space is partitioned into slabs, and one-half of the virial due to the interaction between two particles is assigned to each of the slabs containing the particles. To evaluate local pressure, the Harasima contour was used. The algorithm is based on that of Lindahl and Edholm,[32] with modifications to enable Ewald sums based on Sonne et al.[33] The total virial contains contributions from kinetic energy, bonded interactions, nonbonded interactions, and an Ewald sum. In lipid bilayers, the pressure profiles arise due to the amphipathic nature of the lipids composing it: the hydrophilic head groups are squeezed together to prevent exposure of the hydrophobic tails to the solvent leading to a negative lateral pressure, while the attractive dispersion forces and entropic repulsion between the lipid tails result mainly in a positive lateral pressure.

3. RESULTS AND DISCUSSION

The experimental SAXS curves of the vesicle sample composed of archaeal lipids at 25 and 70 °C are depicted in Figure 1A. These scattering curves show three broad scattering peaks that are increasing in intensity with decreasing scattering vector q and a steep upturn of the scattering intensity at very low values of q. The broad scattering peaks occur in the q region corresponding to the thickness of the lipid bilayer, whereas the steep upturn at very low values of q occurs due to the very large overall dimensions of the bilayer that are above the resolution of the SAXS experiment. As the temperature increases, the broad scattering peaks decrease in intensity and shift toward higher q values. This indicates an increase in the bilayer thickness, which possibly leads also to a slight change in the scattering contrast of the bilayer.

Because of the limited experimental resolution, the information on the overall size of the vesicles is not complete in these SAXS results; therefore, the steep upturn at low q needs to be cut off before the detailed IFT evaluation of the SAXS data containing information on the internal structure of the bilayer. The fits obtained by the IFT analysis are shown as gray lines in Figure 1A, whereas the resulting thickness pair-distance distribution functions $p_t(r)$ are depicted in Figure 1B. These functions reveal a rather similar internal structure of these bilayers in terms of the scattering contrast, with somewhat larger overall thicknesses of the bilayer at lower temperature (6 nm at 25 °C vs 5.5 nm at 70 °C). At higher temperature, the thermal energy of lipid molecules is higher; the hydrophobic tails become more flexible and hydrophobic heads are hydrated to a lesser extent, and so therefore the lipid molecules can obviously pack themselves into thinner bilayers.

The internal structure of the lipid bilayers is revealed in more detail through the electron density profiles. These profiles were obtained via convolution square root procedure of the experimentally obtained $p_t(r)$ functions and also by the MD simulations. The electron density profiles obtained by MD and SAXS method at 25 and 70 °C are shown in Figure 1. These profiles show that the central part of the bilayer is negative, whereas the outer layers have the positive electron density in comparison to the average electron density of the sample; the latter defines $\rho_e = 0$. This is in agreement with the lower electron density of the hydrophobic hydrocarbon parts of the lipid molecules (comprising the central part of the lipid bilayer) in comparison to the higher electron density of the polar headgroup parts of the lipid molecules (comprising the outer shells on each side of the bilayer). They also reveal the approximate thickness of the central hydrophobic part (~3 nm) and the outer hydrophilic shells of the bilayer (~1.5 nm) and their slight changes with the temperature. The comparison of the MD electron density profiles of the bilayers in two different buffers shows (water with counterions (Na+) and 0.45 M KCl) that the buffer has practically no effect on the electron density profile of the bilayer (data not shown). The shift in positions of the $\rho_e(z)$ peaks that is observed with the temperature increase corresponds to the changes in the outer shells in the bilayers increases. Figure 1 also shows that the bilayers at lower temperatures are somewhat thicker.

The comparison of electron density profiles derived from MD simulations and SAXS results shows a good agreement. Slight discrepancies in the absolute values of $\rho_e(z)$ can be noticed (Figure 1). These can arise either from the different nature of the two techniques, from the numerical model of the system itself, or from impurities in the real samples that cannot be taken into account in the simulations. Nevertheless, these results confirm the structural accuracy of the model and the force field used in our study.

The time evolutions of the surface area per molecule (A_m) for archaeal lipid in water with the Na^+ counterions and in the 0.45 M KCl solution at different temperatures show that the bilayers were well equilibrated within few tens of nanosecond (data not shown). The values of A_m and of the bilayer thickness (phosphates peak-to-peak distance) are reported in Table 1.

Table 1. Properties of the Equilibrated Archaeal Lipid Bilayers in Different Buffers and at Different Temperatures from MD Simulations[a]

buffer	T [°C]	A_m [Å^2]	d [Å]
Na^+ counterions	25	83.4 ± 0.4	42.5
	70	86.7 ± 0.7	42.1
0.45 M KCl	25	82.5 ± 0.3	42.5
	70	86.8 ± 0.6	42.1
	90	90.4 ± 0.7	41.8

[a] T, temperature; A_m, area per molecule; d, thickness of the bilayer.

As expected, they increase and decrease, respectively, with increasing temperature. Again, we found that the presence of buffer in the systems has practically no effect on A_m. Shinoda et al.[34] showed that the concentration of NaCl does not affect the structure of DPhPC-ether. This supports our findings of archaeal lipids. On the other hand, Knecht and Klasczyk[35] suggest that chloride ions bind almost as strongly to PC bilayers as sodium ions, and they do not affect the structure of bilayer. This was calculated by experiments and compared to molecular dynamic simulations. They are suggesting that a range of published simulation results on the interaction of NaCl with PC bilayers have to be reconsidered and revised.

To further characterize the systems under study, we derived from the MD simulations the density profiles of the bilayers main components across the membrane normal. The potassium ions penetrate more deeply into the bilayer as compared to the chloride ions, which is expected due to the negative charges carried by the lipid head groups. Quite interestingly, the same components of the AI and AGI molecules (lipid hydrocarbon tails, glycerol, phosphate, inositol, and glucose moieties) have similar distributions along the bilayer normal, although the AGI molecules carry an additional glucose group. The latter partition in the region of phosphate and inositol groups and are indicated by a broader density distribution pointing to its high mobility and conformational freedom.

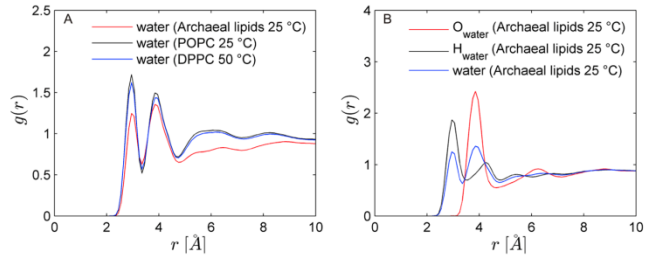

Figure 2. Radial distribution functions (RDFs).

The average location of the lipid components with respect to the solvent indicates that hydration of the head groups in these lipids is quite different from that in simple lipid bilayers. To characterize the latter, we have measured the radial distribution functions (RDF) of the solvent (water molecules) around the phosphorus atom in the archaeal lipids (Figure 2) and that of POPC and DPPC bilayers for the purpose of comparison. The data show that there is hardly any difference between these distribution functions for the two PC-based lipids, but a large one between PC and archaeal lipids. Furthermore, the RDFs at 70 and 90 °C are exactly the same (data not shown). Table 2 reports

Table 2. Coordinate Number, the Number of Atoms in the First Shell around Phosphorous Atom in Archaeal Lipids, POPC, and DPPC

	coordination number		
atom pair	archaeal lipid	POPC	DPPC
P–H_{water}	4.60	5.87	5.64
P–O_{water}	5.64	5.98	5.98
P–water	3.98	5.45	5.20

the coordination numbers and indicates that the phosphorus head groups in archaeal lipid are indeed less hydrated than those in PC-based lipid bilayers.

Interactions between the lipid components probably play a major role in the stability of the bilayer. They moreover slow the overall dynamics of the lipid head groups as well as the lateral diffusion of the lipids, as we further quantify in the following paragraphs. Because of the difference in interactions between the headgroup moieties and the tails, one expects also a difference in the pressure profiles along the membrane normal for these archaeal and simple PC-based lipids with acyl chains. These profiles have been calculated and are reported together with those of POPC and DPPC bilayer in Figure 3. Aside from a difference due to the change in bilayer hydrophobic core thickness, the peaks of the pressure at the interfacial regions are much higher in archaeal lipids as compared to PC-based lipids. As it was observed, the archaeal lipid bilayers have a much larger positive lateral pressure in the hydrophobic region.

Turning back to the dynamical characteristics of the archaeal lipid bilayer, we estimated the molecules lateral diffusion coefficients D from the MSD curves by linear fitting (Figure 4). They indicate that archaeal lipids have much lower lateral diffusion than other phosphatidylcholine (PC) lipids at temperatures above the gel to liquid crystal phase transitions. For instance, the lateral diffusion coefficients of DPPC lipids (measured experimentally or estimated from MD simulations) amount to

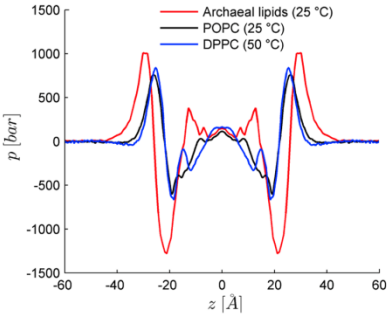

Figure 3. Lateral pressure profile of archaeal lipid (red), POPC (black), and DPPC (blue) bilayers.

~1–4 × 10^{-7} cm^2/s,[36–38] and for 1,2-diphytanoyl-*sn*-glycero-3-phosphocholine (DPhPC)-ether at 25 °C D is ~4.8 × 10^{-8} cm^2/s.[39]

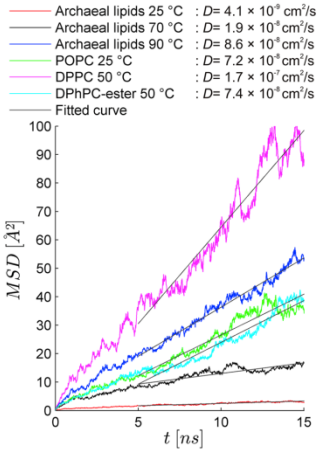

Figure 4. Mean square displacement (MSD) of lipids in the bilayer composed of archaeal lipids, POPC, and DPPC. The gray linear curves are fitted curves to the data from 5 to 15 ns. From fitted curves was the diffusion coefficient (D) calculated. The D values of POPC, DPPC, and DPhPC-ester were determined on our unpublished and published MD system.[40]

dx.doi.org/10.1021/la5014208 | *Langmuir* 2014, 30, 8308–8315

Table 3. Median Values of Angle (α) between V_{Pino}, V_{ino}, and V_{glu}, and Normal to Archaeal Lipid Bilayers Composed of AI and AGI Molecules and Half Time Constant of Reorientation Autocorrelation Function ($\tau_{1/2}$) at 25, 70, and 90 °C

		25 °C		70 °C		90 °C	
vector	molecule	α [deg]	$\tau_{1/2}$ [ns]	α [deg]	$\tau_{1/2}$ [ns]	α [deg]	$\tau_{1/2}$ [ns]
V_{Pino}	AI	51.5	7.51	80.5	0.69	70.5	0.50
V_{Pino}	AGI	70.1	–	80.1	1.78	72.3	0.60
V_{ino}	AI	50.4	5.54	72.1	0.75	69.5	0.19
V_{ino}	AGI	64.2	–	70.5	1.94	66.5	0.69
V_{glu}	AGI	87.6	–	80.1	1.40	84.2	0.58

the conformation of the AI headgroup. It flips to almost perpendicular orientation with respect to the bilayer plane. The glucose in the headgroup has a bimodal distribution. This means that the latter are tilted into or out of the bilayer. The reorientational autocorrelation functions provide insight into the dynamics of the lipid head groups (Figure 5G, I, J, K). As expected, the time constants of the auto correlation decay are higher for larger temperatures, but we also observe that headgroup moieties of AI lipids are moving faster than the headgroup moieties of AGI lipids. The presence of glucose in the AGI molecule appears to lower the dynamic of the headgroup moieties, probably due to the formation of hydrogen bonds with surrounding headgroup moieties. In comparison to simple PC-based lipids (e.g., DPPC), the dynamic of V_{Pino} reorientation even at 90 °C is much slower than the dynamics of P−N vector estimated at 50 °C ($\tau_{1/2}$ = 0.3 ns).[41]

4. SUMMARY AND CONCLUSIONS

The *Aeropyrum pernix* is a rare cell organism, whose membrane is composed predominantly of two polar lipids (AI and AGI). There is no report whether the AI and AGI molecules are randomly distributed or aggregate in the membrane of *A. pernix*. Accordingly, in this study, we modeled archaeal lipid bilayers assuming a random distribution of its components. The bilayers were simulated at a wide range of temperatures and at different salt concentrations. We considered in particular temperatures where the archaeal lipid bilayers are in the liquid crystalline phase. For comparison, DPhPC phospholipids that carry methyl groups in lipid tails as do AI and AGI lipids[2] are also liquid crystalline in a wide range of temperatures (−120 and 120 °C).[42] The structural properties of AI and AGI bilayers were calculated and compared to electron density profiles extracted from SAXS measurements. The agreement obtained provided confidence in the force field parameters and protocols used in the MD simulations.

The properties of the archaeal bilayers as the average area per lipid, the hydrophobic core thickness, the orientation of the lipid head-groups, and the dynamics of the lipids significantly change with temperature in the range studied here (25−90 °C), while the salt nature and content seem to have no effect on the structure of the bilayer (area per lipid and thickness). The presence of salt seems also to have a negligible effect on the bilayer structure as the archaeal lipids associate through hydrogen bonding between their headgroup moieties. As compared to PC-based lipid bilayers, the archaeal lipids head groups are less hydrated than PC-based lipids.

The in-plane dynamics of the archaeal lipids in the bilayers is much slower than that of other PC-based lipids. The lateral diffusion coefficient (D) of AI and AGI lipids is indeed lower than that of other PC-based lipids, even when comparing archaeal bilayers at 90 °C and PC-based bilayers at 25 °C. The slower dynamics is in part due the methyl-branches in the lipid tails,[39] but, more importantly, due to the large sugar moieties of the lipid head groups. Inositol and glucose indeed interact with each other through hydrogen bonding. The orientation of the headgroup moieties is quite similar at all temperatures studied with the exception of that of the AI molecule at 25 °C. The glucose in AGI molecules has a bimodal distribution (facing inward and outward the bilayer plane). The dynamics of the headgroup moieties described by reorientational correlation functions is faster at the higher temperatures studied. Furthermore, this headgroup dynamics is faster for the AI head groups, as compared to AGI, as the former are not only smaller, but lack the glucose groups that form stable hydrogen bonds with neighboring lipids.

The lateral pressure profile of archaeal lipid bilayers also shows significant differences from that of PC-based lipid bilayers. In particular, the lateral pressure in the hydrophobic core is much higher, and the negative pressure due mainly to attractive forces just beneath the head groups is also much higher. The surface tension of bilayers that corresponds to the integral of the pressure profile along the bilayer is important for the function of membrane proteins and determines in general the elastic properties of lipid bilayers.[43] The differences highlighted here, between simple PC-based lipids and archaeal lipids, relate directly to their interesting and unusual physical properties.

■ AUTHOR INFORMATION

Corresponding Authors

*E-mail: mounir.tarek@univ-lorraine.fr.

*Tel.: +386-14-768-456. E-mail: damijan.miklavcic@fe.uni-lj.si.

Notes

The authors declare no competing financial interest.

■ ACKNOWLEDGMENTS

This research was conducted within the scope of the EBAM European Associated Laboratory. This work was in part supported by the Slovenian Research Agency (J2-3639, P1-0201, P2-0249, and P4-0121). This manuscript is a result of the networking efforts of COST Action TD1104 (www.electroporation.net). Part of the calculations of the paper was performed during the Short Term Scientific Mission Grant STSM [070113-021794] to A.P. Simulations were performed using HPC resources from GENCI-CINES (Grant 2012−2013 [076434]).

■ REFERENCES

(1) Benvegnu, T.; Brard, M.; Plusquellec, D. Archaeabacteria Bipolar Lipid Analogues: Structure, Synthesis and Lyotropic Properties. *Curr. Opin. Colloid Interface Sci.* **2004**, *8*, 469−479.

(2) Ulrih, N. P.; Gmajner, D.; Raspor, P. Structural and Physicochemical Properties of Polar Lipids from Thermophilic Archaea. *Appl. Microbiol. Biotechnol.* **2009**, *84*, 249−260.

(3) Ulrih, N. P.; Adamlje, U.; Nemec, M.; Sentjurc, M. Temperature- and pH-Induced Structural Changes in the Membrane of the

Hyperthermophilic Archaeon Aeropyrum Pernix K1. *J. Membr. Biol.* **2007**, *219*, 1−8.
(4) Sako, Y.; Nomura, N.; Uchida, A.; Ishida, Y.; Morii, H.; Koga, Y.; Hoaki, T.; Maruyama, T. Aeropyrum Pernix Gen. Nov., Sp. Nov., a Novel Aerobic Hyperthermophilic Archaeon Growing at Temperatures up to 100°C. *Int. J. Syst. Bacteriol.* **1996**, *46*, 1070−1077.
(5) Morii, H.; Yagi, H.; Akutsu, H.; Nomura, N.; Sako, Y.; Koga, Y. A Novel Phosphoglycolipid Archaetidyl(glucosyl)inositol with Two Sesterterpanyl Chains from the Aerobic Hyperthermophilic Archaeon Aeropyrum Pernix K1. *Biochim. Biophys. Acta, Mol. Cell Biol. Lipids* **1999**, *1436*, 426−436.
(6) Gmajner, D.; Ota, A.; Sentjurc, M.; Ulrih, N. P. Stability of Diether C(25,25) Liposomes from the Hyperthermophilic Archaeon Aeropyrum Pernix K1. *Chem. Phys. Lipids* **2011**, *164*, 236−245.
(7) Napotnik, T. B.; Valant, J.; Gmajner, D.; Passamonti, S.; Miklavcic, D.; Ulrih, N. P. Cytotoxicity and Uptake of Archaeosomes Prepared from Aeropyrum Pernix Lipids. *Hum. Exp. Toxicol.* **2013**.
(8) Polak, A.; Tarek, M.; Tomšič, M.; Valant, J.; Ulrih, N. P.; Jamnik, A.; Kramar, P.; Miklavčič, D. Electroporation of Archaeal Lipid Membranes Using MD Simulations. *Bioelectrochemistry* **2014**.
(9) Milek, I.; Cigic, B.; Skrt, M.; Kaletunç, G.; Ulrih, N. P. Optimization of Growth for the Hyperthermophilic Archaeon Aeropyrum Pernix on a Small-Batch Scale. *Can. J. Microbiol.* **2005**, *51*, 805−809.
(10) Bligh, E. G.; Dyer, W. J. A Rapid Method of Total Lipid Extractin and Purification. *Can. J. Biochem. Physiol.* **1959**, *37*, 911−917.
(11) Kratky, O.; Stabinger, H. X-Ray Small Angle Camera with Block-Collimation System an Instrument of Colloid Research. *Colloid Polym. Sci.* **1984**, *262*, 345−360.
(12) Orthaber, D.; Bergmann, A.; Glatter, O. SAXS Experiments on Absolute Scale with Kratky Systems Using Water as a Secondary Standard. *J. Appl. Crystallogr.* **2000**, *33*, 218−225.
(13) Weyerich, B.; Brunner-Popela, J.; Glatter, O. Small-Angle Scattering of Interacting Particles. II. Generalized Indirect Fourier Transformation under Consideration of the Effective Structure Factor for Polydisperse Systems. *J. Appl. Crystallogr.* **1999**, *32*, 197−209.
(14) Brunner-Popela, J.; Mittelbach, R.; Strey, R.; Schubert, K.-V.; Kaler, E. W.; Glatter, O. Small-Angle Scattering of Interacting Particles. III. D[sub 2]O-C[sub 12]E[sub 5] Mixtures and Microemulsions with N-Octane. *J. Chem. Phys.* **1999**, *110*, 10623.
(15) Fritz, G.; Bergmann, A.; Glatter, O. Evaluation of Small-Angle Scattering Data of Charged Particles Using the Generalized Indirect Fourier Transformation Technique. *J. Chem. Phys.* **2000**, *113*, 9733.
(16) Frühwirth, T.; Fritz, G.; Freiberger, N.; Glatter, O. Structure and Order in Lamellar Phases Determined by Small-Angle Scattering. *J. Appl. Crystallogr.* **2004**, *37*, 703−710.
(17) Fritz, G.; Glatter, O. Structure and Interaction in Dense Colloidal Systems: Evaluation of Scattering Data by the Generalized Indirect Fourier Transformation Method. *J. Phys.: Condens. Matter* **2006**, *18*, S2403−S2419.
(18) Glatter, O. The Interpretation of Real-Space Information from Small-Angle Scattering Experiments. *J. Appl. Crystallogr.* **1979**, *12*, 166−175.
(19) Glatter, O. A New Method for the Evaluation of Small-Angle Scattering Data. *J. Appl. Crystallogr.* **1977**, *10*, 415−421.
(20) Glatter, O. Evaluation of Small-Angle Scattering Data from Lamellar and Cylindrical Particles by the Indirect Transformation Method. *J. Appl. Crystallogr.* **1980**, *13*, 577−584.
(21) Iampietro, D. J.; Brasher, L. L.; Kaler, E. W.; Stradner, A.; Glatter, O. Direct Analysis of SANS and SAXS Measurements of Catanionic Surfactant Mixtures by Fourier Transformation. *J. Phys. Chem. B* **1998**, *102*, 3105−3113.
(22) Sato, T.; Sakai, H.; Sou, K.; Medebach, M.; Glatter, O.; Tsuchida, E. Static Structures and Dynamics of Hemoglobin Vesicle (HBV) Developed as a Transfusion Alternative. *J. Phys. Chem. B* **2009**, *113*, 8418−8428.
(23) Glatter, O. In *Small Angle X-ray Scattering*; Glatter, O., Kratky, O., Eds.; Academic Press Inc. London Ltd.: London, 1983; p 119.
(24) Glatter, O. Convolution Square Root of Band-Limited Symmetrical Functions and Its Application to Small-Angle Scattering Data. *J. Appl. Crystallogr.* **1981**, *14*, 101−108.
(25) Glatter, O.; Hainisch, B. Improvements in Real-Space Deconvolution of Small-Angle Scattering Data. *J. Appl. Crystallogr.* **1984**, *17*, 435−441.
(26) Mittelbach, R.; Glatter, O. Direct Structure Analysis of Small-Angle Scattering Data from Polydisperse Colloidal Particles. *J. Appl. Crystallogr.* **1998**, *31*, 600−608.
(27) Kalé, L.; Skeel, R.; Bhandarkar, M.; Brunner, R.; Gursoy, A.; Krawetz, N.; Phillips, J.; Shinozaki, A.; Varadarajan, K.; Schulten, K. NAMD2: Greater Scalability for Parallel Molecular Dynamics. *J. Comput. Phys.* **1999**, *151*, 283−312.
(28) Essmann, U.; Perera, L.; Berkowitz, M. L.; Darden, T.; Lee, H.; Pedersen, L. G. A Smooth Particle Mesh Ewald Method. *J. Chem. Phys.* **1995**, *103*, 8577.
(29) Darden, T.; York, D.; Pedersen, L. Particle Mesh Ewald: An N log(N) Method for Ewald Sums in Large Systems. *J. Chem. Phys.* **1993**, *98*, 10089.
(30) Shinoda, K.; Shinoda, W.; Baba, T.; Mikami, M. Comparative Molecular Dynamics Study of Ether- and Ester-Linked Phospholipid Bilayers. *J. Chem. Phys.* **2004**, *121*, 9648−9654.
(31) Lindahl, E.; Edholm, O. Spatial and Energetic-Entropic Decomposition of Surface Tension in Lipid Bilayers from Molecular Dynamics Simulations. *J. Chem. Phys.* **2000**, *113*, 3882.
(32) Hess, B.; Kutzner, C.; van der Spoel, D.; Lindahl, E. GROMACS 4: Algorithms for Highly Efficient, Load-Balanced, and Scalable Molecular Simulation. *J. Chem. Theory Comput.* **2008**, *4*, 435−447.
(33) Sonne, J.; Hansen, F. Y.; Peters, G. H. Methodological Problems in Pressure Profile Calculations for Lipid Bilayers. *J. Chem. Phys.* **2005**, *122*, 124903.
(34) Shinoda, K.; Shinoda, W.; Mikami, M. Molecular Dynamics Simulation of an Archaeal Lipid Bilayer with Sodium Chloride. *Phys. Chem. Chem. Phys.* **2007**, *9*, 643−650.
(35) Knecht, V.; Klasczyk, B. Specific Binding of Chloride Ions to Lipid Vesicles and Implications at Molecular Scale. *Biophys. J.* **2013**, *104*, 818−824.
(36) Pfeiffer, W.; Henkel, T.; Sackmann, E.; Knoll, W.; Richter, D. Local Dynamics of Lipid Bilayers Studied by Incoherent Quasi-Elastic Neutron Scattering. *Europhys. Lett.* **1989**, *8*, 201−206.
(37) Essmann, U.; Berkowitz, M. L. Dynamical Properties of Phospholipid Bilayers from Computer Simulation. *Biophys. J.* **1999**, *76*, 2081−2089.
(38) Hofsäß, C.; Lindahl, E.; Edholm, O. Molecular Dynamics Simulations of Phospholipid Bilayers with Cholesterol. *Biophys. J.* **2003**, *84*, 2192−2206.
(39) Shinoda, W.; Shinoda, K.; Baba, T.; Mikami, M. Molecular Dynamics Study of Bipolar Tetraether Lipid Membranes. *Biophys. J.* **2005**, *89*, 3195−3202.
(40) Polak, A.; Bonhenry, D.; Dehez, F.; Kramar, P.; Miklavčič, D.; Tarek, M. On the Electroporation Thresholds of Lipid Bilayers: Molecular Dynamics Simulation Investigations. *J. Membr. Biol.* **2013**, *246*, 843−850.
(41) Niemelä, P.; Hyvönen, M. T.; Vattulainen, I. Structure and Dynamics of Sphingomyelin Bilayer: Insight Gained through Systematic Comparison to Phosphatidylcholine. *Biophys. J.* **2004**, *87*, 2976−2989.
(42) Andersson, M.; Jackman, J.; Wilson, D.; Jarvoll, P.; Alfredsson, V.; Okeyo, G.; Duran, R. Vesicle and Bilayer Formation of Diphytanoylphosphatidylcholine (DPhPC) and Diphytanoylphosphatidylethanolamine (DPhPE) Mixtures and Their Bilayers' Electrical Stability. *Colloids Surf., B: Biointerfaces* **2011**, *82*, 550−561.
(43) Ollila, S. Lateral Pressure in Lipid Membranes and Its Role in Function of Membrane Proteins. Ph.D. Thesis, Tampere University of Technology, 2010; p 70.

Paper 5

Title: Polyoxyethylene glycol ($C_{12}E_8$) decreases the electroporation threshold of POPC lipid bilayers

Authors: Polak A, Velikonja A, Kramar P, Tarek M, Miklavčič D

Publication: The paper was submitted on June 10th 2014 to *Langmuir* and later on June 26th 2014 it was rejected. The paper was submitted on September 30th 2014 to *The Journal of Physical Chemistry*.

DOI: /

Year: /

Volume: /

Issue: /

Pages: /

Polyoxyethylene glycol (C12E8) decreases the electroporation threshold of POPC lipid bilayers

Andraž Polak[a], Aljaž Velikonja[a,b], Peter Kramar[a], Mounir Tarek*[c,d], Damijan Miklavčič*[a]

[a] University of Ljubljana, Faculty of Electrical Engineering, Tržaška cesta 25, SI-1000 Ljubljana, Slovenia (andraz.polak@fe.uni-lj.si, avelik@avelik.homeip.net, peter.kramar@fe.uni-lj.si, Corresponding author: tel.: +386-14-768-456, e-mail: damijan.miklavcic@fe.uni-lj.si)

[b] SMARTEH Research and Development of Electronic Controlling and Regulating Systems, Poljubinj 114,SI-5220 Tolmin, Slovenia

[c] Université de Lorraine, UMR 7565, F-54506 Vandoeuvre-lès-Nancy, France (Corresponding author: mounir.tarek@univ-lorraine.fr)

[d] CNRS, UMR 7565, F-54506 Vandoeuvre-lès-Nancy, France

Keywords: Electroporation, Molecular dynamics, Planar lipid bilayer, polyoxyethylene glycol, palmitoy-oleoyl-phosphatidylcholine.

Abstract

Electroporation relates to a phenomenon in which cell membranes are permeabilized after being exposed to high electric fields. The mechanism of electroporation on molecular level is not yet fully elucidated, although considerable body of experimental results and molecular dynamic simulations were performed on simple lipid bilayers and bilayers composed of lipid mixtures. Here we present the experimental and simulation study of electroporation of palmitoy-oleoyl-phosphatidylcholine (POPC) bilayers with incorporated non-lipid molecules (polyoxyethylene glycol $C_{12}E_8$). The experimental results show slight increase of capacitance of POPC bilayer with incorporated $C_{12}E_8$, with respect to pure POPC bilayers in additions the voltage breakdown measured on planar lipid bilayers decreases by 22% for POPC bilayer with incorporated $C_{12}E_8$ with respect to pure POPC bilayer. The molecular dynamics simulations confirmed these experimental results. The electroporation threshold in molecular dynamics was however reduced by approximately 50%. Molecular dynamics simulations also reveal that surfactant polyoxyethylene glycol molecules play major role in pore formation. These surfactant molecules namely form hydrophilic part embedded in interior of the bilayer core, which favours formation of water wires that are protruding into the bilayer. When the water wire extend across the whole lipid bilayer, they already form water channels stabilized by the $C_{12}E_8$ head groups which already can transport ions across the membrane without the need of rearranging lipid head groups.

Introduction

Electroporation relates to a phenomenon in which cell membranes are permeabilized after being exposed to high electric fields.[1] Cell electroporation is used in several fields like biology, biotechnology, food processing and medicine.[2] It is considered reversible if cells recover their

initial state after electric field is switched off. On the contrary, electroporation is considered irreversible if it leads to the cell death. Among nowadays applications of electroporation based techniques we can list electrochemotherapy,[3] transdermal drug delivery,[4] gene therapy,[5] water cleaning,[6] food processing[7] and tissue ablation.[8] In biotechnology, protocols using electroporation to trigger drug-release from smart-liposome-based nanocarriers are being devised as well.[9] Experimental evidence suggests that the effect of an applied external electric field to cells is to produce aqueous pores specifically in their membrane lipid bilayer. Information about the sequence of events describing the electroporation phenomenon can be gathered from measurements of electrical currents through planar lipid bilayers and from the characterization of molecular transport of molecules into (or out of) cells subjected to electric field pulses. The application of electrical pulses induces rearrangements of the membrane components (water and lipids) that ultimately lead to the formation of transmembrane pores, the presence of which increases substantially ionic and molecular transport through the otherwise impermeable membrane.[5,10–12] To provide a molecular level characterization of the phenomena, several groups have resorted over a decade ago to atomistic simulations that have proven to be effective in providing insights into both the structure and the dynamics of model lipid membranes.[13] Molecular dynamics (MD) simulations have hence provided so far the most informative molecular model of electroporation processes of lipid bilayers.

Electroporation may be triggered by applying long (microseconds) low magnitude (kV/m) electric pulses. These pulses cause accumulation of charges at cell boundaries over a charging time in the order of 100s of ns.[14] As the cell membranes behave as a capacitors, this charge accumulation gives rise to a transmembrane potential U_t. Molecular dynamics *in silico* protocols have so far been developed to mimic the effect of such low magnitude microsecond electric pulses (μsEP) on planar bilayers[15] by imposing a net charge imbalance across the zwitterionic membranes.[15,16] The electric pulses induce formation of hydrophilic pores, in which, transmembrane water columns created above an electroporation threshold are stabilized by lipid head groups. This stabilization is a crucial step in the so-called electropore life cycle[17] and is considered a prerequisite for ion conduction as reported by most MD simulations studies so far.[15,18–21]

Most of these studies have been performed on simple zwitterionic lipids (phosphatidyl choline - PC- head groups) at the exceptions of few that considered also a small fraction of negatively charged lipids to study their externalization.[22] It was shown that applying a large transmembrane voltage induces formation of hydrophilic pores, in which, transmembrane water columns stabilized by the head groups of the lipid bilayer. This step in the so-called electropore life cycle[17] is prerequisite for ion conduction.[15,18–21] Recently,[23,24] we have found that for some particular lipids, pores formed in bilayers subject to high transmembrane voltage may not have the same morphology as the commonly created hydrophilic pores. For lipids from archaea for instance,[23] we did not observe rearrangement of lipid headgroups to stabilize the water wires created in membrane. The cell membranes of these types of archaea have however a unique composition, a high chemical and a high physical stability[25–27] compared to simple phosphatidyl-choline (PC) lipids as they carry head groups formed by sugar moieties, ether linkages instead of ester linkages between the head group and the carbonyl region, and methyl branches in the lipid tails.[28] These properties appear not only to increase the stability of these bilayers to electrical stress manifested by the increase of electroporation threshold, but change also the morphology of the pores. We have found a similar pore behavior for bilayers containing cholesterol.[29] For

specific bilayers such as those composed by POPS, a negatively charged lipid, we also recently found that pores created above an electroporation threshold are not stabilized by the lipid head groups.[24] Overall these studies indicate that the electroporation process is modulated by the nature of the lipids in bilayer and may be different from until recently assumed. We are here revealing that pores formed during electroporation of "real" membranes made of a complex mixture of lipids, cholesterol, sugar and other molecules may take various shapes.

The lipid composition is also known to modulate significantly the electroporation thresholds, i.e. the voltage required to breakdown a bilayer: several experimental studies characterized the impact of cholesterol contents for instance on the electroporation of simple lipid bilayers.[30–33] Most of the authors reported its stabilizing effect, as was later also found in MD simulation studies.[29,34] Yet, this seems not to be a universal behavior: in the case of diphytanoyl- glycero-phosphocholine (DPhPC), lipid of which the saturated hydrocarbon chains are functionalized with methyl groups, cholesterol was found to slightly decrease the electroporation threshold.[35] Electroporation thresholds were also shown to decrease upon addition of DPPC simple lipids to Archea based membrane composition.[23]

Other less studied additives that change lipid bilayers properties as well are surfactants. Troiano et al. studied the effects of incorporating polyoxyethylene glycol (i.e $C_{12}E_8$) into the POPC bilayers.[36] They showed that the voltage breakdown of planar mixed lipid bilayers decreases as the surfactant concentration increases. Consistent with Troiano's observations, Kandušer *et al.* found that incorporation of $C_{12}E_8$ into the membranes of (DC3F) cell lines lowers the irreversible electroporation threshold.[37] Polyoxyethylene glycol surfactants have peculiar properties in particular the size of their hydrophilic head group (see below). Even at normal conditions, their behavior in lipid membranes is quite distinct from that of other additives e.g. cholesterol since they have specific conformations, mobility and interactions with the solvent and the ions present at the lipid water interface. What role such properties play in the modulation of the electric stability of bilayers containing such a surfactant and to what extent pores that may form in the bilayer have also specific properties remains unknown.

In our present paper, we studied in particular planar POPC lipid bilayers containing the surfactant. The techniques of planar lipid bilayers formation were developed over the last 50 years.[38–41] Their electrical properties e.g. capacitance, the resistance and the voltage breakdown (electroproation threshold) can be measured in situ by voltage clamp, current clamp and others special methods.[42] These properties obtained in experiments were then compared to results from atomistic simulations performed on similar mixtures from which a further characterization of the electroporation phenomenon is presented.

Material and Methods

Experimental

Experiments under current-controlled conditions (i.e., current clamp) were performed using a measurement system described in detail elsewhere.[43] Briefly, system allows one to estimate the capacitance using an LCR meter and it measures the voltage breakdown by applying linearly rising current signal. The chamber where planar lipid bilayers are formed consists of two 5.3 cm^3 reservoirs made of Teflon. Between the two compartments, a thin Teflon sheet with a round

aperture (~ 105 μm diameter) is inserted. Planar lipid bilayers were formed by the Montal–Mueller method.[41] We studied bilayers prepared from 1-pamitoyl 2-oleoyl phosphatidylcholine (POPC) (AvantiPolar-Lipids, Alabaster, AL). The lipid powder was dissolved in a 9:1 hexane/ethanol solution 10 mg/ml. A 3:7 mixture of hexadecane and pentane was used for torus formation. The salt solution consisted of 0.1 M KCl and 0.01 M HEPES in the same proportion. 1 M NaOH was added to obtain pH 7.4. For the bilayer with a surfactant content, we followed the protocol set by Troiano et al.:[36] 15 μl of $C_{12}E_8$ solution at 100 times the desired concentration (1 mM) was injected into one of the compartments of the chamber, which contained 1.5 ml of solution at a height just below the aperture.

All together 42 POPC planar lipid bilayers and 42 POPC planar lipid bilayers with $C_{12}E_8$ incorporated were formed. The measuring protocols consisted of two sets of data: the capacitance measurement and the lipid bilayer voltage breakdown measurement. The capacitance was measured using an LCR meter (Agilent 4284A, USA) and a sinusoidal signal with amplitude 0.025 V and frequency 1 kHz. The capacitance was normalized to the surface area of the bilayer providing therefore the specific capacitance (C_{sp}). The voltage breakdown (U_{br}) was determined for each lipid bilayer by applying linear rising current signals of slope 300 μA/s. U_{br} was defined as the voltage at which a voltage drop due to the lipid bilayer rupture was detected. All the measurements were done at room temperature (25 ± 1°C).

Molecular Dynamics Simulations

In this study we considered hydrated POPC bilayers with incorporated $C_{12}E_8$ (Figure 1). The molecular dynamics (MD) simulations presented here were carried out using NAMD.[44] The systems were examined at constant pressure and constant temperature (NPT), or at constant volume and constant temperature (NVT) employing Langevin dynamics and the Langevin piston method. The time step for integrating the equations of motion was set at 2.0 fs. Short- and long-range forces were calculated every one and two time steps, respectively. Bonds between hydrogen and heavy atoms were constrained to their equilibrium value. Long-range electrostatic forces were taken into account using the particle mash Ewald (PME) approach.[45]

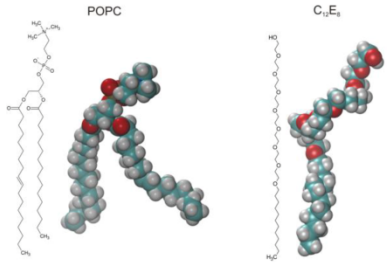

Figure 1: Representation of the structure and models of the POPC and $C_{12}E_8$ molecules. Configuration taken from the simulation of the POPC bilayer with $C_{12}E_8$ incorporated (red – oxygen, cyan – carbon, grey - hydrogen).

The bilayers were built of 64 POPC lipids with 0 mol% and 10 mol% incorporated $C_{12}E_8$ surfactant molecules in a 0.1 M KCl solution. First, simulations were performed at 50 °C (NPT) for 70 ns to relax the initial configurations. Then we run equilibration at lower temperature 25 °C (NPT) for 40 ns. The final systems were constructed by replication four times of these small bilayer patches then equilibrated at 25 °C (NPT) for 40 ns.

From the equilibrated bilayers, we calculated the average area per molecule (A_m) and the electrostatic properties of simulated lipid bilayers. The electrostatic potential profiles along the membrane normal was derived from the MD simulations using the linear Poisson's equation and expressed as the double integral of the molecular charge density distributions $\rho(z)$:

$$\Phi(z) = -\varepsilon_0^{-1} \iint \rho(z'')\, dz''\, dz',$$

z being the position of the charge in the direction along the normal to the bilayer. The dipole potential (U_d) of the bilayers is defined as the electrostatic potential difference between the middle of the bilayer (hydrophobic core) and the bulk (solvent), while the transmembrane voltage (U_t) was defined as the electrostatic potential difference between the two bulk regions surrounding the bilayer. The electron density profiles, along the bilayer normal were derived directly from MD simulations.

The capacitance of each simulated membrane was estimated using the charge imbalance method.[46,47] Briefly, configurations from the equilibrated NPT runs were used to set new systems, where the simulation box size was extended in direction perpendicular to the membrane to create air water interfaces. For these runs, the temperature was maintained at 25 °C and the volume was maintained constant. Systems with charge imbalances of 0e, 2e, 4e, 6e and 8e were simulated for over 1 ns each. The last 0.5 ns of simulation were used to determine the electrostatic potential distribution, from which the transmembrane voltages (U_t) were calculated. For all simulations, U_t was found in a linear correlation with q the charge imbalance normalized to the membrane area. Accordingly the capacitance of the bilayers was estimated as $C_{sp} = q / U_t$.

The electroporation of the lipid bilayers was induced by applying high transmembrane voltages created by means of charge imbalance method. This method is mimicking the effect of low magnitude microsecond electric pulses.[15,47] The MD simulations of systems with 0 mol% and 10 mol% incorporated $C_{12}E_8$ were run at several voltages. Here we report the electroporation threshold ($U_{EPthres}$) as interval between the highest U_t at which lipid bilayer were not electroporated in the 60 ns time scale and the lowest U_t at which pores were created in the membrane within 60 ns.

Results

Experiments

We formed 42 planar lipid bilayers composed of POPC lipids and 42 POPC planar lipid bilayers with $C_{12}E_8$ incorporated. The average capacitance of the POPC planar lipid bilayer determined in this study is 0.59 μF/cm^2, which compares well to the 0.6 μF/cm^2 determined in other studies.[36,48,49] This capacitance increases mildly to 0.63 μF/cm^2 for the POPC planar lipid bilayers with $C_{12}E_8$ incorporated. In previous study the authors did not found out $C_{12}E_8$ has an effect to the capacitance of POPC bilayer.[36]

The Figure 2 reports a representative current and voltage trace from a single measurement in which a steady current ramp is applied to the planar lipid bilayer. As can be seen, when the transmembrane voltage exceeds certain value U_{br}, it abruptly collapses, indicating that the planar lipid bilayer is broken. Considering all data, incorporation of 10 mol% of $C_{12}E_8$ in the POPC

planar lipid bilayer lowers U_{br}. Indeed for POPC U_{br} amounts to 0.374 V and decreases by about 22% to 0.293 V for POPC with $C_{12}E_8$ (c.f. Table 1). Student's t-test showed statistically significant difference ($P < 0.001$) between POPC bilayers and POPC bilayers with $C_{12}E_8$ incorporated for both specific capacitance and voltage breakdown.

Table 1: Specific capacitance (C_{Esp}) and voltage breakdown (U_{br}) of POPC planar lipid bilayers without and with $C_{12}E_8$ incorporated in 0.1 M KCl measured experimentaly.

Bilayer	n	C_{Esp} [μF/cm^2]	U_{br} [V]
POPC	42	0.59 ± 0.03*	0.374 ± 0.046**
POPC + 10 μM $C_{12}E_8$	42	0.63 ± 0.03*	0.293 ± 0.044**

Values given are mean ± standard deviation. The number of measurements n in each experimental group is given in the first column. Specific capacitances are statistically different ($P < 0.001$) and voltage breakdowns are statistically different ($P < 0.001$). They were compared using Student's t-test.

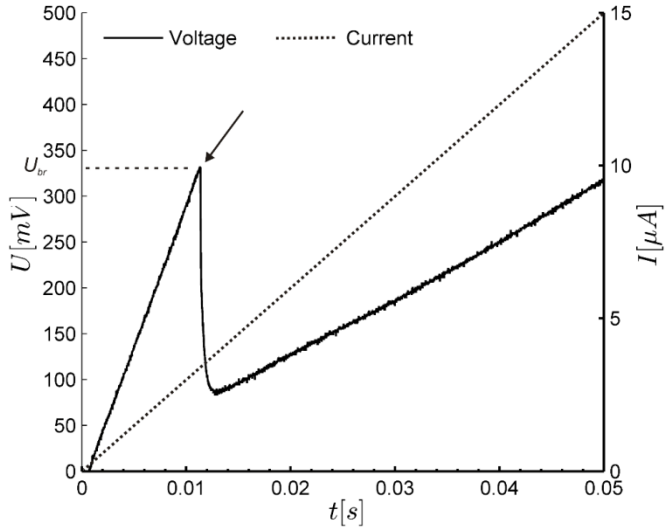

Figure 2: The voltage (U) and current (I) signals acquired in experiments using the current clamp method. The rising current is applied and the voltage response is measured. The planar lipid bilayer is broken when the measured voltage drops (indicated by arrow). The voltage value at which the planar lipid bilayer is broken is voltage breakdown (U_{br}).

MD Simulations

The evolution of the average area per molecule (A_m) determined from the runs shows that the systems were well equilibrated within few tens of ns (data not shown). Quite interestingly, A_m of the POPC bilayer and of the POPC bilayers with incorporated $C_{12}E_8$ are almost the same (Table 2) indicating that within this construct (the bilayer) $C_{12}E_8$ occupies a similar area as POPC. Using CHARMM 36 force field the area per lipid of pure POPC bilayers was estimated to be 64.7 ± 0.2 Å^2 at 30 °C.[50] This value is higher than the A_m calculated in our study, but in our study the temperature was 25 °C. The experimental value of A_m of POPC bilayer is 68.3 ± 1.5 Å^2 at 30 °C.[51]

Table 2: Area per lipid (A_m), membrane dipole potential (U_d) and specific capacitance (C_{Msp}) of the POPC bilayers with and without incorporated surfactant $C_{12}E_8$ in 0.1 M KCl from MD simulations.

Bilayer	A_m [Å^2]	U_d [V]	C_{Msp} [µF/cm^2]
POPC	60.4 ± 0.7	0.68	0.88
POPC + 10 mol% $C_{12}E_8$	60.7 ± 0.9	0.66	0.97

Values given are mean ± standard deviation.

There is no large differences between the POPC bilayer with and without incorporated $C_{12}E_8$ density profiles (Figure 3A). These are note almost symmetrical across the plane placed in the middle of bilayer, which means that the membranes are well equilibrated. The $C_{12}E_8$ molecules present a bimodal distribution (Figure 3B). In particular, the hydrophilic head group of the molecules is mainly located near the glycerol lipid head groups but extends also out of the bilayer where it interacts with ions of the surrounding solution. For $C_{12}E_8$ molecules reaching out to this outer interface, we note the formation of specific configurations where when a potassium ion from solution comes close to the hydrophilic part of $C_{12}E_8$, the latter wraps the potassium ion (Figure 4).

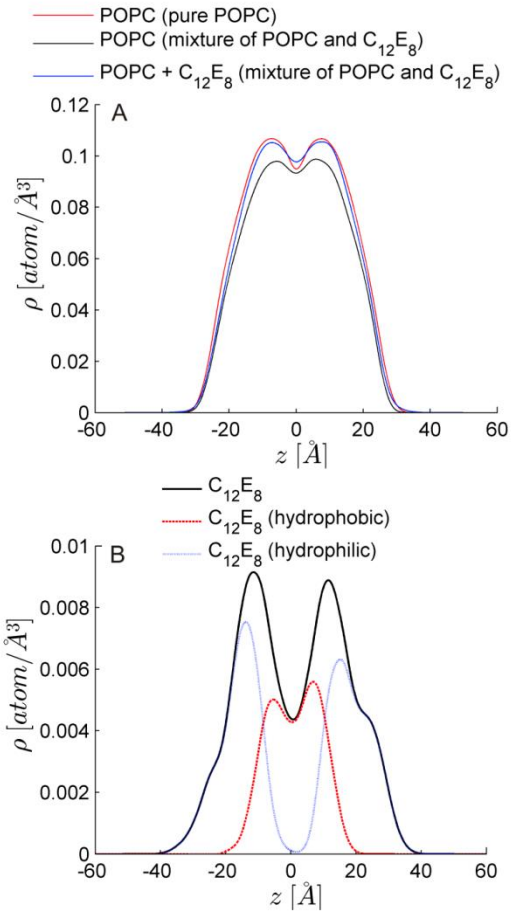

Figure 3: A) The density profiles of lipids and $C_{12}E_8$ molecules; B) the density profile of $C_{12}E_8$ molecules and their hydrophobic and hydrophilic parts in the POPC bilayer.

8

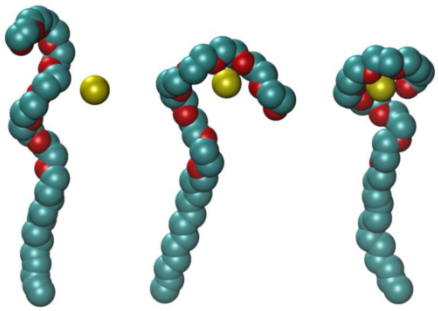

Figure 4: The snapshots of $C_{12}E_8$, when it wraps the potassium ion (red – oxygen, cyan – carbon, yellow - potassium).

The electrostatic potential profiles across the POPC bilayers with $C_{12}E_8$ incorporated were estimated from the charge distribution in the system. These analyses indicate that adding $C_{12}E_8$ into the bilayer does not change significantly the membrane dipole potential (cf Table 1). The membranes dipole potentials derived from our MD simulations are less than 0.7 V. The dipole potential measured experimentally is ~0.363 V,[52] but other MD simulation studies also showed that membrane dipole potential is 0.6 V.[53]

The lipid bilayers were subjected to transmembrane voltages (U_t) created by means of charge imbalance method. This allowed us to estimate first the capacitances of the POPC bilayers with 0 mol% and 10 mol% incorporated $C_{12}E_8$. The values obtained were 0.88 μF/cm^2 and 0.97 μF/cm^2, respectively (Table 1). These values are higher than those measured experimentally (0.6 μF/cm^2),[36] but in the range of other values estimated by means of molecular dynamic simulations.[47] These data obtained from simulations reproduced the slight increase in capacitance between pure POPC bilayer and POPC bilayer with $C_{12}E_8$ incorporated determined experimentally.

We then performed additional simulations at higher transmembrane voltages to trigger electroporation of the lipid bilayers under investigation (cf Table 3). In the cases where test voltages did not lead to the creation of a pore (in simulation times less than 60 ns), we concluded that the electroporation threshold $U_{EPthres}$ is higher. We have determined electroporation threshold as lying between the U_t values where the pores have not occurred and the U_t values where we observed the pore creation. The $U_{EPthres}$ intervals found for POPC bilayers with 0 mol% and 10 mol% incorporated $C_{12}E_8$ are 1.9-2.3 V and less than 1.1 V, respectively. The $U_{EPthres}$ of POPC lipid bilayer with incorporated $C_{12}E_8$ is about 50% lower than $U_{EPthres}$ of the pure POPC bilayer (more than 0.8 V lower). This, is in qualitatively agreement with the experimental data, where U_{br} of POPC bilayers with incorporated $C_{12}E_8$ was 22% lower than U_{br} of pure POPC bilayers and in agreement with Troiano et al. study.[36]

Table 3: Electric characteristics of the POPC bilayers with incorporated surfactant $C_{12}E_8$ under various transmembrane voltages created by a net charge imbalance.

Bilayer	Q_{im} [e]	U_t [V]	t_{sim} [ns]	t_{water} [ns]	t_{ion} [ns]	*Pore observed*
POPC	8	1.9	71	-	-	No
	10	2.3	105	41.1	42.6	Yes
POPC + 10 mol% $C_{12}E_8$	6	1.1	37	29.7	-	Yes
	8	1.5	68	47.9	51.6	Yes
	10	1.9	78	14.7	15.8	Yes
	12	2.3	10	2.3	3.3	Yes

Q_{im} – charge imbalance, U_t – transmembrane voltage, t_{sim} – simulation time, t_{water} – time when first water wire is formed, t_{ion} – time when first ion goes through the pore.

The pore formation in pure POPC bilayers under high transmembrane voltage was studied and was described before.[13,15,17] We observed similar behaviour. Electroporation starts by protrusion of water molecules into the hydrophobic region to form water fingers. Water fingers either extend or coalesce with other forming from the opposite side to form water wire that extends through the bilayer (hydrophobic pore) (Figure 5B). As these water columns become larger, the lipids from both leaflets migrate into the interior of bilayer to stabilize them thus forming hydrophilic pores. If the voltage is maintained, the hydrophilic pores conduct the ions present in the solution (Figure 5C).

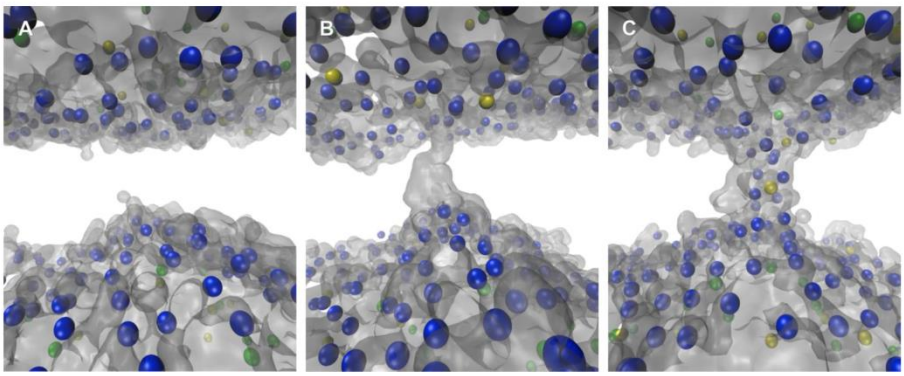

Figure 5: The electroporation of POPC bilayer at $U_t = 2.3$ V (snapshots at successive times after imposing a transmembrane voltage above the threshold): A) initial configuration, B) formation of water wire and C) formation of conducting 'hydrophobic' pore (blue – phosphorous atom, yellow – potassium ion, green – chloride ion, water – grey surface).

POPC bilayers with $C_{12}E_8$ incorporated at the concentration considered in our study have a peculiar way of forming pores when subject to high transmembrane voltages. Initially, the hydrophobic and hydrophilic segments of $C_{12}E_8$ are mostly aligned with the hydrophobic and hydrophilic segments of the POPC lipids (Figure 6C). Some $C_{12}E_8$ molecules also form small clusters with their hydrophilic part embedded in interior of the bilayer core. These clusters

appear to favour the formation of the water wires that are dragged into the bilayer by $C_{12}E_8$ molecules. When the water wire extends across the whole lipid bilayer (Figure 6C), it already form water channels stabilized by the $C_{12}E_8$ head groups. So stabilized pore can now transport ions across the membrane (Figure 6E). It is only much later if the transmembrane voltage is maintained that few lipid molecules migrate into the interior of POPC bilayer and stabilize the pore even further (Figure 6F).

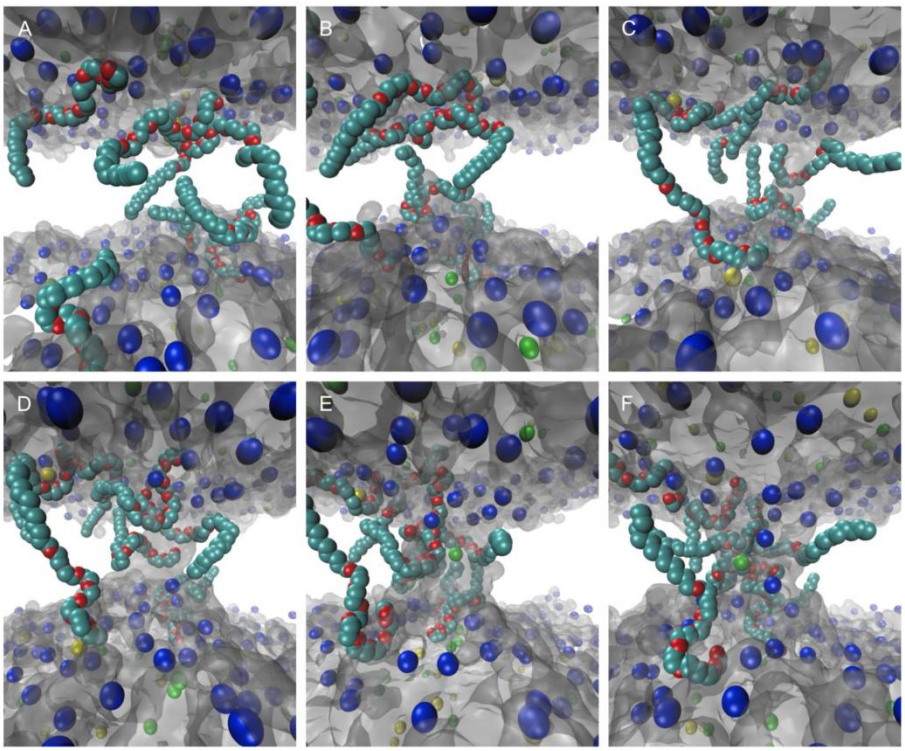

Figure 6: The electroporation of POPC bilayer with incorporated $C_{12}E_8$ at U_t=1.5 V (snapshots at successive times after imposing a transmembrane voltage above the threshold): A) initial configuration, B) $C_{12}E_8$ molecules go into the bilayer, C) formation of water channel stabilized by $C_{12}E_8$, D) wider water channel stabilized by $C_{12}E_8$, E) conducting water channel stabilized by $C_{12}E_8$ and F) conducting water channel stabilized by $C_{12}E_8$ and POPC lipids. (blue – phosphorous atom, yellow - potassium ion, green - chloride ion, water – grey surface, cyan and red – $C_{12}E_8$ molecules).

Discussion

In this study we focused on studying the change of properties of POPC bilayers, due to addition and incorporation of $C_{12}E_8$ into the POPC bilayer experimentally and using MD simulations. The experiments on planar lipid bilayers showed that $C_{12}E_8$ has only a very mild effect on the lipid bilayer capacitance. The capacitances of formed bilayers are in the range of those reported in other studies.[36] Our MD results show however that $C_{12}E_8$ molecules increases sensibly the

capacitance of POPC bilayer. We note however that in experiments, the concentration of surfactant in the bilayer is unknown at a given molar ratio of the two compounds in solution. It is likely that the concentration that we have considered here in the simulations is higher than that attained in experiments.

The MD simulations allows one to investigate how, at the molecular level, the POPC and $C_{12}E_8$ molecules are distributed in the equilibrated bilayer. The $C_{12}E_8$ surfactant is mostly oriented with their hydrophobic tail inside lipid bilayer and their hydrophilic part located in head group region and out of the lipid/water interface. The simulations indicated however that often, $C_{12}E_8$ hydrophilic head groups also partition in the hydrophobic region, though no specific flip-flop of $C_{12}E_8$ was observed, perhaps due to too short time of simulation. Experimentally, the latter was shown to occur on the seconds timescale.[54,55] Quite noticeably, in the simulations, one could detect penetration of the $C_{12}E_8$ head group, wrapping potassium ions toward the lipid inner core.

The voltage breakdown of POPC bilayers in experiments were measured using current clamp method.[43] The absolute values of breakdown voltages, therefore cannot be directly compared to those determined in another studies, due to their dependence on the shape and nature of applied signal.[36] However when comparing POPC bilayers with the POPC bilayers with $C_{12}E_8$ incorporated the reduction of voltage breakdown by 22% at planar lipid bilayers was observed. It was found out that 0.490 V is the minimum value to break the POPC planar lipid bilayer. Trioano *et. al.* applied voltage pulses to the planar lipid bilayers ranging from 10 μs to 10 s. Pure POPC bilayers had breakdown voltage ranging from 0.450 V to 0.167 V. POPC bilayers with incorporated $C_{12}E_8$ had 15%, 26% and 33% lower voltage breakdown upon the addition of 0.1, 1 and 10 μM $C_{12}E_8$, respectively.

The electroporation threshold estimated from the MD simulations agrees with experimental results. The electroporation threshold estimated from MD simulations namely decreases from 1.9–2.3 V for the pure POPC bilayer to value bellow 1.1 V, when $C_{12}E_8$ is added. The simulations allowed us to investigate further the morphologies of the pores formed in systems containing the surfactant. These have indeed a topology which is distinct from the pore forming in pure POPC bilayer. Consistent with previous simulations,[13,15,17] in the PC pure bilayers, the pores start forming with water wires and then expands to form conducting hydrophilic pores stabilized by the PC head groups that migrate toward the lipid hydrophobic core. Note that it has been reported that for some bilayers, such as those formed by archaeal lipids, water wires may form conducting hydrophobic pore that are not stabilized by rearrangement of the lipids.[23] In POPC bilayers containing the polyoxyethylene glycol surfactant, probably because of their higher mobility, $C_{12}E_8$ molecules appear to form the hydrophilic pore immediately by $C_{12}E_8$ stabilizing the water columns and ensuring that the pore conducts ions. Eventually, the pores are further stabilized by lipid head groups migrate into the bilayer core. Hence, the present study indicates that $C_{12}E_8$ plays an important role in forming the conducting pore through the POPC lipid bilayer. Gurtovenko and Lyulina studied bilayers composed of PC and PE lipid monolayers. The electric-field-induced water-filled pore occur mainly on the PC side. The structure of the molecule has strong effect to the electroporation process.[56]

In order to investigate the reason for changes in the electroporation threshold as $C_{12}E_8$ is added to the POPC lipid bilayers, we have estimated the dipole potential across the lipid bilayer from MD simulations. The latter provides direct estimate of the local electric field present at the lipid/water interface and might have an effect on the electroporation threshold since it modulates the forces

applied on the dipole of the interfacial water molecules.[57] The data at hand shows that the dipole potential at the concentrations investigated here does not change drastically the dipole potential when the surfactant is present.

In light of recent findings,[23] we have also estimated the local pressure profiles along z,[58] the bilayer normal for the two systems studied here. Namely, we have recently proposed that the lateral pressure in the hydrophobic region of lipid bilayers has an effect to the electroporation threshold.[23,28] The pressure profiles were calculated on the fly[44] (from simulations performed at constant temperature and pressure as $p(z)=\frac{1}{\Delta V}\left[\sum_i m_i \mathbf{v}_i \otimes \mathbf{v}_i - \sum_{i<j} \mathbf{F}_{ij} \otimes \mathbf{r}_{ij} f\left(z, z_i, z_j\right)\right]$ where $p(z)$ is the local pressure tensor in the slab centred on the coordinate z, the sum over the kinetic term running over all atoms in the slab and $f\left(z, z_i, z_j\right)$ a weighting function. In lipid bilayers, the pressure profiles arise due to the amphipathic nature of the lipids composing it: the hydrophilic head groups are squeezed together to prevent exposure of the hydrophobic tails to the solvent leading to a negative lateral pressure, while the attractive dispersion forces and entropic repulsion between the lipid tails results mainly in a positive lateral pressure. Here, the comparison of the pressure profiles of POPC and POPC bilayers containing $C_{12}E_8$ (Figure 7) shows only mild decrease for the latter in the upper region of the hydrophobic tails.

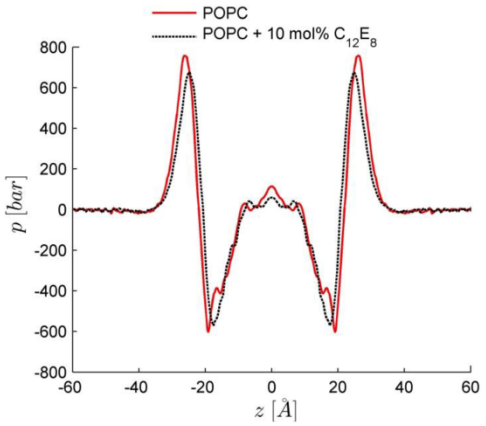

Figure 7: Pressure profile of POPC bilayer and POPC bilayer with incorporated 10 mol% $C_{12}E_8$.

The water permeability or diffusion toward the interior of lipid bilayers is the very initial and key step in membrane electroporation.[21,59] A significant change in the lateral pressure in the hydrophobic core of the bilayers has an effect on $U_{EPthres}$. Here, the analyses show however that that the change in the lateral pressure upon addition of the surfactant is noticeable but not large.

Another important factor that plays a role in the systems studied here, is the presence of hydrophilic moieties within the bilayer hydrophobic core upon addition of $C_{12}E_8$ (Figure 3). One expects that such moieties increase the "hydrophilicity" of the lipid core and increase therefore water permeability inside the hydrophobic core. Accordingly, we posit here that specific

configurations of the surfactant are at the origin and reason of the decrease of the electroporation thresholds observed experimentally and in MD simulations.

In conclusion, the present study reveals some key molecular properties of lipid bilayers incorporating polyoxyethylene glycol $C_{12}E_8$. Using combined experiments and for the first time molecular dynamics simulations the $C_{12}E_8$ has been found to modulate of the electric stability of POPC bilayers even at low (10 mol%) concentration in the lipid bilayer. The properties of the surfactant, in particular its high mobility and the way its hydrophilic head group moiety changes the intrinsic properties of the host bilayer were shown to be at the origin of such modulation. Incorporation of such a surfactant may serve to tune the electroporation threshold of liposomes for instance providing new routes for the design of efficient drug delivery carriers. Controlled electroporation can be indeed used to release the drug when such carriers have reached proper location in a variety of applications or to reduce irreversible threshold of electroporation in tissue ablation by means of non-thermal irreversible electroporation.[37,60]

Acknowledgement

Research was conducted within the scope of the EBAM European Associated Laboratory. This work was in part supported by the Slovenian Research Agency and bilateral cooperation programs between France and Slovenia (PROTEUS). The manuscript is a result of the networking efforts of COST Action TD1104 (www.electroporation.net). Part of the calculations of the paper was performed during the Short Term Scientific Mission *Grant STSM [**070113-021794**]* to Andraž Polak. Simulations were performed using HPC resources from GENCI-CINES *(Grant 2012-2013 [**076434**])*. A.V. was also supported by the European Social Fund and SMARTEH.

References

(1) Neumann, E.; Rosenheck, K. Permeability Changes Induced by Electric Impulses in Vesicular Membranes. *J. Membr. Biol.* **1972**, *10*, 279–290.

(2) Haberl, S.; Miklavcic, D.; Sersa, G.; Frey, W.; Rubinsky, B. Cell Membrane Electroporation-Part 2: The Applications. *IEEE Electr. Insul. Mag.* **2013**, *29*, 29–37.

(3) Matthiessen, L. W.; Johannesen, H. H.; Hendel, H. W.; Moss, T.; Kamby, C.; Gehl, J. Electrochemotherapy for Large Cutaneous Recurrence of Breast Cancer: A Phase II Clinical Trial. *Acta Oncol.* **2012**, *51*, 713–721.

(4) Denet, A.-R.; Vanbever, R.; Préat, V. Skin Electroporation for Transdermal and Topical Delivery. *Adv. Drug Deliv. Rev.* **2004**, *56*, 659–674.

(5) Daud, A. I.; DeConti, R. C.; Andrews, S.; Urbas, P.; Riker, A. I.; Sondak, V. K.; Munster, P. N.; Sullivan, D. M.; Ugen, K. E.; Messina, J. L.; et al. Phase I Trial of Interleukin-12 Plasmid Electroporation in Patients with Metastatic Melanoma. *J. Clin. Oncol.* **2008**, *26*, 5896–5903.

(6) Vernhes, M. .; Benichou, A.; Pernin, P.; Cabanes, P. .; Teissié, J. Elimination of Free-Living Amoebae in Fresh Water with Pulsed Electric Fields. *Water Res.* **2002**, *36*, 3429–3438.

(7) Toepfl, S.; Heinz, V.; Knorr, D. High Intensity Pulsed Electric Fields Applied for Food Preservation. *Chem. Eng. Process. Process Intensif.* **2007**, *46*, 537–546.

(8) Davalos, R. V.; Mir, L. M.; Rubinsky, B. Tissue Ablation with Irreversible Electroporation. *Ann. Biomed. Eng.* **2005**, *33*, 223–231.

(9) Elbayoumi, T. A.; Torchilin, V. P. Current Trends in Liposome Research. *Methods Mol. Biol.* **2010**, *605*, 1–27.

(10) C. Heller, L.; Heller, R. Electroporation Gene Therapy Preclinical and Clinical Trials for Melanoma. *Curr. Gene Ther.* **2010**, *10*, 312–317.

(11) Teissié, J.; Escoffre, J. M.; Paganin, A.; Chabot, S.; Bellard, E.; Wasungu, L.; Rols, M. P.; Golzio, M. Drug Delivery by Electropulsation: Recent Developments in Oncology. *Int. J. Pharm.* **2012**, *423*, 3–6.

(12) Pucihar, G.; Kotnik, T.; Miklavcic, D.; Teissié, J. Kinetics of Transmembrane Transport of Small Molecules into Electropermeabilized Cells. *Biophys. J.* **2008**, *95*, 2837–2848.

(13) Tieleman, D. P. The Molecular Basis of Electroporation. *BMC Biochem.* **2004**, *5*, 10.

(14) Kotnik, T.; Kramar, P.; Pucihar, G.; Miklavcic, D.; Tarek, M. Cell Membrane Electroporation- Part 1: The Phenomenon. *IEEE Electr. Insul. Mag.* **2012**, *28*, 14–23.

(15) Delemotte, L.; Tarek, M. Molecular Dynamics Simulations of Lipid Membrane Electroporation. *J. Membr. Biol.* **2012**, *245*, 531–543.

(16) Vernier, P. T.; Ziegler, M. J.; Sun, Y.; Gundersen, M. a; Tieleman, D. P. Nanopore-Facilitated, Voltage-Driven Phosphatidylserine Translocation in Lipid Bilayers--in Cells and in Silico. *Phys. Biol.* **2006**, *3*, 233–247.

(17) Levine, Z. A.; Vernier, P. T. Life Cycle of an Electropore: Field-Dependent and Field-Independent Steps in Pore Creation and Annihilation. *J. Membr. Biol.* **2010**, *236*, 27–36.

(18) Gurtovenko, A. a; Vattulainen, I. Pore Formation Coupled to Ion Transport through Lipid Membranes as Induced by Transmembrane Ionic Charge Imbalance: Atomistic Molecular Dynamics Study. *J. Am. Chem. Soc.* **2005**, *127*, 17570–17571.

(19) Böckmann, R. a; de Groot, B. L.; Kakorin, S.; Neumann, E.; Grubmüller, H. Kinetics, Statistics, and Energetics of Lipid Membrane Electroporation Studied by Molecular Dynamics Simulations. *Biophys. J.* **2008**, *95*, 1837–1850.

(20) Gurtovenko, A. A.; Anwar, J.; Vattulainen, I. Defect-Mediated Trafficking across Cell Membranes: Insights from in Silico Modeling. *Chem. Rev.* **2010**, *110*, 6077–6103.

(21) Kramar, P.; Delemotte, L.; Maček Lebar, A.; Kotulska, M.; Tarek, M.; Miklavčič, D. Molecular-Level Characterization of Lipid Membrane Electroporation Using Linearly Rising Current. *J. Membr. Biol.* **2012**, *245*, 651–659.

(22) Vernier, P. T.; Ziegler, M. J.; Sun, Y.; Chang, W. V; Gundersen, M. a; Tieleman, D. P. Nanopore Formation and Phosphatidylserine Externalization in a Phospholipid Bilayer at High Transmembrane Potential. *J. Am. Chem. Soc.* **2006**, *128*, 6288–6289.

(23) Polak, A.; Tarek, M.; Tomšič, M.; Valant, J.; Ulrih, N. P.; Jamnik, A.; Kramar, P.; Miklavčič, D. Electroporation of Archaeal Lipid Membranes Using MD Simulations. *Bioelectrochemistry* **2014**.

(24) Dehez, F.; Delemotte, L.; Kramar, P.; Miklavčič, D.; Tarek, M. Evidence of Conducting Hydrophobic Nanopores Across Membranes in Response to an Electric Field. *J. Phys. Chem. C* **2014**, *118*, 6752–6757.

(25) Benvegnu, T.; Brard, M.; Plusquellec, D. Archaeabacteria Bipolar Lipid Analogues: Structure, Synthesis and Lyotropic Properties. *Curr. Opin. Colloid Interface Sci.* **2004**, *8*, 469–479.

(26) Ulrih, N. P.; Gmajner, D.; Raspor, P. Structural and Physicochemical Properties of Polar Lipids from Thermophilic Archaea. *Appl. Microbiol. Biotechnol.* **2009**, *84*, 249–260.

(27) Ulrih, N. P.; Adamlje, U.; Nemec, M.; Šentjurc, M. Temperature- and pH-Induced Structural Changes in the Membrane of the Hyperthermophilic Archaeon Aeropyrum Pernix K1. *J. Membr. Biol.* **2007**, *219*, 1–8.

(28) Polak, A.; Bonhenry, D.; Dehez, F.; Kramar, P.; Miklavčič, D.; Tarek, M. On the Electroporation Thresholds of Lipid Bilayers: Molecular Dynamics Simulation Investigations. *J. Membr. Biol.* **2013**, *246*, 843–850.

(29) Casciola, M.; Bonhenry, D.; Liberti, M.; Apollonio, F.; Tarek, M. A Molecular Dynamic Study of Cholesterol Rich Lipid Membranes: Comparison of Electroporation Protocols. *Bioelectrochemistry* **2014**.

(30) Needham, D.; Hochmuth, R. M. Electro-Mechanical Permeabilization of Lipid Vesicles. Role of Membrane Tension and Compressibility. *Biophys. J.* **1989**, *55*, 1001–1009.

(31) Neumann, E.; Kakorin, S.; Toensing, K. Fundamentals of Electroporative Delivery of Drugs and Genes. *Bioelectrochemistry Bioenerg.* **1999**, *48*, 3–16.

(32) Kakorin, S.; Brinkmann, U.; Neumann, E. Cholesterol Reduces Membrane Electroporation and Electric Deformation of Small Bilayer Vesicles. *Biophys. Chem.* **2005**, *117*, 155–171.

(33) Naumowicz, M.; Figaszewski, Z. A. Pore Formation in Lipid Bilayer Membranes Made of Phosphatidylcholine and Cholesterol Followed by Means of Constant Current. *Cell Biochem. Biophys.* **2013**, *66*, 109–119.

(34) Fernández, M. L.; Marshall, G.; Sagués, F.; Reigada, R. Structural and Kinetic Molecular Dynamics Study of Electroporation in Cholesterol-Containing Bilayers. *J. Phys. Chem. B* **2010**, *114*, 6855–6865.

(35) Van Uitert, I.; Le Gac, S.; van den Berg, A. The Influence of Different Membrane Components on the Electrical Stability of Bilayer Lipid Membranes. *Biochim. Biophys. Acta* **2010**, *1798*, 21–31.

(36) Troiano, G. C.; Tung, L.; Sharma, V.; Stebe, K. J. The Reduction in Electroporation Voltages by the Addition of a Surfactant to Planar Lipid Bilayers. *Biophys. J.* **1998**, *75*, 880–888.

(37) Kandušer, M.; Fošnarič, M.; Šentjurc, M.; Kralj-Iglič, V.; Hägerstrand, H.; Iglič, A.; Miklavčič, D. Effect of Surfactant Polyoxyethylene Glycol (C12E8) on Electroporation of Cell Line DC3F. *Colloids Surfaces A Physicochem. Eng. Asp.* **2003**, *214*, 205–217.

(38) Coronado, R.; Latorre, R. Phospholipid Bilayers Made from Monolayers on Patch-Clamp Pipettes. *Biophys. J.* **1983**, *43*, 231–236.

(39) Funakoshi, K.; Suzuki, H.; Takeuchi, S. Lipid Bilayer Formation by Contacting Monolayers in a Microfluidic Device for Membrane Protein Analysis. *Anal. Chem.* **2006**, *78*, 8169–8174.

(40) Mueller, P.; Rudin, D. O.; Tien, H. T.; Wescott, W. C. Methods for the Formation of Single Bimolecular Lipid Membranes in Aqueous Solution. *J. Phys. Chem.* **1963**, *67*, 534–535.

(41) Montal, M.; Mueller, P. Formation of Bimolecular Membranes from Lipid Monolayers and a Study of Their Electrical Properties. *Proc. Natl. Acad. Sci. U. S. A.* **1972**, *69*, 3561–3566.

(42) Kramar, P.; Miklavčič, D.; Kotulska, M.; Maček Lebar, A. Voltage- and Current-Clamp Methods for Determination of Planar Lipid Bilayer Properties. In *Advances in Planar Lipid Bilayers and Liposomes*; Iglič, A., Ed.; Elsevier: Amsterdam, 2010; Vol. 11, pp. 29–69.

(43) Polak, A.; Mulej, B.; Kramar, P. System for Measuring Planar Lipid Bilayer Properties. *J. Membr. Biol.* **2012**, *245*, 625–632.

(44) Kalé, L.; Skeel, R.; Bhandarkar, M.; Brunner, R.; Gursoy, A.; Krawetz, N.; Phillips, J.; Shinozaki, A.; Varadarajan, K.; Schulten, K. NAMD2: Greater Scalability for Parallel Molecular Dynamics. *J. Comput. Phys.* **1999**, *151*, 283–312.

(45) Essmann, U.; Perera, L.; Berkowitz, M. L.; Darden, T.; Lee, H.; Pedersen, L. G. A Smooth Particle Mesh Ewald Method. *J. Chem. Phys.* **1995**, *103*, 8577.

(46) Sachs, J. N.; Crozier, P. S.; Woolf, T. B. Atomistic Simulations of Biologically Realistic Transmembrane Potential Gradients. *J. Chem. Phys.* **2004**, *121*, 10847–10851.

(47) Delemotte, L.; Dehez, F.; Treptow, W.; Tarek, M. Modeling Membranes under a Transmembrane Potential. *J. Phys. Chem. B* **2008**, *112*, 5547–5550.

(48) Diederich, A.; Bähr, G.; Winterhalter, M. Influence of Surface Charges on the Rupture of Black Lipid Membranes. *Phys. Rev. E* **1998**, *58*, 4883.

(49) Meier, W.; Graff, A.; Diederich, A.; Winterhalter, M. Stabilization of Planar Lipid Membranes: A Stratified Layer Approach. *Phys. Chem. Chem. Phys.* **2000**, *2*, 4559–4562.

(50) Klauda, J. B.; Venable, R. M.; Freites, J. A.; O'Connor, J. W.; Tobias, D. J.; Mondragon-Ramirez, C.; Vorobyov, I.; MacKerell, A. D.; Pastor, R. W. Update of the CHARMM All-Atom Additive Force Field for Lipids: Validation on Six Lipid Types. *J. Phys. Chem. B* **2010**, *114*, 7830–7843.

(51) Kucerka, N.; Tristram-Nagle, S.; Nagle, J. F. Structure of Fully Hydrated Fluid Phase Lipid Bilayers with Monounsaturated Chains. *J. Membr. Biol.* **2005**, *208*, 193–202.

(52) Haldar, S.; Kanaparthi, R. K.; Samanta, A.; Chattopadhyay, A. Differential Effect of Cholesterol and Its Biosynthetic Precursors on Membrane Dipole Potential. *Biophys. J.* **2012**, *102*, 1561–1569.

(53) Gurtovenko, A. a; Vattulainen, I. Calculation of the Electrostatic Potential of Lipid Bilayers from Molecular Dynamics Simulations: Methodological Issues. *J. Chem. Phys.* **2009**, *130*, 215107.

(54) Kragh-Hansen, U.; le Maire, M.; Møller, J. V. The Mechanism of Detergent Solubilization of Liposomes and Protein-Containing Membranes. *Biophys. J.* **1998**, *75*, 2932–2946.

(55) Le Maire, M.; Møller, J. V; Champeil, P. Binding of a Nonionic Detergent to Membranes: Flip-Flop Rate and Location on the Bilayer. *Biochemistry* **1987**, *26*, 4803–4810.

(56) Gurtovenko, A. a; Lyulina, A. S. Electroporation of Asymmetric Phospholipid Membranes. *J. Phys. Chem. B* **2014**, *118*, 9909–9918.

(57) Aliste, M. P.; Tieleman, D. P. Computer Simulation of Partitioning of Ten Pentapeptides Ace-WLXLL at the Cyclohexane/water and Phospholipid/water Interfaces. *BMC Biochem.* **2005**, *6*, 30.

(58) Lindahl, E.; Edholm, O. Spatial and Energetic-Entropic Decomposition of Surface Tension in Lipid Bilayers from Molecular Dynamics Simulations. *J. Chem. Phys.* **2000**, *113*, 3882.

(59) Tokman, M.; Lee, J. H.; Levine, Z. a; Ho, M.-C.; Colvin, M. E.; Vernier, P. T. Electric Field-Driven Water Dipoles: Nanoscale Architecture of Electroporation. *PLoS One* **2013**, *8*, e61111.

(60) Yarmush, M. L.; Golberg, A.; Serša, G.; Kotnik, T.; Miklavčič, D. Electroporation-Based Technologies for Medicine: Principles, Applications, and Challenges. *Annu. Rev. Biomed. Eng.* **2014**, *16*, 295–320.

4 Discussion

4.1 System for measuring properties of planar lipid bilayers

A system for planar lipid bilayers' formation and measurement of their properties was developed. The capacitance is measured by methods of LCR meter. The voltage breakdown can be measured using voltage or current-clamp method. The system enables generation of arbitrary shaped signals, which can be applied to the planar lipid bilayer. The idea of electrical circuits for voltage and current-clamp methods was adopted and upgraded from Kalinowski and Figaszewski (1995a).

The key feature of the developed system is the automated planar lipid bilayers formation by folding method, which allows temperature regulation. The automatic formation was achieved by precise regulation of the liquid level in each reservoir of the chamber. The reservoirs are separated by thin Teflon sheet with aperture. With such a set-up, the same hydrostatic pressure on both sides of the planar lipid bilayer can be reached, and each planar lipid bilayer is exposed to the same pressure conditions. This automation allows reproducible planar lipid bilayer formation and measurements at constant conditions which in turn provide quantitative and qualitative results. Since electrical interference from other sources interferes with the measured signals, the measurement chamber with electrodes is guarded and grounded. Moreover, the guard is an isolated bath with the temperature regulation with accuracy of 0.5 °C. The temperature in reservoirs is measured as close as possible to the formed planar lipid bilayers. The temperature can be regulated between 15 and 55 °C. Furthermore the temperature can be precisely regulated also around room temperature, as the heating and cooling is realized using peltier element (Figure 11).

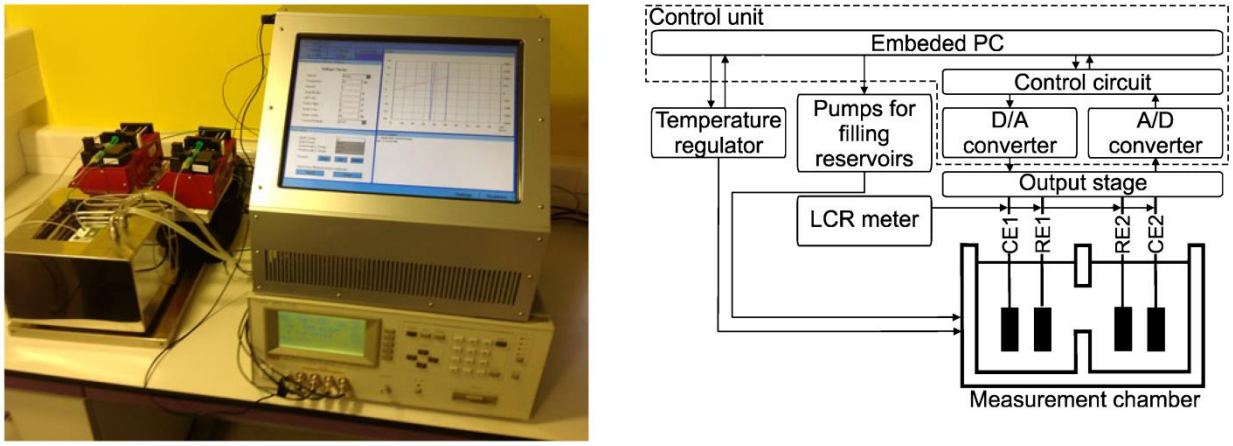

Figure 11: Left: The photography of the system for measuring the properties of planar lipid bilayers. On the left are two pumps for filling reservoirs and the bath with temperature regulation. The measurement chamber with four electrodes is inserted into the bath. The cables from the electrodes lead to the control unit, which is on the right. Below the control unit is the LCR meter. Right: Scheme of the system for measuring the properties of planar lipid bilayer, which consists of the control unit, the LCR meter, the output stage, the pumps for filling reservoirs, the measurement chamber with four electrodes and the bath with temperature regulation. The control unit consists of the embedded PC, the control circuit, the digital to analog converter and the analog to digital converter.

The system generates voltage signals with 1 mV accuracy by using the voltage-clamp method, while with the current-clamp method the system is able to measure voltage with 4 mV accuracy. The voltage and current signals can be generated as a pulse, step change, linear rising signal or arbitrarily shaped signals. The cutoff frequencies of the system output stage are 11 and 17 kHz for the voltage-clamp and current-clamp methods, respectively. These two values show the dynamics with open connectors of the system in question.

The measurement of the planar lipid bilayer capacitance was tested on lecithin planar lipid bilayers at 25 °C. They were formed round the apertures with diameters of 126 and 197 µm. The specific capacitances were 0.39 ± 0.0302 µF/cm^2 and 0.38 ± 0.02 µF/cm^2, respectively. These values are similar to the data available in literature (Naumowicz et al. 2003). The results also showed that aperture size has no effect on specific capacitance values. The voltage and current-clamp methods were tested using linear rising signals with slopes of 20 V/s and 150 µA/s, respectively. The voltage breakdown values were estimated to 480.0 ± 5.0 mV and 480.5 ± 6.5 mV, respectively and they were in the expected range.

The possibility of the temperature regulation within the system is important since it reveals the basic principles of bilayer formation, considering the fact that the planar lipid bilayers' structure and properties change with the temperature. At lower temperatures the lipid bilayers are in gel phase. The lipids are more ordered and have lower permeability. When the lipid bilayer is heated it can change to liquid-crystalline phase. In this phase the lipid tails are not ordered, which increases the lipids' mobility. Also the electrical properties change with the temperature. The capacitance of DPPC and DMPC planar lipid bilayer is higher when they are in liquid-crystalline phase compared to the gel

phase (Yoshida et al. 1989). It has also been established that the capacitance of egg lecithin has a temperature hysteresis. At heating the capacitance increases at 57–59 °C and at cooling the capacitance decreases at 42–43 °C. The conductance increases when the temperature is around the temperature of the phase transition of DPPC and DSPC lipid bilayers (Antonov et al. 1990).

4.2 The properties of archaeal lipid bilayers

The specific structure of lipids in archaeal membranes enables them to live in harsh environments. The archaeal lipids can form lipid monolayers or bilayers. The structure depends on the lipid type. The tetraether lipids form monolayers and other lipids form bilayers. The archaeal lipids have a number of special moieties, but in this thesis the focus was on the archaeal lipids which are found in the archaea *Aeropyrum pernix* membrane. Its membrane is predominantly composed of 2,3-di-O-sesterterpanyl-sn-glicerol-1-phospho-myo-inositol (AI) and 2,3-di-O-sesterterpanyl-sn-glicerol-1-phospho-1'(2'-O-α-D-glucosyl)-myo-inositol (AGI) at a molar ratio 9:91 mol% (Morii et al. 1999). *Sn*-glycerol-1-phosphate forms the backbone of these lipids. Hydrogen chains are methyl-branched isopranoids bonded with ether linkages to glycerol. The inositol is bonded to the phosphate group. The AGI molecule is composed of glucose, which is bonded to the inositol. Structural properties of the bilayers composed of AI and AGI molecules and behavior of the special moieties in AI and AGI molecules under electrical stress have been investigated.

The AI and AGI lipid molecules have not yet been described by molecular dynamics force fields, therefore the models and parameters in CHARMM force field were built. Morii et al. suggested that two stereo-structures of phospho-myo-inositol (1D and 1L) of AGI may compose the membrane of *A. pernix* (Morii et al. 1999). For simplicity only the 1D conformation was chosen to be modeled. The AI and AGI molecules were modeled by combining of CHARMM 36 lipids force field (Klauda et al. 2010) and that of carbohydrates. The force field parameters of ether linkage were adopted from (Shinoda et al. 2004a). We considered hydrated bilayers composed of AI and AGI at a 9:91 molar ratio (Morii et al. 1999).

4.2.1 Structure of archaeal lipid bilayers

The structure of lipid bilayers composed of AI and AGI molecules was examined using SAXS measurements and MD simulations. The SAXS measurements were performed at vesicles composed of pure archaeal lipids and their mixtures with DPPC in the same molar ratio, at 25 and 70 °C. Electron density profiles were calculated on the base of SAXS results. The electron density profiles were compared with the electron density profiles derived from MD simulations. In **paper 3** and **paper 4** we show good agreement between both profiles' values. Since there is no knowledge whether the AI and AGI molecules in the *A. pernix* membrane are randomly distributed or aggregated, the archaeal lipid bilayers were modeled assuming a random distribution of its components. The

configurational sampling of the lipids partitioning in a mixed composition bilayer is a very slow process, and there is always a nagging question whether the results of finite time simulations depend on the initial membrane configuration. One possibility to overcome this would be to perform MD simulations using coarse grain models (Ingólfsson et al. 2013), but today, robust force fields to represent archaeal lipids are not available yet. In our studies it has been assumed that the AI at the applied concentration (9 mol% lipid content) does not aggregate but partitions uniformly in the bilayer. Therefore to gain confidence in the membrane model it has mainly been relied on the comparison of the structural features to SAXS data.

The **paper 4** focused on the structural properties of the pure archaeal lipid bilayers. Static and dynamic characteristic of the bilayers were investigated. The bilayers were simulated at different temperatures (25, 70 and 90 °C) and in different salt solutions (KCl and Na^+ counter ions). The properties of the archaeal bilayers as the average area per lipid, the hydrophobic core thickness, the orientation of the lipid head groups and the dynamics of the lipids significantly change with temperature in the studied range (25 to 90 °C) while the salt nature and content seem to have no effect on the structure of the bilayer (area per lipid and thickness). The presence of salt seems also to have no effect to the bilayer structure as the archaeal lipids associate through hydrogen bonding between their head group moieties. Compared to PC-based lipid bilayers, the archaeal lipids head groups are less hydrated than PC-based lipids.

The in-plane dynamics of the archaeal lipids in the bilayers is much lower compared to that of other PC-based lipids. The lateral diffusion coefficient (*D*) of AI and AGI lipids is indeed lower than that of other PC-based lipids, even when comparing archaeal bilayers at 90 °C and PC-based bilayers at 25 °C. The lower dynamics is in part due the methyl-branches in lipid tails (Shinoda et al. 2005), but more importantly, due to the large sugar moieties of the archaeal lipid head groups. Inositol and glucose interact indeed with each other via hydrogen bonding. The head groups appear to form small clusters that stabilize the bilayer. The orientation of the head group moieties is rather similar at all temperatures studied with the exception of that of the AI molecule at 25 °C. The glucose in AGI molecules has a bimodal distribution (facing inward and outward the bilayer plane). The dynamics of the head group moieties described by reorientational correlation functions is faster at higher temperatures applied in the study. Furthermore, the head group dynamics is higher for the AI molecules head groups, compared to AGI, as the former are not only smaller, but lack the glucose groups that form stable hydrogen bonds with neighboring lipids.

The lateral pressure profile of archaeal lipid bilayers also shows significant differences compared to that of PC-based lipid bilayers. In particular, the lateral pressure in the hydrophobic core is much higher, and the negative pressure mainly due to attractive forces just beneath the head groups is also much higher. The surface tension of bilayers, which corresponds to the integral of the pressure profile

along the bilayer is important for the functioning of membrane proteins and determines the elastic properties of lipid bilayers in general (Ollila 2010). The differences highlighted here, between simple PC-based lipids and archaeal lipids, relate directly to archaeal interesting and unusual physical properties.

4.2.2 The electroporation of archaeal lipid bilayers

The AI and AGI molecules have complex structures; therefore the research was focused on the role of methyl branches in lipid tails and the effect of the difference between ester and ether linkages on the electrical stability. In **paper 2**, we compared DPPC, DPhPC-ester and DPhPC-ether based lipid bilayers under electric stress. The DPhPC-ester lipids have methyl-branched hydrogen chains in addition to the DPPC lipids. The difference between DPhPC-ester and DPhPC-ether is in linkages between glycerol and hydrogen chains. The DPhPC-ether lipids have ether linkages instead of ester linkages. In **paper 2** it was revealed that methyl-groups have small effect on membrane dipole potential. On the other hand changing ester linkages with ether linkages, decreases membrane dipole potential. The membrane dipole potentials were in good agreement with experimental results measured using Cryo-EM (Wang et al. 2006). As all bilayers are of similar thickness, all the specific capacitances are around 0.9 $\mu F/cm^2$. The moieties like methyl-groups and ester linkages have significant effect on the electroporation threshold. The electroporation thresholds of DPPC, DPhPC-ester and DPhPC-ether are on intervals 1.8–2.2 V, 2.3–2.7 V, 3.0–3.4 V, respectively. The intervals do not overlap, therefore the differences are clear. The methyl groups increase the bilayer's electroporation threshold. Changing the ester and ether linkages increases electroporation threshold even further. Comparison of the lateral pressure profiles between DPPC and DPhPC-ester, revealed that DPhPC-ester bilayer exhibits a wider and higher pressure in the middle hydrophobic part of the region.

In **paper 3** the electroporation of bilayers formed of archaeal lipids (AI and AGI) and their mixtures with DPPC in the same ratio were investigated. The obtained calculations show that the archaeal lipid bilayers have a much higher electroporation threshold compared to any other bilayers composed of simple phospholipids studied so far. The properties of lipids which contribute to the stability of membranes might be numerous and diverse, but include at least the structure of the lipid tails, the chemical nature of the head group and the nature of the head to tail linkage (ester or ether). The studied archaeal lipids have special head groups carrying inositol and glucose. In comparison to simple phosphatidylcholine (PC) head groups these carbohydrates are larger moieties that move much slower. Furthermore and as importantly, the carbohydrates in the lipid head groups are packed and involved in hydrogen bonds. As clearly evident from **paper 4** and comparing electroporation thresholds between DPhPC and archaeal lipids, these special head group moieties contribute substantially to the increase of these bilayers electroporation thresholds.

The dipole potential and capacitance as we have previously shown can be directly estimated from simulations and compared to experimental values. The charge and molecular dipole distributions in the anisotropic lipid bilayers are at the origin of an intrinsic electrostatic profile across the membrane. In their pioneering work, Liberman and Topaly (1968) hypothesized, from the measurements of the partition coefficients of fat-soluble tetraphenylboron anions and fat-soluble triphenylphosphonium cations between the membrane and aqueous phases, that the inner part of the bilayer membrane must initially be positively charged. The absolute value of this "dipole potential" has been very difficult to measure or predict (Clarke 2001; Wang et al. 2006; Demchenko and Yesylevskyy 2009), and estimates obtained from various methods and for various lipids range from 200 to 1000 mV. More recent and direct measurements based on Cryo-EM imaging (Wang et al. 2006) and atomic force microscopy (AFM) (Yang et al. 2008) techniques showed that the dipole potential can be "measured" in a noninvasive manner and estimate its value to a few 100 mV. The large body of data from the simulations of fully hydrated lipid bilayers are found in qualitative agreement with experiments, showing that the electrostatic profile monotonically increases across the membrane–water interface (Gawrisch et al. 1992; Peterson et al. 2002; Shinoda et al. 2004a; Wang et al. 2006; Klauda et al. 2010). Given the diversity of the lipids studied and more significantly of the force fields used, values of dipole potentials ranging from 500 to 1200 mV have been reported (Smondyrev and Berkowitz 1999; Mashl et al. 2001; Sachs et al. 2004; Berkowitz et al. 2006; Wang et al. 2006; Demchenko and Yesylevskyy 2009). The dipole potentials of archaeal lipids measured in our study were also found in this range (~ 200 mV). Though direct experimental estimates for bilayers of the used composition are not available, it is worth noticing that the results which were published in **paper 3** for DPhPC, a lipid with tails similar to those of the archaeal lipids, amount to 700 mV and 360 mV for the ester and ether forms which matches very well the data from (Wang et al. 2006) 510 mV and 260 mV, respectively. In particular the force fields used are good enough to reproduce the 50% decrease in the dipole potential from ester to ether lipids.

The MD protocols used allowed also to estimate the capacitance of the bilayer at specific ionic strength and for a given salt composition. The value determined for the archaeal lipids, to the best of our knowledge not yet determined experimentally, amounts to 0.7 $\mu F\ cm^{-2}$, which is within the magnitude of the capacitances found in similar systems (DPhPC). Taken together, these initial analyses of the MD simulations strengthen our confidence in the force fields used as far as the electrostatic properties of the AI and AGI bilayers modeled are concerned.

More so the head group/head group and tail/tail moieties interactions in bilayers composed of lipid mixtures play a key, yet not evident role in their electrical stability. Uitert et al. showed for instance that stability of lipid bilayers composed of two types of lipids is not necessarily linearly dependent on the concentration of one species, highlighting the fact that the behavior of mixtures cannot easily be predicted. Other similar examples are found in the literature. For instance, the electrical stability of

POPC membranes increases with the addition of cholesterol up to 50% (Naumowicz and Figaszewski 2013), while the stability of DPhPC membranes increases with addition of cholesterol only up to 10%, then decreases at higher concentration; at cholesterol ratios of ~50%, the electrical stability of DPhPC is even lower than stability of pure DPhPC (van Uitert et al. 2010).

The archaeal lipids studied here have very complex structure in comparison to the DPPC or even DPhPC. It is hard to predict, how will the electrical stability of archaeal lipids mixtures with a second component (DPPC) vary with the lipid composition. The DPPC lipid tails are not as long as those of archaeal lipids and they are formed of simple acyl chains. It is unclear how their zwittterionic and smaller head groups affect the bilayer electrical stability. Namely, both characteristics influence the packing of the lipids in to a bilayer.

Shinoda et al. have performed an extensive study of water permeability (Shinoda et al. 2004b) in DPPC and DPhPC which can perhaps provide a rationale for the increased electroporation threshold, due to branched lipid tails. Based on analyses of local diffusion coefficients, the authors have shown that water molecules in the DPhPC bilayer interior exhibit considerably lower mobility when compared to the DPPC bilayer interior. As a result of reduced water diffusion in the branch-chained bilayer, the DPhPC bilayer water permeability was lower compared to that of the DPPC bilayer for about 30%. As such permeability or diffusion toward the interior of the bilayer is the very initial and key step in electroporation, we expect that this has a direct effect on electroporation threshold. One can note along these lines that in **paper 2** the bilayers composed of DPhPC-ester showed an increase of electroporation threshold compared to DPPC bilayers, due to change in the lipid tails' composition.

Seeking to identify how characteristics of archaeal lipids can change the electroporation thresholds, lateral pressure profiles of the archaeal lipid bilayers and their mixtures with DPPC and pure DPPC were computed (**paper 3**). The profiles show higher peaks in hydrophilic head group region as well as in the hydrophobic core region in comparison to regular PC-based lipids bilayers. The same effect was observed at DPPC and DPhPC lipids' comparison (**paper 2**). One may speculate that a direct implication of higher pressure in hydrophobic region lowers the permeability of water and therefore increases the electroporation threshold. Similarly, the temperature, another key factor in the lipid chains mobility has also shown to affect electroporation threshold.

In contrast, the capacitances of the archaeal lipid bilayer do not seem to correlate to any extent with the electroporation thresholds, since these were found essentially unchanged with changes in bilayers composition. Counter intuitively also to what was expected, the bilayers dipole potentials' magnitudes are not directly correlated to the electroporation threshold value. These dipole potentials are proportional to the strength of the electric field at the bilayer head group/water interfaces. The archaeal lipid bilayers one is much lower compared to that of pure PC-lipids and increases with increasing

concentration of DPPC lipids in the mixtures, while the electroporation thresholds subsequently decrease.

In the Table 1 we gathered the bilayers' properties composed of PC lipids and archaeal lipids. The area per lipid in bilayers strongly depends on temperature and the type of lipids which compose the bilayer. The lipids occupy larger area at higher temperature. Ester and ether linkages and charges in the head group exhibit the main effect on the membrane dipole potential. The intervals of the electroporation thresholds do not overlap, therefore increase of electroporation threshold from DPPC, DPhPC-ester DPhPC-ether, archaeal lipids with DPPC to pure archaeal lipids at 50 °C can be observed. The electroporation thresholds calculated are probably overestimated since they were so far all determined from MD simulations (Delemotte and Tarek 2012; Kramar et al. 2012a). Indeed, the electroporation threshold of planar lipid bilayers formed of phospholipids are, by using simulations, estimated to be above 1.5 V (Vernier et al. 2006; Delemotte and Tarek 2012; Polak et al. 2013) while the experimentally measured voltage breakdown of planar lipid bilayers ranges from 200 mV to 600 mV (Kramar et al. 2010). So far, the reasons behind such large discrepancies remain unclear, but it is believed that they arise from a large difference of timescale between experiments and simulations. Namely, the electroporation on planar lipid bilayers takes milliseconds; on the other hand we are able to perform simulation up to a few nanoseconds.

Table 1: Properties of equilibrated phosphatidylcholine (PC) and archaeal lipid bilayers MD simulations (T – temperature, A_m – area per molecule, U_d –membrane dipole potential, C_{Msp} – specific capacitance derived from MD simulations, $U_{EPthres}$ – electroporation threshold).

Bilayer		Buffer	T [°C]	A_m [Å^2]	U_d [V]	C_{Msp} [μF/cm^2]	$U_{EPthres}$ [V]
PC-lipids	256 DPPC	0.45 M KCl	50	60.0 ± 0.9	0.70	0.94	1.8–2.2
	256 DPhPC-ester	0.45 M KCl	50	80.1 ± 0.6	0.62	0.93	2.3–2.7
	256 DPhPC-ether	0.45 M KCl	50	74.6 ± 0.7	0.36	0.90	3.0–3.4
Archaeal lipids	12 AI, 116 AGI, 128 DPPC	0.45 M KCl	70	73.8 ± 0.7	0.42	-	-
		Na^+ counter ions	70	74.6 ± 0.9	-	-	-
		0.45 M KCl	50	72.0 ± 0.9	0.42	0.68	3.6–4.1
		0.45 M KCl	25	69.1 ± 0.7	0.42	0.68	3.9–4.3
		Na^+ counter ions	25	68.9 ± 0.4	-	-	-
	24 AI, 232 AGI	0.45 M KCl	90	90.4 ± 0.7	0.18	-	-
		0.45 M KCl	70	86.8 ± 0.6	0.20	-	-
		Na^+ counter ions	70	86.7 ± 0.7	-	-	-
		0.45 M KCl	50	86.0 ± 0.6	0.23	0.72	4.1–4.5
		0.45 M KCl	25	82.5 ± 0.3	0.23	0.67	5.0–5.4
		Na^+ counter ions	25	83.4 ± 0.4	-	-	-

Values given in A_m column are mean ± standard deviation.

The electroporation process at zwitterionic lipid bilayers consists of several stages. First the water fingers protrude either from one side or both sides of the bilayer. Water defects appear within few nanoseconds then merge to form a complete transmembrane wire (Figure 12B). Such a defect is hereafter called a "hydrophobic pore" to indicate that water columns are in contact with hydrophobic lipid tails; later they expand in width and the lipid head groups band into the interior of the pore (Figure 12C). This lipids' reorganization stabilizes the pore and ions can be conducted through the pore and across the bilayer. This is called a hydrophilic pore. This process was observed and reported in **paper 2** on DPPC, DPhPC-ester and DPhPC-ether bilayers as well as in other studies (Tieleman et al. 2003; Leontiadou et al. 2004; Delemotte and Tarek 2012).

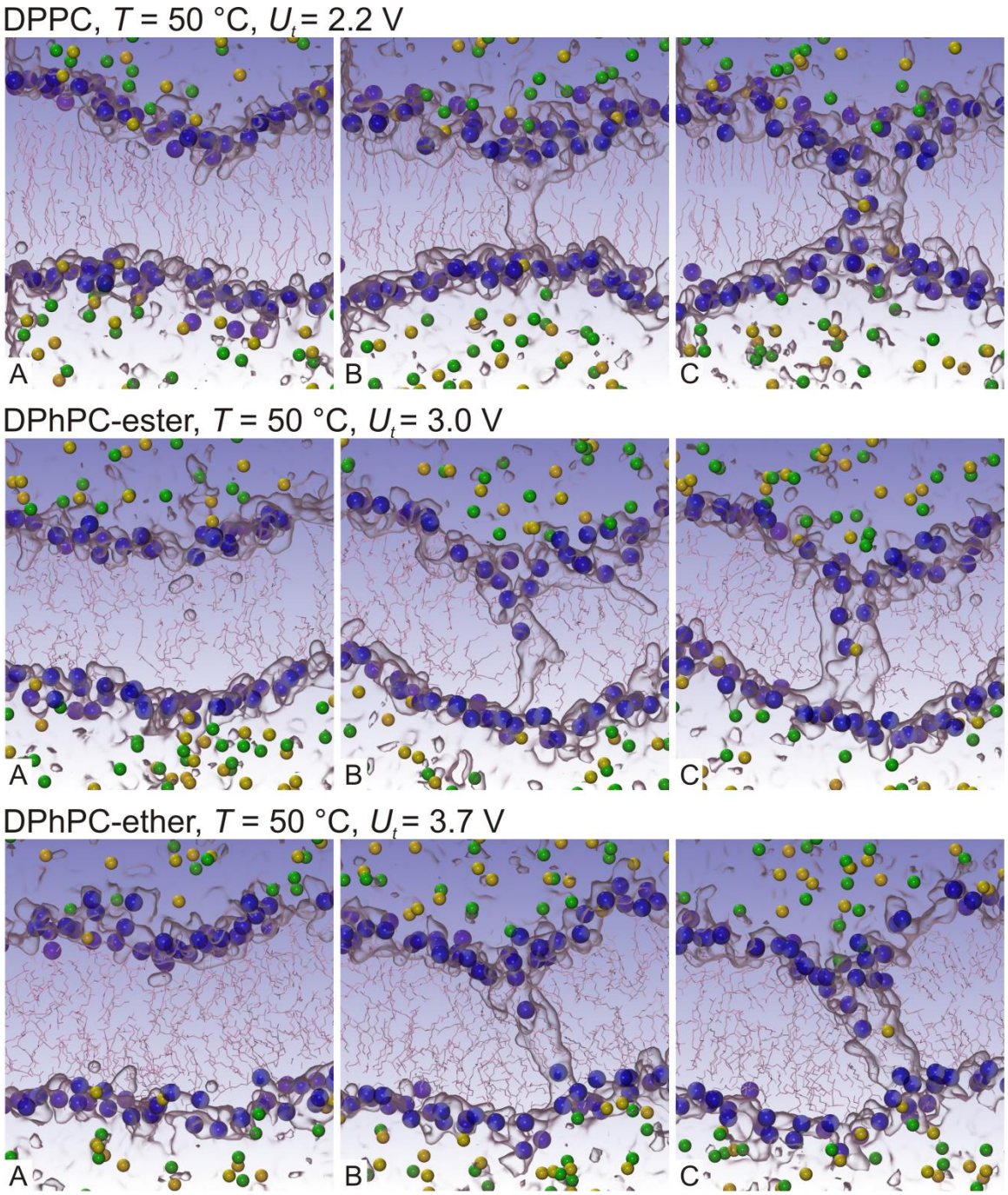

Figure 12: Electroporation process of DPPC, DPhPC-ester and DPhPC-ether lipid bilayers (snapshots at successive times after imposing a transmembrane voltage above the threshold): A) initial configuration, B) formation of water wire and C) formation of conducting 'hydrophilic' pore (white – lipid tails (between lipid headgroups), blue – lipid headgroups, yellow – potassium ion, green – chloride ion, gray surface – water, T – temperature, U_t – transmembrane voltage).

In **paper 3** pore formation in archaeal lipid bilayers was studied. The process of electroporation starts with the protrusion of water fingers from either one or both sides of the membrane. Water defects appear within few nanoseconds then merge to form a complete transmembrane wire (Figure 13B). Such a defect is also called a "hydrophobic pore" to indicate that the water columns are in contact with the hydrophobic lipid tails, which later expand in width. Surprisingly, in all the trajectories, the pores

remained “hydrophobic” i.e. no lipid head groups bent toward the interior of the lipid hydrophobic core along these water wires (Figure 13C). Regardless of the nature of the pore, ions were then driven along the electrical gradient. Hence, in contrast to previously reported behavior of PC based lipids (**paper 2**), the archaeal lipids forming the bilayer did not migrate towards the interior of the hydrophobic core to stabilize the water conducting pores. Similar behavior was also noted for the systems containing a fraction of DPPC. Similar process of hydrophobic pore formation under electrical stress was also observed in the POPS bilayers (Dehez et al. 2014).

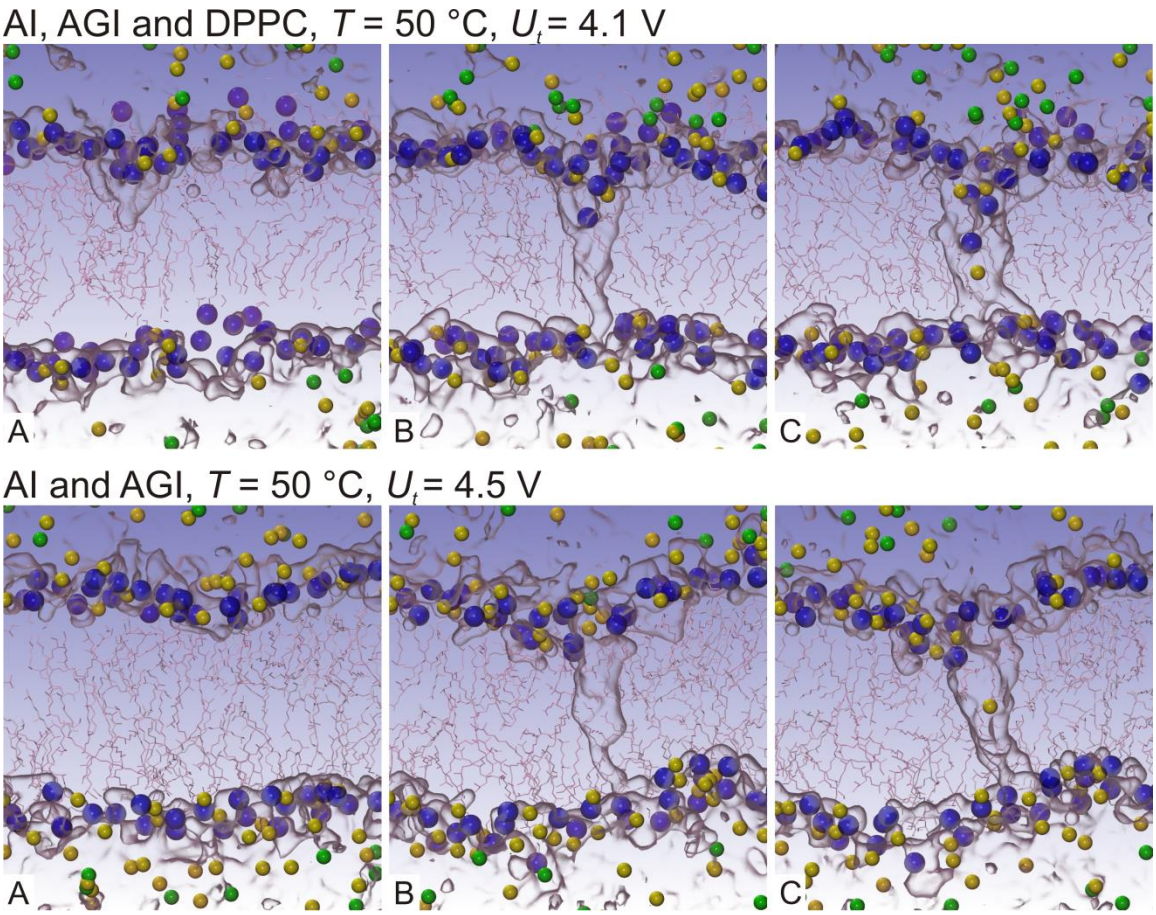

Figure 13: Electroporation process of archaeal lipid bilayers and theirs mixtures with DPPC in the same molar ratio (snapshots at successive times after imposing a transmembrane voltage above the threshold): A) initial configuration, B) formation of water wire and C) formation of conducting 'hydrophobic' pore (white – lipid tails (between lipid headgroups), blue – lipid headgroups, yellow – potassium ion, green – chloride ion, gray surface – water, *T* – temperature, U_t – transmembrane voltage).

4.3 The role of surfactant $C_{12}E_8$ at the electroporation of POPC lipid bilayer

In this chapter the research was focused on the change of properties of POPC bilayers, due to $C_{12}E_8$ addition and incorporation into the POPC bilayer. However it has to be emphasized that the concentration of surfactant in the bilayer at a given molar ratio of the two compounds in solution was unknown in the experiments. It is likely that the concentration used in the simulations is higher than the one attained from experiments.

Two groups of researchers showed that surfactant $C_{12}E_8$ affects the electroporation process in lipid membranes. Kandušer et al. showed that incorporation of the $C_{12}E_8$ surfactant into the DC3F cell line membranes lowered the irreversible electroporation. The reversible electroporation however remained the same (Kandušer et al. 2003). Troiano et al. studied the effect of $C_{12}E_8$ surfactant incorporated into POPC planar lipid bilayers (Troiano et al. 1998). They found that POPC planar lipid bilayers with $C_{12}E_8$ incorporated exhibit much lower voltage breakdown compared to the pure POPC planar lipid bilayers. However, no significant difference between capacitances of the POPC planar lipid bilayers and POPC lipid bilayers with $C_{12}E_8$ incorporated was found. The voltage breakdown was measured by voltage pulses application. In **paper 5** the properties of planar lipid bilayers composed of POPC lipids and $C_{12}E_8$ surfactant were measured and properties of similar bilayers using MD simulations were calculated. The experimentally measured capacitances values were in the same range as reported by Troiano et al., but it can be emphasised that statistically significant increase of capacitance in the POPC planr lipid bilayers with $C_{12}E_8$ incorporated was observed. The voltage breakdowns of POPC planar lipid bilayers and POPC planar lipid bilayers with $C_{12}E_8$ incorporated are 0.374 V and 0.293 V, respectively. It can be concluded that $C_{12}E_8$ incorporation decreases voltage breakdown by 22% (Table 2). Trioano et al. applied voltage pulses to the planar lipid bilayers ranging from 10 μs to 10 s. Pure POPC bilayers exhibit voltage breakdown ranging from 450 mV to 167 mV. POPC bilayers with incorporated $C_{12}E_8$ exhibited 15%, 26% and 33% lower voltage breakdown upon the 0.1, 1 and 10 μM $C_{12}E_8$ addition, respectively. The absolute values of voltage breakdowns cannot be compared directly to those determined from other studies, due to their dependence on the shape and nature of applied signal (Sabotin et al. 2009).

Table 2: Properties of POPC planar lipid bilayers and POPC planar lipid bilayers with $C_{12}E_8$ incorporated (*n* – number of measurements, U_{br} – voltage breakdown, C_{Esp} – specific capacitance).

Bilayer	*n*	U_{br} [V]	C_{Esp} [μF/cm^2]
POPC	42	0.374 ± 0.046	0.59 ± 0.03
POPC + 10 μM $C_{12}E_8$	42	0.293 ± 0.044	0.63 ± 0.03

Values given in U_{br} and C_{Esp} column are mean ± standard deviation.

The MD simulations enable the investigation on how, on the molecular level, the POPC and $C_{12}E_8$ molecules are distributed in the equilibrated bilayer. The hydrophobic tail of the $C_{12}E_8$ surfactant is mostly oriented towards the interior of the lipid bilayer and their hydrophilic part located in the head group region is oriented outwards towards the lipid/water interface. The simulations also indicated that $C_{12}E_8$ hydrophilic head groups in the hydrophobic region often partition, though no specific flip-flop of $C_{12}E_8$ was observed. Experimentally, the latter was shown to occur in the seconds timescale (le Maire et al. 1987; Kragh-Hansen et al. 1998)., In the simulations, one could quite noticeably detect the $C_{12}E_8$ head group penetration, wrapping potassium ions toward the lipid inner core.

The electroporation threshold estimated on the MD simulations supports the experimental results. The obtained values decrease from 1.9–2.3 V for the POPC bilayer to less than 1.1 V (Table 3). The POPC bilayer's electroporation threshold with $C_{12}E_8$ incorporated is lower than 1.1 V. Simulations allowed further morphology investigation of the pores formed in systems containing the surfactant. Their topology can indeed be distinct from the pore formation in pure POPC bilayer. Consistent with previous simulations (Tieleman 2004; Levine and Vernier 2010; Delemotte and Tarek 2012) in the pure PC bilayers, the pores start forming with water wires (Figure 14B) and later expand to form conducting hydrophilic pores, stabilized by the PC head groups which migrate toward the lipid hydrophobic core (Figure 14C). However for some bilayers, such as those formed by archaeal lipids and POPS it has been reported that the water wires may be expand to conducting hydrophobic pore which is not stabilized by lipids' rearrangement (Polak et al. 2014; Dehez et al. 2014). POPC bilayers with $C_{12}E_8$ incorporated have a peculiar way of pore formation when subject to high transmembrane voltages, at the concentrations used in the study. Initially, the hydrophobic and hydrophilic segments of $C_{12}E_8$ are rather aligned with the hydrophobic and hydrophilic segments of the POPC lipids. Some $C_{12}E_8$ molecules also form small clusters with their hydrophilic part embedded in the interior of the bilayer core (Figure 14A). These clusters appear to favor the formation of the water wires which are dragged into the bilayer by $C_{12}E_8$ molecules (Figure 14B). When the water wire extends across the whole lipid bilayer, it simultaneously forms water channels, stabilized by the $C_{12}E_8$ head groups (Figure 14C). The channels can transport ions across the membrane. Only a while later when the transmembrane voltage values are maintained when a few lipid molecules move into the interior of POPC bilayer and stabilize the pore even further.

Table 3: Properties of equilibrated POPC bilayers and POPC bilayers with incorporated $C_{12}E_8$ molecules in 0.1 M KCl from MD simulations (A_m – area per molecule, U_d –membrane dipole potential, C_{Msp} – specific capacitance derived from MD simulations, $U_{EPthres}$ – electroporation threshold).

Bilayer	A_m [Å^2]	U_d [V]	C_{Msp} [μF/cm^2]	$U_{EPthres}$ [V]
POPC	60.4 ± 0.7	0.68	0.88	1.9–2.3
POPC + 10 mol% $C_{12}E_8$	60.7 ± 0.9	0.66	0.97	< 1.1

Values given in A_m column are mean ± standard deviation.

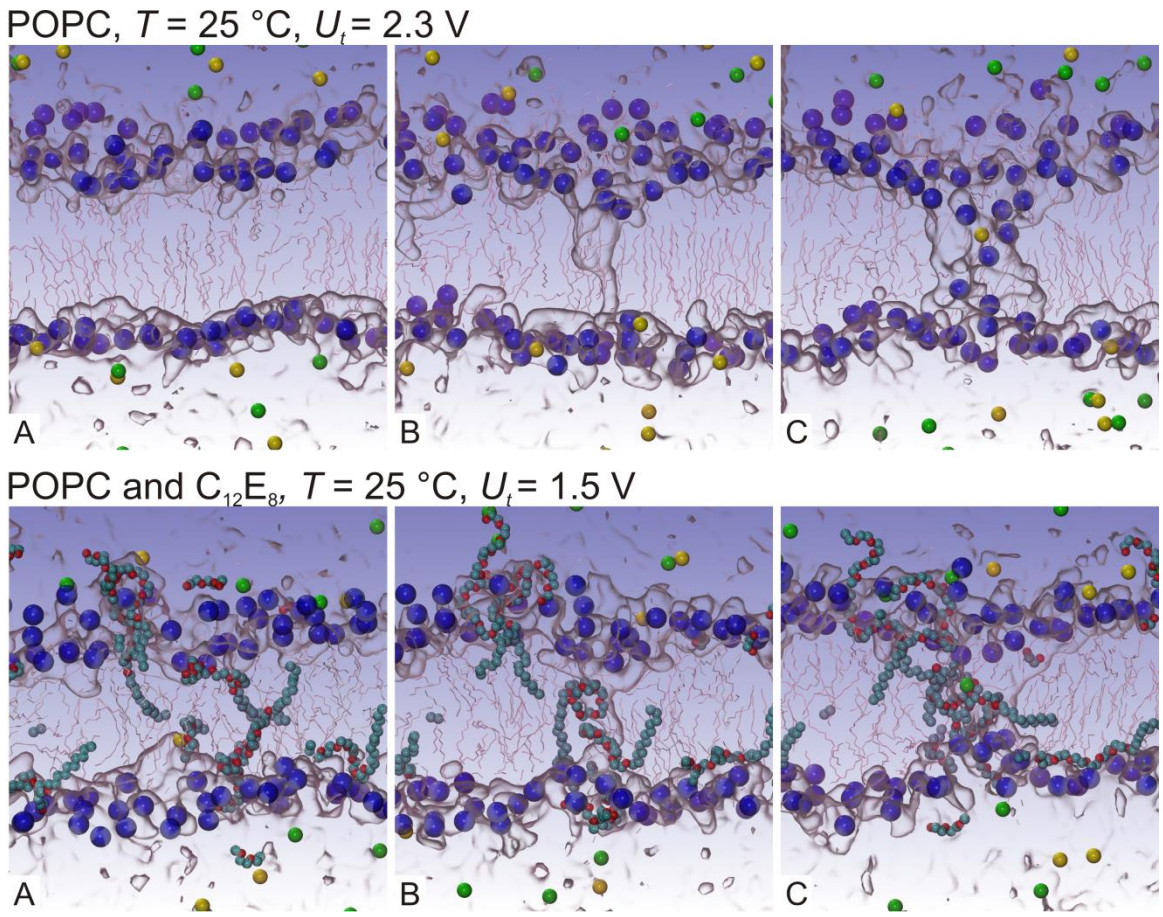

Figure 14: Electroporation process of POPC bilayers and POPC bilayers with surfactant $C_{12}E_8$ incorporated (snapshots at successive times after imposing a transmembrane voltage above the threshold): A) initial configuration, B) formation of water wire in hydrophilic region formed by $C_{12}E_8$ molecules and C) formation of conducting 'hydrophilic' pore (white – lipid tails (between lipid headgroups), blue – lipid headgroups, yellow – potassium ion, green – chloride ion, gray surface – water, red and cyan – $C_{12}E_8$ molecules, T – temperature, U_t – transmembrane voltage).

In order to investigate the reason for changes in the electroporation threshold when $C_{12}E_8$ is added to the POPC lipid bilayers, the dipole potential across the lipid bilayer was estimated from the MD simulations (Table 3). The latter provides a direct estimate of the local electric field present at the lipid/water interface and could influence the electroporation threshold since it modulates the forces applied on the dipole of the interfacial water molecules.(Aliste and Tieleman 2005) The data at hand shows that the dipole potential is not drastically altered when the surfactant is present at the investigated concentrations. The water permeability or diffusion toward the interior of lipid bilayers is the very initial key step in membranes electroporation.(Kramar et al. 2012b; Tokman et al. 2013) A significant change in lateral pressure in the bilayers' hydrophobic core has an influence on electroporation threshold. The analyses show that that the lateral pressure change is not drastic upon addition of the surfactant.

5 Conclusion and future work

The system for measuring planar lipid properties allows measurements of capacitance and voltage breakdown of the formed planar lipid bilayer. The properties can be measured using voltage or current-clamp methods with arbitrary shaped signals. The temperature of planar lipid bilayers' can be regulated between 15 and 55 °C. The planar lipid bilayers can be formed by painting or folding methods. The system for measuring planar lipid bilayers' properties formed in measurement chambers by double well chip and cross-channel chip method is suggested to be upgraded (Funakoshi et al. 2006).

The experiments on archaeal lipids' planar lipid bilayers are in the evaluation stage. Preliminary results show good agreement with the results obtained from the MD simulations. More experimental results have to be performed to obtain good statistic. The experimental results should be compared to MD simulations. A difference in absolute values between experiments and simulations was expected, but relative differences among bilayers of different composition at different temperatures should be in agreement.

A systematic study of the archaeal lipid bilayers' electroporation using MD simulations was performed. An increase in the electroporation threshold by methyl groups' addition to the lipid tail has been confirmed. Ester linkages replacement by ether linkages further increases electroporation threshold. Bilayers composed of AI and AGI lipids have much higher electroporation threshold compared to other lipid bilayers. The electroporation threshold can be decreased by adding the DPPC molecules into the bilayer. Very high electroporation thresholds of archaeal lipid bilayers can be related to special properties of the archaeal lipid bilayers. They exhibit very high lateral pressure in the hydrophobic region and very high negative pressure beneath the head group region. The lateral diffusion of archaeal lipids in a bilayer is slower when compared to other lipids. The head groups form numerous hydrogen bonds among each other. In archaeal lipid bilayers specific pore formation was observed. In these lipids the pore creation starts with water wire formation which permeates through the bilayer. In the next step the water wire expands and forms a channel to conduct ions. The archaeal lipids do not bend into the interior of the bilayer to stabilize the pore. This type of pore formation has also been noticed in POPS membranes (Dehez et al. 2014). Extent simulations on the sites of pore formation and also the study of the pore closure is suggested.

The study of effect of $C_{12}E_8$ incorporation into POPC membranes on electroporation rate showed good agreement with other studies (Troiano et al. 1998; Kandušer et al. 2003) and revealed the principle of decreasing electroporation threshold on molecular level. The electroporation threshold is decreased due to hydrophilic region being formed by $C_{12}E_8$ in the bilayer even before the water penetrates into the bilayer. For the future work more experiments and MD simulations at different $C_{12}E_8$ concentration

are suggested to be performed. It would also be interesting to study how the $C_{12}E_8$ behaves in case when it is incorporated into other lipid bilayers.

6 Original contributions

Based on results in this doctoral thesis, the following original scientific contributions to the research area were recognized:

6.1 Development of the system for measuring planar lipid bilayer properties

We developed a system for measuring the planar lipid bilayers properties. The measurement methods were adopted from literature. The developed system enables measurement of planar lipid bilayers' properties at regulated temperature in the range from 15 to 55 °C, due to use of temperature regulated bath. The planar lipid bilayer is formed by painting or folding method (**paper 1**). When using folding method the planar lipid bilayers are automatically formed using two syringe pumps which are filling the reservoirs of the measurement chamber.

6.2 Development of archaeal lipid models (AI and AGI) for use in molecular dynamics simulations

The lipids which are found in the membranes of archaea *Aeropyrum pernix* have not yet been described as MD models in literature. Therefore we built models of these two lipids, by combining the CHARMM force fields. The parameters from force field for lipids and carbohydrates was used and the parameters for ether linkages were adopted from Shinoda et al. (2004a). The models were evaluated in **paper 3** and **paper 4** and will be available online to those who work on molecular dynamic simulations.

6.3 Analysis of electroporation of archaeal lipid bilayers using molecular dynamics

Due to complex structure of the archaeal lipids AI and AGI, the study was divided into three parts. In the first part it has been showed that methyl groups in lipid tails increase the electroporation threshold and that changing ester linkages with ether linkages increases the electroporation threshold even further (**paper 2**). In the second part the electroporation thresholds of archaeal lipid bilayers were calculated. The comparison showed that they have much higher electroporation threshold than PC-based lipids, due to special moieties like methyl head groups, ether linkages, and special structure of head groups, which are composed of carbohydrates. In archaeal lipid bilayers also specific creation of conducting hydrophobic pore was observed (**paper 3**). Similar kind of pore formation was also observed in the POPS bilayers. Finally, in the third part we investigated the structure and dynamics of

archaeal lipid bilayers. The dynamics of the archaeal lipids and their head groups is much slower compared to other PC-based lipids (**paper 4**).

6.4 Analysis of molecule $C_{12}E_8$ influence on the electroporation of POPC bilayers

Due to better understanding on how to compose a lipid bilayer with desired electrical properties, we studied how incorporation of $C_{12}E_8$ into the POPC bilayers affects the electroporation (**paper 5**). The study was divided into experiments and molecular dynamics simulations. Experimentally obtained results are in agreement with the data from literature - the results confirm the literature data. The MD simulations support the experimental data and give explanation of changing characteristic at molecular level. The drastic change in electroporation threshold is caused by specific pore creation. The $C_{12}E_8$ molecules form hydrophilic cluster in the interior of the bilayer, followed by water penetration into the bilayer and its expansion to form a pore.

7 References

Aliste MP, Tieleman DP (2005) Computer simulation of partitioning of ten pentapeptides Ace-WLXLL at the cyclohexane/water and phospholipid/water interfaces. BMC Biochem 6:30. doi: 10.1186/1471-2091-6-30

Al-Sakere B, André F, Bernat C, et al. (2007) Tumor ablation with irreversible electroporation. PLoS One 2:e1135. doi: 10.1371/journal.pone.0001135

Antonov VF, Smirnova EY, Shevchenko EV (1990) Electric field increases the phase transition temperature in the bilayer membrane of phosphatidic acid. Chem Phys Lipids 52:251–257. doi: 10.1016/0009-3084(90)90121-7

Basu R, De S, Ghosh D, Nandy P (2001) Nonlinear conduction in bilayer lipid membranes - effect of temperature. Physica A 292:146–152.

Benvegnu T, Brard M, Plusquellec D (2004) Archaeabacteria bipolar lipid analogues: structure, synthesis and lyotropic properties. Curr Opin Colloid Interface Sci 8:469–479. doi: 10.1016/j.cocis.2004.01.005

Benz R, Beckers F, Zimmermann U (1979) Reversible electrical breakdown of lipid bilayer membranes: A charge-pulse relaxation study. J Membr Biol 48:181–204. doi: 10.1007/BF01872858

Benz R, Fröhlich O, Läuger P, Montal M (1975) Electrical capacity of black lipid films and of lipid bilayers made from monolayers. Biochim Biophys Acta - Biomembr 394:323–334. doi: 16/0005-2736(75)90287-4

Benz R, Janko K (1976) Voltage-induced capacitance relaxation of lipid bilayer membranes Effects of membrane composition. Biochim Biophys Acta - Biomembr 455:721–738. doi: 16/0005-2736(76)90043-2

Berkowitz ML, Bostick DL, Pandit S (2006) Aqueous solutions next to phospholipid membrane surfaces: insights from simulations. Chem Rev 106:1527–39. doi: 10.1021/cr0403638

Brooks BR, Brooks CL, Mackerell AD, et al. (2009) CHARMM: the biomolecular simulation program. J Comput Chem 30:1545–614. doi: 10.1002/jcc.21287

C. Heller L, Heller R (2010) Electroporation Gene Therapy Preclinical and Clinical Trials for Melanoma. Curr Gene Ther 10:312–317. doi: 10.2174/156652310791823489

Chanturiya AN (1990) Detection of transient capacitance increase associated with channel formation in lipid bilayers. Biochim Biophys Acta - Biomembr 1026:248–250. doi: 10.1016/0005-2736(90)90071-U

Clarke RJ (2001) The dipole potential of phospholipid membranes and methods for its detection. Adv Colloid Interface Sci 89-90:263–81.

Coronado R, Latorre R (1983) Phospholipid bilayers made from monolayers on patch-clamp pipettes. Biophys J 43:231–236. doi: 16/S0006-3495(83)84343-4

Corovic S, Lackovic I, Sustaric P, et al. (2013) Modeling of electric field distribution in tissues during electroporation. Biomed Eng Online 12:16. doi: 10.1186/1475-925X-12-16

Darold W (1972) Voltage dependence of bilayer membrane capacitance. J Colloid Interface Sci 40:417–423. doi: 10.1016/0021-9797(72)90351-7

Dehez F, Delemotte L, Kramar P, et al. (2014) Evidence of Conducting Hydrophobic Nanopores Across Membranes in Response to an Electric Field. J Phys Chem C 118:6752–6757. doi: 10.1021/jp4114865

Delemotte L, Dehez F, Treptow W, Tarek M (2008) Modeling membranes under a transmembrane potential. J Phys Chem B 112:5547–50. doi: 10.1021/jp710846y

Delemotte L, Tarek M (2012) Molecular dynamics simulations of lipid membrane electroporation. J Membr Biol 245:531–43. doi: 10.1007/s00232-012-9434-6

Demchenko AP, Yesylevskyy SO (2009) Nanoscopic description of biomembrane electrostatics: results of molecular dynamics simulations and fluorescence probing. Chem Phys Lipids 160:63–84. doi: 10.1016/j.chemphyslip.2009.05.002

Diederich A, Bähr G, Winterhalter M (1998) Influence of surface charges on the rupture of black lipid membranes. Phys Rev E 58:4883. doi: 10.1103/PhysRevE.58.4883

Elbayoumi TA, Torchilin VP (2010) Current trends in liposome research. Methods Mol Biol 605:1–27. doi: 10.1007/978-1-60327-360-2_1

Essmann U, Perera L, Berkowitz ML, et al. (1995) A smooth particle mesh Ewald method. J Chem Phys 103:8577. doi: 10.1063/1.470117

Funakoshi K, Suzuki H, Takeuchi S (2006) Lipid Bilayer Formation by Contacting Monolayers in a Microfluidic Device for Membrane Protein Analysis. Anal Chem 78:8169–8174. doi: 10.1021/ac0613479

Gawrisch K, Ruston D, Zimmerberg J, et al. (1992) Membrane dipole potentials, hydration forces, and the ordering of water at membrane surfaces. Biophys J 61:1213–23. doi: 10.1016/S0006-3495(92)81931-8

Goldman DE (1943) POTENTIAL, IMPEDANCE, AND RECTIFICATION IN MEMBRANES. J Gen Physiol 27:37–60. doi: 10.1085/jgp.27.1.37

Gurtovenko AA, Anwar J, Vattulainen I (2010) Defect-Mediated Trafficking across Cell Membranes: Insights from in Silico Modeling. Chem Rev 110:6077–6103. doi: 10.1021/cr1000783

Gusbeth C, Frey W, Volkmann H, et al. (2009) Pulsed electric field treatment for bacteria reduction and its impact on hospital wastewater. Chemosphere 75:228–33. doi: 10.1016/j.chemosphere.2008.11.066

Gutberlet T, Katsaras J (2001) Lipid bilayers: structure and interactions. 320.

Haberl S, Miklavcic D, Sersa G, et al. (2013) Cell membrane electroporation-Part 2: the applications. IEEE Electr Insul Mag 29:29–37. doi: 10.1109/MEI.2013.6410537

Hanai T, Haydon DA, Taylor J (1964) An Investigation by Electrical Methods of Lecithin-in-Hydrocarbon Films in Aqueous Solutions. Proc R Soc London Ser A Math Phys Sci 281:377 – 391. doi: 10.1098/rspa.1964.0188

Hanford MJ, Peeples TL (2002) Archaeal Tetraether Lipids: Unique Structures and Applications. Appl Biochem Biotechnol 97:45–62. doi: 10.1385/ABAB:97:1:45

Hanyu Y, Yamada T, Matsumoto G (1998) Simultaneous measurement of spectroscopic and physiological signals from a planar bilayer system: detecting voltage-dependent movement of a membrane-incorporated peptide. Biochemistry 37:15376–82. doi: 10.1021/bi981003f

Herrera FE, Pantano S (2009) Salt induced asymmetry in membrane simulations by partial restriction of ionic motion. J Chem Phys 130:195105. doi: 10.1063/1.3132705

Hess B, Kutzner C, van der Spoel D, Lindahl E (2008) GROMACS 4: Algorithms for Highly Efficient, Load-Balanced, and Scalable Molecular Simulation. J Chem Theory Comput 4:435–447. doi: 10.1021/ct700301q

Huang C, Wheeldon L, Thompson TE (1964) The properties of lipid bilayer membranes separating two aqueous phases: Formation of a membrane of simple composition. J Mol Biol 8:148–160. doi: 10.1016/S0022-2836(64)80155-8

Immordino ML, Dosio F, Cattel L (2006) Stealth liposomes: review of the basic science, rationale, and clinical applications, existing and potential. Int J Nanomedicine 1:297–315.

Ingólfsson HI, Lopez C a., Uusitalo JJ, et al. (2013) The power of coarse graining in biomolecular simulations. Wiley Interdiscip Rev Comput Mol Sci. doi: 10.1002/wcms.1169

Kalé L, Skeel R, Bhandarkar M, et al. (1999) NAMD2: Greater Scalability for Parallel Molecular Dynamics. J Comput Phys 151:283–312. doi: 10.1006/jcph.1999.6201

Kalinowski S, Figaszewski Z (1995a) A 4-electrode system for measurement of bilayer lipid membrane capacitence. Meas Sci Technol 6:1043–1049.

Kalinowski S, Figaszewski Z (1995b) A 4-electrode potentiostat-galvanostat for studies of bilayer lipid membranes. Meas Sci Technol 6:1050–1055.

Kalinowski S, Ibron G, Bryl K, Figaszewski Z (1998) Chronopotentiometric studies of electroporation of bilayer lipid membranes. Biochim Biophys ACTA-BIOMEMBRANES 1369:204–212.

Kandušer M, Fošnarič M, Šentjurc M, et al. (2003) Effect of surfactant polyoxyethylene glycol (C12E8) on electroporation of cell line DC3F. Colloids Surfaces A Physicochem Eng Asp 214:205–217. doi: 10.1016/S0927-7757(02)00410-7

Klauda JB, Venable RM, Freites JA, et al. (2010) Update of the CHARMM all-atom additive force field for lipids: validation on six lipid types. J Phys Chem B 114:7830–43. doi: 10.1021/jp101759q

Koronkiewicz S, Kalinowski S, Bryl K (2002) Programmable chronopotentiometry as a tool for the study of electroporation and resealing of pores in bilayer lipid membranes. Biochim Biophys ACTA-BIOMEMBRANES 1561:222–229.

Kotnik T, Kramar P, Pucihar G, et al. (2012) Cell membrane electroporation- Part 1: The phenomenon. IEEE Electr Insul Mag 28:14–23. doi: 10.1109/MEI.2012.6268438

Kragh-Hansen U, le Maire M, Møller J V (1998) The mechanism of detergent solubilization of liposomes and protein-containing membranes. Biophys J 75:2932–46. doi: 10.1016/S0006-3495(98)77735-5

Kramar P, Delemotte L, Maček Lebar A, et al. (2012a) Molecular-level characterization of lipid membrane electroporation using linearly rising current. J Membr Biol 245:651–9. doi: 10.1007/s00232-012-9487-6

Kramar P, Delemotte L, Maček Lebar A, et al. (2012b) Molecular-level characterization of lipid membrane electroporation using linearly rising current. J Membr Biol 245:651–9. doi: 10.1007/s00232-012-9487-6

Kramar P, Miklavc D, Kotulska M, Maček Lebar A (2010) Voltage- and Current-Clamp Methods for Determination of Planar Lipid Bilayer Properties. In: Iglič A (ed) Adv. Planar Lipid Bilayers Liposomes, Volume 11. Elsevier, Amsterdam, pp 29–69

Kramar P, Miklavcic D, Lebar A (2009) A System for the Determination of Planar Lipid Bilayer Breakdown Voltage and Its Applications. IEEE Trans Nanobioscience 8:132–138. doi: 10.1109/TNB.2009.2022834

Kramar P, Miklavcic D, Lebar AM (2007) Determination of the lipid bilayer breakdown voltage by means of linear rising signal. Bioelectrochemistry 70:23–7. doi: 10.1016/j.bioelechem.2006.03.022

Lehninger AL, Nelson DL, Cox MM (2008) Lehninger principles of biochemistry. 1100.

Leontiadou H, Mark AE, Marrink SJ (2004) Molecular dynamics simulations of hydrophilic pores in lipid bilayers. Biophys J 86:2156–64. doi: 10.1016/S0006-3495(04)74275-7

Levine ZA, Vernier PT (2010) Life cycle of an electropore: field-dependent and field-independent steps in pore creation and annihilation. J Membr Biol 236:27–36. doi: 10.1007/s00232-010-9277-y

Liberman E, Topaly V (1968) Permeability of bimolecular phospholipid membranes for fat-soluble ions. Biophysic 477–487.

Luckey M (2008) Membrane structural biology: with biochemical and biophysical foundations. 345.

Le Maire M, Møller J V, Champeil P (1987) Binding of a nonionic detergent to membranes: flip-flop rate and location on the bilayer. Biochemistry 26:4803–10.

Marrink SJ, Lindahl E, Edholm O, Mark a E (2001) Simulation of the spontaneous aggregation of phospholipids into bilayers. J Am Chem Soc 123:8638–9.

Marrink SJ, Risselada HJ, Yefimov S, et al. (2007) The MARTINI force field: coarse grained model for biomolecular simulations. J Phys Chem B 111:7812–24. doi: 10.1021/jp071097f

Mashl RJ, Scott HL, Subramaniam S, Jakobsson E (2001) Molecular simulation of dioleoylphosphatidylcholine lipid bilayers at differing levels of hydration. Biophys J 81:3005–15. doi: 10.1016/S0006-3495(01)75941-3

Meier W, Gra A, Diederichb A, Winterhalter M (2000a) Stabilization of planar lipid membranes : A stratiÐed layer approach. 4559–4562.

Meier W, Graff A, Diederich A, Winterhalter M (2000b) Stabilization of planar lipid membranes: A stratified layer approach. Phys Chem Chem Phys 2:4559–4562. doi: 10.1039/B004073H

Miklavčič D, Mali B, Kos B, et al. (2014) Electrochemotherapy: from the drawing board into medical practice. Biomed Eng Online 13:29. doi: 10.1186/1475-925X-13-29

Montal M, Mueller P (1972) Formation of bimolecular membranes from lipid monolayers and a study of their electrical properties. Proc Natl Acad Sci U S A 69:3561–3566.

Morii H, Yagi H, Akutsu H, et al. (1999) A novel phosphoglycolipid archaetidyl(glucosyl)inositol with two sesterterpanyl chains from the aerobic hyperthermophilic archaeon Aeropyrum pernix K1. Biochim Biophys Acta - Mol Cell Biol Lipids 1436:426–436. doi: 10.1016/S0005-2760(98)00157-X

Mueller P, Rudin DO, Tien HT, Wescott WC (1963) Methods for the formation of single bimolecular lipid membranes in aqueous solution. J Phys Chem 67:534–535. doi: 10.1021/j100796a529

Napotnik TB, Rebersek M, Kotnik T, et al. (2010) Electropermeabilization of endocytotic vesicles in B16 F1 mouse melanoma cells. Med Biol Eng Comput 48:407–13. doi: 10.1007/s11517-010-0599-9

Naumowicz M, Figaszewski ZA (2013) Pore Formation in Lipid Bilayer Membranes made of Phosphatidylcholine and Cholesterol Followed by Means of Constant Current. Cell Biochem Biophys 66:109–19. doi: 10.1007/s12013-012-9459-6

Neumann E, Schaefer-Ridder M, Wang Y, Hofschneider P. (1982) Gene transfer into electric fields. EMBO J 1:841–845.

Ollila S (2010) Lateral Pressure in Lipid Membranes and Its Role in Function of Membrane Proteins, PhD thesis. 70.

Ottova A, Tien H (2002) The 40th anniversary of bilayer lipid membrane research. Bioelectrochemistry 56:171–173.

Pace NR (2006) Time for a change. Nature 441:289. doi: 10.1038/441289a

Pavšelj N, Miklavčič D (2008) Numerical modeling in electroporation-based biomedical applications. Radiol Oncol 42:159–168. doi: 10.2478/v10019-008-0008-2

Peterson U, Mannock D a, Lewis RNA., et al. (2002) Origin of membrane dipole potential: Contribution of the phospholipid fatty acid chains. Chem Phys Lipids 117:19–27. doi: 10.1016/S0009-3084(02)00013-0

Phillips JC, Braun R, Wang W, et al. (2005) Scalable molecular dynamics with NAMD. J Comput Chem 26:1781–802. doi: 10.1002/jcc.20289

Polak A, Bonhenry D, Dehez F, et al. (2013) On the electroporation thresholds of lipid bilayers: molecular dynamics simulation investigations. J Membr Biol 246:843–50. doi: 10.1007/s00232-013-9570-7

Polak A, Mulej B, Kramar P (2012) System for measuring planar lipid bilayer properties. J Membr Biol 245:625–32. doi: 10.1007/s00232-012-9476-9

Polak A, Tarek M, Tomšič M, et al. (2014) Electroporation of Archaeal Lipid Membranes using MD Simulations. Bioelectrochemistry. doi: 10.1016/j.bioelechem.2013.12.006

Portet T, Camps i Febrer F, Escoffre J-M, et al. (2009) Visualization of membrane loss during the shrinkage of giant vesicles under electropulsation. Biophys J 96:4109–21. doi: 10.1016/j.bpj.2009.02.063

Punnamaraju S, Steckl AJ (2010) Voltage Control of Droplet Interface Bilayer Lipid Membrane Dimensions. Langmuir 27:618–626. doi: 10.1021/la1036508

Rems L, Miklavčič D (2014) Različni modeli elektroporacije in transporta molekul prek celične membrane. Elektroteh Vestn 81:64–72.

Robello M, Gliozzi A (1989) Conductance transition induced by an electric field in lipid bilayers. Biochim Biophys Acta - Biomembr 982:173–176. doi: 16/0005-2736(89)90189-2

Rosen D, Sutton AM (1968) The effects of a direct current potential bias on the electrical properties of bimolecular lipid membranes. Biochim Biophys Acta - Biomembr 163:226–233. doi: 10.1016/0005-2736(68)90101-6

Rubinsky B (2007) Irreversible electroporation in medicine. Technol Cancer Res Treat 6:255–60.

Ruiz M (2007) Cell membrane. http://en.wikipedia.org/wiki/File:Cell_membrane_de.

Sabotin I, Lebar AM, Miklavcic D, Kramar P (2009) Measurement protocol for planar lipid bilayer viscoelastic properties. IEEE Trans Dielectr Electr Insul 16:1236–1242. doi: 10.1109/TDEI.2009.5293933

Sachs JN, Crozier PS, Woolf TB (2004) Atomistic simulations of biologically realistic transmembrane potential gradients. J Chem Phys 121:10847–51. doi: 10.1063/1.1826056

Sako Y, Nomura N, Uchida A, et al. (1996) Aeropyrum pernix gen. nov., sp. nov., a Novel Aerobic Hyperthermophilic Archaeon Growing at Temperatures up to 100°C. Int J Syst Bacteriol 46:1070–1077. doi: 10.1099/00207713-46-4-1070

Salomon-Ferrer R, Case D a., Walker RC (2013) An overview of the Amber biomolecular simulation package. Wiley Interdiscip Rev Comput Mol Sci 3:198–210. doi: 10.1002/wcms.1121

Sersa G, Cufer T, Paulin SM, et al. (2012) Electrochemotherapy of chest wall breast cancer recurrence. Cancer Treat Rev 38:379–86. doi: 10.1016/j.ctrv.2011.07.006

Sharma V, Stebe K, Murphy JC, Tung L (1996) Poloxamer 188 decreases susceptibility of artificial lipid membranes to electroporation. Biophys J 71:3229–3241. doi: 10.1016/S0006-3495(96)79516-4

Shinoda K, Shinoda W, Baba T, Mikami M (2004a) Comparative molecular dynamics study of ether- and ester-linked phospholipid bilayers. J Chem Phys 121:9648–54. doi: 10.1063/1.1806791

Shinoda W, Mikami M, Baba T, Hato M (2004b) Molecular Dynamics Study on the Effects of Chain Branching on the Physical Properties of Lipid Bilayers: 2. Permeability. J Phys Chem B 108:9346–9356. doi: 10.1021/jp035998+

Shinoda W, Shinoda K, Baba T, Mikami M (2005) Molecular dynamics study of bipolar tetraether lipid membranes. Biophys J 89:3195–202. doi: 10.1529/biophysj.105.060962

Smondyrev AM, Berkowitz ML (1999) Structure of dipalmitoylphosphatidylcholine/cholesterol bilayer at low and high cholesterol concentrations: molecular dynamics simulation. Biophys J 77:2075–89. doi: 10.1016/S0006-3495(99)77049-9

Stampfli R (1958) Reversible electrical breakdown of the excitable membrane of a Ranvier node. Ann Brazilian Acid Sci 30:57–63.

Tarek M (2005) Membrane electroporation: a molecular dynamics simulation. Biophys J 88:4045–53. doi: 10.1529/biophysj.104.050617

Teissié J (1998) Transfer of foreign receptors to living cell surfaces: the bioelectrochemical approach. Bioelectrochemistry Bioenerg 46:115–120. doi: 10.1016/S0302-4598(98)00098-1

Tekle E, Astumian RD, Friauf WA, Chock PB (2001) Asymmetric Pore Distribution and Loss of Membrane Lipid in Electroporated DOPC Vesicles. Biophys J 81:960–968. doi: 16/S0006-3495(01)75754-2

Tieleman DP (2004) The molecular basis of electroporation. BMC Biochem 5:10. doi: 10.1186/1471-2091-5-10

Tieleman DP, Leontiadou H, Mark AE, Marrink S-J (2003) Simulation of pore formation in lipid bilayers by mechanical stress and electric fields. J Am Chem Soc 125:6382–3. doi: 10.1021/ja029504i

Tien HT, Ottova A (2003) Planar Lipid Bilayers (BLMs) and their Aplications, First. 1028.

Toepfl S, Heinz V, Knorr D (2007) High intensity pulsed electric fields applied for food preservation. Chem Eng Process Process Intensif 46:537–546. doi: 10.1016/j.cep.2006.07.011

Tokman M, Lee JH, Levine Z a, et al. (2013) Electric field-driven water dipoles: nanoscale architecture of electroporation. PLoS One 8:e61111. doi: 10.1371/journal.pone.0061111

Tokumasu F, Jin AJ, Dvorak JA (2002) Lipid membrane phase behaviour elucidated in real time by controlled environment atomic force microscopy. J Electron Microsc (Tokyo) 51:1 –9. doi: 10.1093/jmicro/51.1.1

Troiano GC, Tung L, Sharma V, Stebe KJ (1998) The reduction in electroporation voltages by the addition of a surfactant to planar lipid bilayers. Biophys J 75:880–8. doi: 10.1016/S0006-3495(98)77576-9

Van Uitert I, Le Gac S, van den Berg A (2010) The influence of different membrane components on the electrical stability of bilayer lipid membranes. Biochim Biophys Acta 1798:21–31. doi: 10.1016/j.bbamem.2009.10.003

Ulrih NP, Adamlje U, Nemec M, Sentjurc M (2007) Temperature- and pH-induced structural changes in the membrane of the hyperthermophilic archaeon Aeropyrum pernix K1. J Membr Biol 219:1–8. doi: 10.1007/s00232-007-9061-9

Ulrih NP, Gmajner D, Raspor P (2009) Structural and physicochemical properties of polar lipids from thermophilic archaea. Appl Microbiol Biotechnol 84:249–60. doi: 10.1007/s00253-009-2102-9

Usaj M, Trontelj K, Miklavcic D, Kanduser M (2010) Cell-cell electrofusion: optimization of electric field amplitude and hypotonic treatment for mouse melanoma (B16-F1) and Chinese Hamster ovary (CHO) cells. J Membr Biol 236:107–16. doi: 10.1007/s00232-010-9272-3

Vargas J, Alarcón JM, Rojas E (2000) Displacement Currents Associated with the Insertion of Alzheimer Disease Amyloid β-Peptide into Planar Bilayer Membranes. Biophys J 79:934–944. doi: 10.1016/S0006-3495(00)76348-X

Vernier PT, Ziegler MJ, Sun Y, et al. (2006) Nanopore-facilitated, voltage-driven phosphatidylserine translocation in lipid bilayers--in cells and in silico. Phys Biol 3:233–47. doi: 10.1088/1478-3975/3/4/001

Vries AH De, Ho H, Tieleman DP (2003) Methodological Issues in Lipid Bilayer Simulations. 9424–9433.

Wang L, Bose PS, Sigworth FJ (2006) Using cryo-EM to measure the dipole potential of a lipid membrane. Proc Natl Acad Sci U S A 103:18528–33. doi: 10.1073/pnas.0608714103

Weaver JC (2003) Electroporation of biological membranes from multicellular to nano scales. IEEE Trans Dielectr Electr Insul 10:754–768. doi: 10.1109/TDEI.2003.1237325

White SH (1970) A Study of Lipid Bilayer Membrane Stability Using Precise Measurements of Specific Capacitance. Biophys J 10:1127–1148. doi: 16/S0006-3495(70)86360-3

Wobschall D (1971) Bilayer membrane elasticity and dynamic response. J Colloid Interface Sci 36:385–396. doi: 10.1016/0021-9797(71)90010-5

Yamaguchi H, Nakanishi H (1993a) Photoresponsive planar bilayer lipid membranes containing azobenzene amphiphilic derivatives. Sensors Actuators B Chem 13:376–379. doi: 10.1016/0925-4005(93)85405-Y

Yamaguchi H, Nakanishi H (1993b) Characterization of the preparation process and the photochemical control of electrical properties of bilayer lipid membranes containing azobenzene chromophores. Biochim Biophys Acta - Biomembr 1148:179–184. doi: 10.1016/0005-2736(93)90127-L

Yang Y, Mayer KM, Wickremasinghe NS, Hafner JH (2008) Probing the lipid membrane dipole potential by atomic force microscopy. Biophys J 95:5193–9. doi: 10.1529/biophysj.108.136507

Yoshida T, Taga K, Okabayashi H, et al. (1989) Changes in surface capacitance and conductance parallel to phospholipid membranes associated with phase transition: effects of halothane. Biochim Biophys Acta 984:253–6.

Zorec B, Préat V, Miklavčič D, Pavšelj N (2013) Active enhancement methods for intra- and transdermal drug delivery : a review. Zdr Vetnik 339–356.

Declaration

The author hereby declares that the content of the thesis is a result of his own research work supervised by Prof. Damijan Miklavčič, Ph.D. and Mounir Tarek, Ph.D. The results, which were collected in collaboration with other colleagues, are published in the presented papers. The assistance from other colleagues is stated in the Acknowledgements. The published results of other authors are presented in the literature.

Andraž Polak

Izjava

Izjavljam, da sem doktorsko disertacijo izdelal sam, pod mentorstvom prof. dr. Damijana Miklavčiča in somentorstvom dr. Mounirja Tareka. Rezultati, ki so nastali v sodelovanju z drugimi sodelavci, so bili objavljeni v predstavljenih člankih. Izkazano pomoč ostalih sodelavcev sem v celoti navedel v zahvali. Že objavljeni dosežki drugih avtorjev so navedeni v spisku literature.

Andraž Polak